

Faculty of Science & Engineering
Department of Chemical Engineering

**Mathematical Modelling of LNG Dispersion Under Various
Conditions**

Walter Chukwunonso Ikealumba

This thesis is presented for the Degree of

Doctor of Philosophy

of

Curtin University

November 2016

DECLARATION

To the best of my knowledge and belief this thesis contains no material previously published by any other person except where due acknowledgement has been made. This thesis contains no material which has been accepted for the award of any other degree or diploma in any university.

15/11/2016

Walter Chukwunonso Ikealumba

Date

ABSTRACT

The global demand of liquefied natural gas (LNG) rises rapidly in recent years for the reasons of energy security and sustainable development. This has led to considerable recent research interests and efforts in the LNG production chain and associated risks in handling, storage and transport of LNG, largely driven by the intrinsic process safety issues of LNG, potential terrorist threats and public confidence in LNG safety.

This thesis firstly presents a comprehensive review on some recent advances in LNG value chain, covering upstream gas production and gathering, liquefaction, shipping and regasification processes. Recent developments in the experimentation and modelling of LNG spills associated with LNG value chain are then summarized, covering the events following an LNG spill including LNG pool formation, vapour dispersion and combustion. The consequent hazards and safety issues are also discussed, with a focus on the methods for improving the safety of personnel, facilities and ships. The key technical gaps in the related research areas have been identified and future research directions are outlined.

Following the review on recent advances in LNG value chain and focusing on LNG spill, pool formation and dispersion, this PhD study has developed a CFD code that directly models the complete spill and pool formation process (Direct CFD simulation method), taking into consideration heat and mass transfer governing equations and the Monin-Obukhov similarity theory for atmospheric stability. The model (direct CFD simulation method) was validated against the experimental data from the Burro and Falcon test series. The direct CFD simulation method was shown to provide better predictions than the conventional approach that simply estimates the pool size from natural gas inlet conditions and uses fixed vaporization rate.

This PhD study further applies the direct CFD simulation method to investigate: a) the effect of an impoundment on LNG spill and dispersion mitigation; b) the thermal effect of substrate and atmosphere on LNG spill, pool formation and vapour cloud dispersion; and c) the stability effect of atmosphere and sea on LNG pool formation and vapour cloud dispersion process and implications to Australian LNG transport.

It was clearly shown that an impoundment can confine the LNG spill and control the dispersion by both increasing air flow turbulence and generation of a swirl/recirculation at the upwind walls resulting in reduction of vapour cloud dispersion by up to 55%.

The simulations on the thermal effect simulations show that increasing thermal conditions has little effect on the initial growth rate of the LNG pool (0 – 50 s); however as the LNG discharge rate starts to decrease (~50 – 400 s), the effect of increasing thermal conditions becomes more apparent, with the pool size decreasing. Overall this led to a significant increase in downwind dispersion (by up to 26%) accompanied with a slight decrease in lateral dispersion (by up to 6%) and a slight increase in the vertical dispersion (by up to 5%). The prediction also shows that thermal conditions of spill substrate (in this case, the sea surface) have a greater impact on the dispersion process than that of the atmosphere.

By incorporating a wave modelling method into the previously develop direct CFD simulation method, the stability effect of atmospheric and sea (sea waves in particular) on LNG pool formation and dispersion process was then investigated. Pasquill stability was used to determine the stability classes for each of the scenarios and cases studied. The importance of modelling the roll and pitch of LNG carriers was investigated; with sloshing leading to an increase of up to 31% on tank wall pressure and an increase of 100 seconds on spill time. Analyses show that as stability increase, LNG pool radius also increase; and a larger pool radius was indicative of a lower evaporation rate. The increasing stability (more stable conditions) was shown to have little effect on the earlier growth of the LNG pool and the temporal evolution of evaporation rate (0 – 50 s); once the discharge of LNG from the tanker starts decreasing, the effect of increasing stability in each case , starts becoming visible (~50 s and onwards). The results showed that stability effects induced by the sea waves were noted to have a greater impact on the whole spill and dispersion process. Overall the increasing stability conditions led to an 8% increase in downwind dispersion of the vapour cloud, 11% increase in the crosswind dispersion and a 19% decrease in vertical dispersion. Finally the implications of this study to Australian LNG export was investigated, from which it was concluded that LNG exports during winter can lead to

the least affected areas compared to that in summer. In order to mitigate LNG spill hazards from an LNG carrier, the areas of focus should be on travel routes in close proximity to islands; and following an LNG spill, stopping the LNG carrier would minimize the hazard zone.

ACKNOWLEDGEMENT

The first and biggest acknowledgement is to my supervisor Professor Hongwei Wu, who gave me the opportunity to undertake this PhD and assisted me in many ways to help me complete this PhD program by answering all my questions patiently and providing his knowledge of the LNG value chain, mathematical modelling and preparation of reports/publication papers.

I am also grateful to Sam Mannan from the Mary Kay O'Connor Process Safety Center, Texas A&M University for providing some experimental data, which provided initial stepping stone in understanding and modelling of LNG spill and dispersion process. Thanks also go to Jeff Roberts from the Lawrence Livermore National Laboratory for providing the Burro 8 reports, without which I could not have been able to validate my direct CFD simulation code. I would also like to acknowledge David Chan from James Cook University for drafting the initial LNG ship model; his drafting expertise was valuable towards creating simplified LNG ship models and overall modelling process.

In addition, I am grateful to the Australian Postgraduate Awards for supporting my PhD study. My study would have also not been possible without the allocated computer times on the Epic and Magnus super computers in Pawsey Supercomputing Centre; I am very grateful for their generosity.

Last but not least, I am thankful for my family for their unconditional and continual support. Many thanks to my dad, Professor Ndidi Victor Ikealumba who read both the proposal and this final thesis document to provide me with as much feedback on structure, grammar and spelling to ensure the quality of the document. My mum, Mrs Ebele Gladys Ikealumba for her persistent prayers, my brothers (Nnaemeka & Jachike) as well as my sisters (Chiamaka & Nnemdi), for their encouragement and well wishes.

PUBLICATIONS

1. Walter Chukwunonso Ikealumba and Hongwei Wu. "Effect of atmospheric and sea stability on liquefied natural gas (LNG) dispersion: Implications to Australian LNG marine transport." *Fuel*, **2017**, 197, 8-19
2. Walter Chukwunonso Ikealumba and Hongwei Wu. "Effect of Air and Sea Surface Temperatures on LNG Dispersion." *Energy & Fuels*, **2016**, 30 (11), 9266-9274
3. Walter Chukwunonso Ikealumba and Hongwei Wu. "Modelling of Liquefied Natural Gas Release and Dispersion: Incorporating a Direct Computational Fluid Dynamics Simulation Method for LNG Spill and Pool Formation." *Industrial & Engineering Chemistry Research*, **2016**, 55, 1778-1787.
4. Walter Chukwunonso Ikealumba and Hongwei Wu. "Some recent advances in liquefied natural gas (LNG) production, spill, dispersion, and safety." *Energy & Fuels*, **2014**, 28, 3556-3586.

CONTENTS

DECLARATION	I
ABSTRACT	II
ACKNOWLEDGEMENT	V
PUBLICATIONS	VI
LIST OF TABLES	X
LIST OF FIGURES	XII
NOMENCLATURE	XV
1 INTRODUCTION	1
1.1 Background and Motives	1
1.1.1 Global Energy Outlook and the Role of Natural Gas	1
1.1.2 Importance of Liquefied Natural Gas (LNG) for Natural Gas Utilisation.....	3
1.1.3 Life Cycle Performance of Natural Gas and LNG.....	5
1.2 Scope and Objectives	7
1.3 Thesis Outline	8
2 LITERATURE REVIEW	10
2.1 Introduction	10
2.2 LNG Production Chain	12
2.2.1 Upstream Gas Production and Gathering.....	12
2.2.2 Liquefaction and Storage	14
2.2.3 Shipping	16
2.2.4 Regasification Terminals	20
2.2.5 LNG Value Chain Potential Hazards	21
2.3 LNG Spill, Vapour Production, Dispersion and Combustion.....	22
2.3.1 Pool Formation.....	23
2.3.2 Vapour Dispersion	29
2.3.3 Combustion	47
2.4 Safety	54
2.4.1 Facilities	55
2.4.2 Ships.....	59

2.5	Conclusion and Research Gaps.....	63
2.5.1	LNG Spill, Vapour Production, Dispersion, and Combustion.....	63
2.5.2	Safety	64
2.6	Research Objectives of Current Study	65
3	METHODOLOGY	66
3.1	Introduction.....	66
3.2	Pre-Processing.....	66
3.2.1	Geometry.....	66
3.2.2	Meshing.....	66
3.2.3	Controls.....	67
3.3	Processing	67
3.4	Post Processing	68
3.5	Utilisation of Methodology.....	69
4	A CFD MODEL FOR THE SIMULATION AND ANALYSIS OF LNG DISPERSION.....	70
4.1	Direct CFD Simulation Method Development	70
4.1.1	Introduction.....	70
4.1.2	The Burro Series Test	71
4.1.3	Mathematical Formulation.....	74
4.2	Direct CFD Simulation Method Validation.....	77
4.2.1	Computation Geometry and Grid.....	77
4.2.2	Boundary Conditions and Initial Conditions	78
4.2.3	Solution Method.....	79
4.2.4	Crosswind Dispersion	79
4.2.5	Downwind Dispersion.....	80
4.2.6	Time Variant Vapour Gas Concentration Comparison.....	83
4.3	Effect of Impoundments on LNG Dispersion.....	87
4.3.1	Vapour Cloud Dispersion.....	88
4.3.2	Time Variant Vapour Gas Concentration Comparison.....	92
4.4	Conclusion	95
5	EFFECT OF SEA SURFACE AND AIR TEMPERATURE ON LNG DISPERSION	96
5.1	Modelling and Validation According to Sea Surface and Air Temperatures	96
5.1.1	Introduction.....	96

5.1.2	Falcon Series Test	98
5.1.3	Mathematical Formulation	100
5.1.4	Computation Geometry and Grid.....	100
5.1.5	Boundary Conditions and Initial Conditions	101
5.1.6	Solution Method.....	103
5.1.7	Vapour Cloud Dispersion Analysis.....	104
5.1.8	Time Variant Vapour Gas Concentration Comparison.....	105
5.2	Effect of Sea Surface and Air Temperature Analysis.....	109
5.3	Conclusion	115
6	EFFECT OF ATMOSPHERIC AND SEA STABILITY ON LNG DISPERSION AND IMPLICATIONS TO AUSTRALIAN LNG MARINE TRANSPORT ...	116
6.1	Wave Modelling and Stability Effect Simulation Methodology	116
6.1.1	Introduction.....	116
6.1.2	Pasquill Stability	118
6.1.3	Mathematical Formulation.....	119
6.1.4	Computation Geometry and Grid.....	121
6.1.5	Boundary Conditions and Initial Conditions	122
6.1.6	Solution Method.....	124
6.2	Analysis of Stability Effect on LNG Spill and Vapour Cloud Dispersion	124
6.2.1	Effect of Sloshing on LNG Dispersion	124
6.2.2	Stability Effect and Vapour Cloud Dispersion Analysis	125
6.3	Implications to Australian LNG Marine Transport	132
6.4	Conclusion	139
7	CONCLUSION AND FUTURE WORK.....	141
7.1	Introduction.....	141
7.2	Conclusion	141
7.2.1	Simulation and Analysis of LNG Dispersion	141
7.2.2	Effect of Sea Surface and Air Temperatures Simulation	142
7.2.3	Stability Effect Simulation and Analysis of LNG Dispersion	142
7.3	Future Work	143
REFERENCES.....		145

LIST OF TABLES

Table 1: Emission of air pollutants from the direct combustion of coal, oil and natural gas ^a	2
Table 2: Average levelised capital costs of new power generation resources ^a	2
Table 3: Fuel properties of natural gas at standard temperature and pressure (STP) ⁸⁻¹¹ compared to those of LNG (-162 °C) ^{3, 12-15}	4
Table 4: Some key LNG projects worldwide ¹⁶⁻²⁴	4
Table 5: LNG value chain costs for a typical 8 mtpa process ^{29, 31}	5
Table 6: LCA of different energy sectors for a 20-year ^a period ^{6, 32-35}	6
Table 7: LCA of LNG vs. pipeline transport ^a	7
Table 8: Published review papers regarding different aspects of the LNG value chain ¹	11
Table 9: Typical composition of natural gas compared to LNG. ⁴⁵	13
Table 10: Commonly used LNG liquefaction processes ^a	15
Table 11: Comparison of refrigeration cycle configurations ^a	16
Table 12: A summary of various cargo containing systems for LNG ⁹⁵⁻⁹⁸	18
Table 13: Some well-known pool formation models for LNG pool modelling.....	26
Table 14: LNG dispersion test on water ³⁸	29
Table 15: Some well-known Similarity-Profile/Modified Gaussian models for LNG vapour dispersion	35
Table 16: Some well-known Navier-Stokes models for LNG vapour dispersion	37
Table 17: The effect of hole size and breach diameter on spill and dispersions using the FERC model ^a	40
Table 18: Comparison of LNGMAP to Sandia predictions ^a	41
Table 19: Test conditions for spills into impoundments followed by dispersion. ¹	45
Table 20: Comparison of the distance to LFL for LNG dispersion in BFTF ^a	45
Table 21: One of the test cases comparing the addition of the fuzzy and MC methods to the source term modelling of the Classical model ^a	46
Table 22: LNG fire tests on water and land ^a	49
Table 23: Some well-known models for LNG fire modelling	52
Table 24: Distribution of known relevant LNG accidents ²³⁸	60
Table 25: Burro 8 Spill: Atmospheric and Boundary Layer Conditions ^a	73

Table 26: Comparison of simulation crosswind and downwind dispersion to experimental data ²⁶⁷	82
Table 27: Peak vapour gas concentrations at sensor locations ²⁶⁷	87
Table 28: Statistical performance comparison for the two source modelling methods ²⁶⁷	87
Table 29: Comparison of vapour cloud spatial evolution without impoundment vs with impoundment ²⁶⁷	89
Table 30: Comparison of peak vapour gas concentrations at different locations ²⁶⁷	93
Table 31: Falcon 1 Spill: Atmospheric and Boundary Layer Conditions ^a	100
Table 32: Air and Sea Surface Temperatures for the Different Scenarios and Corresponding Cases. ²⁷⁵	102
Table 33: Comparison of simulation crosswind and downwind dispersion to experimental data. ²⁷⁵	107
Table 34: Peak vapour gas concentrations at sensor locations. ²⁷⁵	107
Table 35: Statistical performance of the direct CFD simulation method. ²⁷⁵	109
Table 36: Meteorological Conditions Defining Pasquill Turbulence ^a	118
Table 37: Base Stability Conditions and Resultant Sea and Atmospheric temperatures (Conditions used in Scenario I). ²⁸⁵	119
Table 38: Scenario I as realistic scenario under varying wind and sea conditions. ²⁸⁵	123
Table 39: Scenario II under varying wave conditions while wind speed and surrounding temperatures are constant. ²⁸⁵	123
Table 40: Scenario III at varying wind speed while wave conditions and surround temperatures are held constant. ²⁸⁵	123
Table 41: Sea surface temperature and wave conditions during LNG transport in summer. ²⁸⁵	134
Table 42: Sea surface temperature and wave conditions during LNG transport in winter. ²⁸⁵	134
Table 43: $\frac{1}{2}$ LFL of vapour cloud in summer. ²⁸⁵	135
Table 44: $\frac{1}{2}$ LFL of vapour cloud in winter. ²⁸⁵	136

LIST OF FIGURES

Figure 1: Growth of world energy mix from 1990 and extrapolated to 2030 (data were extracted from literature; ² 1EJ = 0.9478 quadrillion Btu)	2
Figure 2: Transport cost of natural gas technologies relative to distance (data extracted from literature, ⁷ 1\$/GJ = 1.055\$/MMBtu).....	3
Figure 3: Thesis Map	9
Figure 4: Natural gas pre-treatment and liquefaction diagram (adapted from the literature ⁴⁶)	13
Figure 6: LNG spill events. ¹	22
Figure 6: Calculated heat loss by water curtain (data were extracted from Rana et al. ¹⁴⁶)	31
Figure 7: Small-scale experimental setup for measuring the evaporation rate of LNG from a water surface by controlling the turbulence (adapted from the study by Morse and Kytömaa ¹⁵²)	33
Figure 8: Schematic diagrams of LNG cargo containment system composed of primary and secondary barriers: a) overall drawing; b) enlarged view of the corner of top bridge pad; and c) insulation panels with level difference (adapted from the study by Bang et al. ²⁴³)	61
Figure 9: Yielding and buckling pressures of corrugations under symmetric loading a) symmetric loading b) asymmetric loading (data were extracted from the study by Chul Kim et al. ²⁵⁰)	62
Figure 10: Spill facility and water pond ²⁶²	72
Figure 11: Gas sensor stations arrangement ^{113, 114}	73
Figure 12: (a) Experimental layout and (b) hexahedral mesh with refinements towards the center of the water pond and approaching the ground surface ²⁶⁷	77
Figure 13: Comparison of CFD vapour cloud dispersion contours at a height of 1m to experimental results ²⁶⁷	81
Figure 14: Comparison of time variant vapour gas volume concentration for predicted LNG pool formation vs direct CFD simulation method at different sensory locations with sensor's (x, y, z) coordinates given. ²⁶⁷	86

Figure 15: a) Experimental layout b) hexahedral mesh with refinements around water pond and vapour fence ²⁶⁷	88
Figure 16: Comparison of CFD vapour cloud dispersion contours 15%, 5% and 1% respectively at a height of 1 m. ²⁶⁷	90
Figure 17: Comparison of 2.5% v/v at different times: (a) no impoundment (b) with impoundment. ²⁶⁷	91
Figure 18: Comparison of time variant vapour gas volume concentration without impoundment vs with impoundment at different locations with sample points (x, y, z) coordinates given. ²⁶⁷	94
Figure 19: (a) Major LNG trade movement in 2014 (billion cubic meters) ²⁷³ and (b) correspond sea surface temperatures ²⁷⁴	97
Figure 20: Falcon series experimental setup. ¹¹⁸	99
Figure 21: (a) Experimental layout and (b) hexahedral mesh with refinements around the water pond and approaching the ground surface. ²⁷⁵	101
Figure 22: (a) Experimental layout and (b) hexahedral mesh with refinements in areas of high flow gradient. ²⁷⁵	103
Figure 23: Comparison of CFD vapour cloud dispersion to experimental results at the 150 m sensory row. ²⁷⁵	106
Figure 24: Comparison of time variant vapour gas volume concentration at different sensory locations with sensor's (x, y and z) coordinates given. ²⁷⁵	108
Figure 25: Pool radius (m) versus time (s) comparison for a realistic scenario with (air and sea) temperatures given for each case. ²⁷⁵	110
Figure 26: Effect of the temperature on vapour cloud dispersion of (air and sea) temperatures for each case, with varying air and sea surface temperatures (results obtained at $\frac{1}{2}$ LFL). ²⁷⁵	111
Figure 27: Effect of the temperature on vapour cloud dispersion of (air and sea) temperature for each case, with varying air temperatures and constant sea surface temperatures (results obtained at $\frac{1}{2}$ LFL). ²⁷⁵	113
Figure 28: Effect of the temperature on vapour cloud dispersion of (air and sea) temperatures for each case, with constant air temperatures and varying sea surface temperatures (results obtained at $\frac{1}{2}$ LFL). ²⁷⁵	114
Figure 29: (a) Major LNG trade movement in 2014 (billion cubic meters) ²⁷³ and (b) Correspond wave conditions ²⁸²	117

Figure 30: (a) Experimental layout and (b) hexahedral mesh with refinements in areas of high flow gradient. ²⁸⁵	121
Figure 31: The effect of sloshing (in Scenario I) on (a) Maximum pressure on tank wall and (b) total LNG spill time with each case's (sea, air) temperatures given. ²⁸⁵ .	125
Figure 32: Scenario I case comparison: a) Pool evaporation rate (kg/s) vs time (s); b) Pool radius (m) vs time (s) with each case's (sea, air) temperatures given. ²⁸⁵	127
Figure 33: Stability effect on vapour could dispersion for Scenario I under varying ocean and atmospheric conditions, with each case's (sea, air) temperatures given (results obtained at $\frac{1}{2}$ LFL). ²⁸⁵	129
Figure 34: Stability effect on vapour could dispersion for Scenario II under varying wave conditions, constant wind speed and constant temperatures, with each case's (sea, air) temperatures given (results obtained at $\frac{1}{2}$ LFL). ²⁸⁵	130
Figure 35: Stability effect on vapour could dispersion for Scenario III at varying wind speeds, constant wave conditions and constant temperatures, with each case's (sea, air) temperatures given (results obtained at $\frac{1}{2}$ LFL). ²⁸⁵	131
Figure 36: LNG carrier travel routes with segmented sections for analysis; China: a-e and Japan: a-d-f. ²⁸⁵	133
Figure 37: Summer vs. winter comparison of vapour cloud dimensions in each section (results obtained at $\frac{1}{2}$ LFL). ²⁸⁵	137

NOMENCLATURE

ALOHA	Area Locations of Hazardous Atmospheres
avg	average
bcm	billion cubic meters
BFTF	Brayton Fire Training Field
BLEVE	boiling liquid expanding vapour explosion
BOG	boil-off gas
Btu	British thermal units
CFD	computational fluid dynamics
CFR	Code of Federal Regulations
cm	centimetres
CWHE	coil wound heat exchanger
DFDE	dual fuel diesel electric propulsion
DFGE	dual fuel gas-turbine electric propulsion
DFSM	dual fuel steam-turbine mechanical propulsion
DMR	dual mixed refrigerant
DOT	Department Of Transport
DSF	dispersion safety factor
E	exa ($\times 10^{18}$)
ESD	emergency shutdown
FB	fractional bias
FERC	Federal Energy Regulatory Commission
FLNG	floating liquefied natural gas
FS	fuzzy sets
Ft	feet
G	giga ($\times 10^9$)
GA	genetic algorithm
GBS	gravity-based structure
h	hour
HAZOP	hazards and operability study
IGC	international gas carriers
in	inches
J	joules
k	kilo ($\times 10^3$)
K	kelvins
L or l	litres
lb	pounds (mass)
LFL	low flammability limit

LLNL	Lawrence Livermore National Laboratory
LNG	liquefied natural gas
LOPA	layer of protection analysis
M	mega ($\times 10^6$)
m	meters
MC	Monte Carlo
MED	model evaluation protocol
MEM	TNO-Multi Energy Method
MFC	mixed fluid cascade
MG	geometric mean bias
min	minutes
MM	million
mol	moles
MR	mixed refrigerant
N	newtons
N/A	not applicable or not available
NFPA	National Fire Protection Association
NMSE	normalised mean square error
NWC	Naval Weapons Center
Pa	pascal
PFHE	parallel fin heat exchanger
PHAST	Process Hazard Analysis Software Tool
PMR	parallel mixed refrigerant
POC	Phillips' Optimised Cascade
Psig	pounds (force) per square inch gauge
PUF	Polyurethane foam
RANS	Reynolds averaged Navier-Stokes
RPT	rapid phase transition
RPUF	reinforced polyurethane foam
RSM	Reynolds stress models
s	seconds
SFDM+R	diesel mechanical propulsion with reliquefaction
SHIPP	system hazard identification, prediction and prevention
SWE	shallow water equations
Tcf	trillion cubic feet
VCE	vapour cloud explosion
VG	geometric mean variance
W	watts
X _{LFL}	downwind length to the flammable cloud at the low flammability limit (m)
X _{vis}	downwind length to the visible cloud (m)

A	Wave amplitude (m)
c	Wave speed (m/s)
C	Concentration (kg/m^3)
d	Bubble diameter or pool length (m)
E	total energy (J)
F	vaporization-condensation flux
g	gravitational acceleration (m/s^2)
h	Liquid height (m)
H	Wave height (m)
I	unit tensor (1/s)
k	Turbulent kinetic energy (m^2/s^2)
k	Wave number
L	latent heat (KJ/kg)
L	Monin-Obukhov length (m)
M	molar mass (kg/mol)
P	Pressure (Pa)
R	universal gas constant
t	Time (s)
T	Temperature (K)
U	Uniform flow velocity magnitude (m/s)
\vec{j}_j	diffusion flux ($\text{kg}/\text{m}^2 \text{s}$)
\dot{m}_{gl}	mass transfer rate from gas to liquid phase (kg/s)
\dot{m}_{lg}	mass transfer rate from liquid to gas phase (kg/s)
ϕ	Velocity potential (m^2/s)
ϕ_h	Monin-Obukhov similarity profile function for heat transfer
ϕ_m	Monin-Obukhov similarity profile function for momentum transfer
h_j	sensible enthalpy (J/kg)
A_c	Wave amplitude at crest (m)
A_i	interfacial area between phases (m^2)
A_t	Wave amplitude at trough (m)
C_{con}	condensation coefficient
C_{ev}	vaporization coefficient
$D_{T,i}$	thermal diffusion coefficient
$D_{i,m}$	mass diffusion coefficient
\vec{F}	sum of body forces (N)
G_b	turbulence kinetic energy generation due to buoyancy ($\text{kg}/\text{m}^3 \text{s}^3$)
G_k	turbulence kinetic energy generation due to velocity gradients ($\text{kg}/\text{m}^2 \text{s}^3$)
k_x	Wave number in direction of flow
k_z	Wave number in the cross flow direction

P_{sat}	saturated pressure (Pa)
P_v	vapour pressure (Pa)
R_i	net rate of species production (kg/m ³ *s)
S_h	energy for chemical reaction and other heat sources (J)
S_i	species source term (kg/m ³ s)
S_k	user defined source term for turbulent kinetic energy (m ² /s ²)
S_ε	user defined source term for turbulent dissipation rate (m ² /s ³)
T_L	liquid temperature (K)
T_{sat}	saturated temperature (K)
V_{cell}	cell volume (m ³)
Y_i	mass fraction of each species
$a_{l,v}$	volume fraction of liquid or vapour phase
k_{eff}	effective thermal conductivity (W/m*K)
\vec{v}	velocity vector (m/s)
μ_t	turbulence viscosity (Pa*s)
ρ_g	vapour density (kg/m ³)
ρ_l	liquid density (kg/m ³)
$\bar{\tau}$	stress tensor (kg/m*s ²)
β	accommodating coefficient
ε	turbulence dissipation rate (m ² /s ³)
ε	Phase difference (°)
λ	Wave length (m)
μ	dynamic viscosity (Pa*s)
ρ	Density (kg/m ³)
ω	Wave frequency (Hz)
ω_e	Effective wave frequency (Hz)

1 INTRODUCTION

1.1 Background and Motives

1.1.1 Global Energy Outlook and the Role of Natural Gas

The global energy demand is rapidly growing and at a time when the threat of climate change needs to be addressed by reducing carbon dioxide emissions, most of which comes from the use of fossil fuels. Figure 1 illustrates the growth of the world energy mix with a forecast to 2030 derived from the BP statistical review of world energy 2013.² This figure depicts the growth of energy consumption by fuel source, with natural gas approaching the consumption levels of coal and oil. The total global energy use for the year 2012 was 521.97 EJ (494.73 Quadrillion Btu), with oil as the leading energy source at 33%, followed by coal at 30%, natural gas at 24%, nuclear at 4% and other sources (wind, solar etc.) at 9%. In Australia however, the total energy use is 521.97 EJ (494.73 Quadrillion Btu), with coal as the leading energy source at 39%, followed by oil at 37%, natural gas at 18%, other sources (wind, solar etc.) at 6% and without nuclear (0%).

Of the three largest energy sources (coal, oil and natural gas), natural gas continues to be favour, due to its environmental friendly nature and is arguably the cleanest fossil fuel.³ In comparison to oil and coal, it emits virtually no sulfur, far less nitrogen oxide, no solid waste and significantly less carbon dioxide than oil and coal. The direct greenhouse gas emissions from combustion for coal and oil are significantly higher per unit of energy compared to that of natural gas (Table 1) based on the review paper by Lim et al.⁴ and the carbon dioxide emission coefficient of the U.S. Energy Information Administration⁵. In addition, according to US Energy Information Administration,⁶ new gas power plants required ~50% of the levelised capital cost of coal per MWh, less than 33% the cost of nuclear, and less than 20% the cost of onshore wind, let alone off-shore wind, as detailed in Table 2.

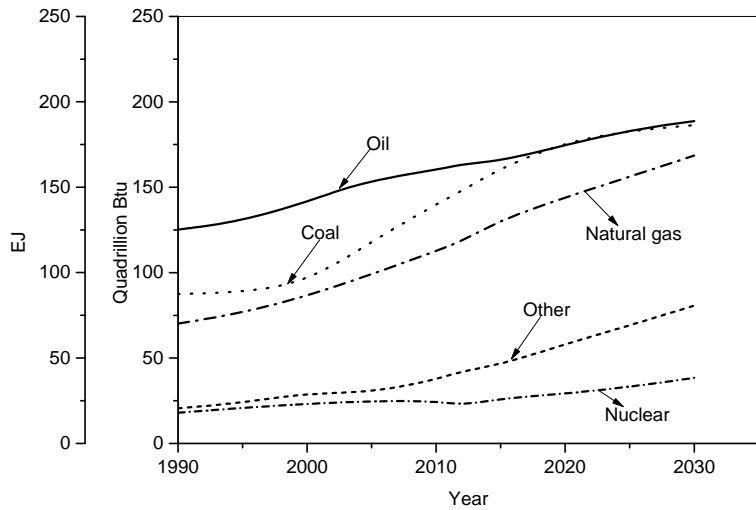


Figure 1: Growth of world energy mix from 1990 and extrapolated to 2030 (data were extracted from literature;² 1EJ = 0.9478 quadrillion Btu).

Table 1: Emission of air pollutants from the direct combustion of coal, oil and natural gas^a

	Carbon dioxide	Nitrogen oxides	Sulphur dioxide
	kg/GJ	kg/GJ	kg/GJ
	(lbs/MMBtu)	(lbs/MMBtu)	(lbs/MMBtu)
Coal	90.37 (210.2)	196.47 (457)	1113.93 (2591)
Oil	70.50 (164)	209.80 (488)	482.37 (1122)
Natural Gas	50.30 (117)	39.55 (92)	0.26 (0.6)

^aData were extracted and converted from the literature^{4, 5}

Table 2: Average levelised capital costs of new power generation resources^a

Energy Source for the Plant	Levelised capital cost ^b (\$/MWh)	Levelised capital cost (\$/MMBtu)	Total system capital cost (\$/MWh)	Total system capital cost (\$/MMBtu)
Natural Gas	15.8 – 44.2	4.63 – 12.95	65.6 – 130.3	19.23 – 38.19
Coal	65.7 – 88.4	19.25 – 25.91	100.1 – 135.5	29.34 – 39.71
Nuclear	83.4	24.44	108.4	31.77
Wind (onshore)	70.3	20.60	86.6	25.38
Wind (offshore)	193.4	56.68	221.5	64.92

^aData were extracted and converted from the U.S. Energy Information Administration⁶

^bLevelised capital cost is the price that the generating asset must receive over its lifetime to break even

Within the next fifteen years, many coal-fired power plants will likely be retired, and if these power stations are replaced with gas-fired power plants, overall emissions can be reduced by up to 50% per unit of energy produced as depicted in Table 2.

1.1.2 Importance of Liquefied Natural Gas (LNG) for Natural Gas Utilisation

Although natural gas is considered to be the most favoured fossil fuel, it still faces challenges such as transportation to demand sites; mainly due to its gaseous state. The two most common transportation methods are via pipeline or as LNG. An economic analysis (Figure 2) by the Center for Energy Economics in the University of Texas at Austin⁷ shows that transport of natural gas as LNG becomes cheaper compared to offshore pipelines for distances greater than 1130 km (~700 miles) or 3540 km (~2200 miles) for onshore pipelines. A comparison of the fuel properties of natural gas at standard temperature and pressure (STP) and LNG (-162 °C), is shown in Table 3. It can be seen that the liquefaction of natural gas into LNG is ideal as it increase the energy density of the fuel, enabling for more economic long-distance transportation of the fuel. In addition, international trade of natural gas is typically in distances exceeding 3540 km (~2200 miles), further reinforcing the value of transporting natural gas as LNG.

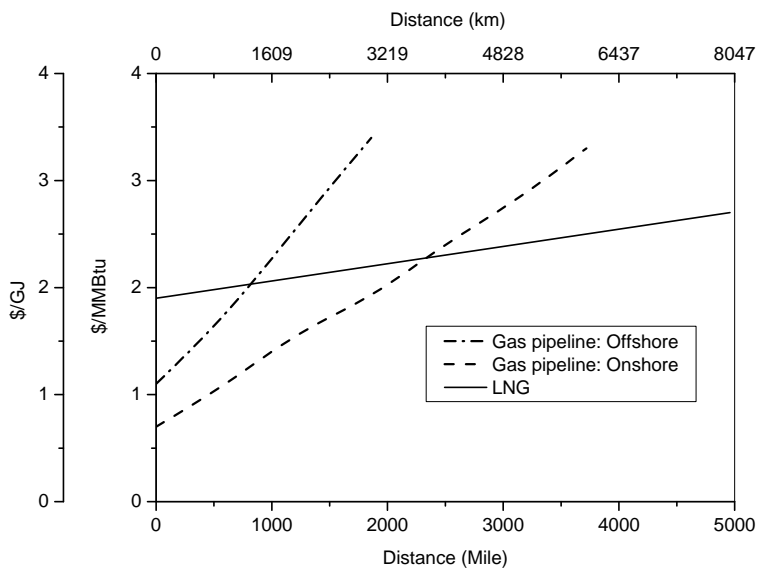


Figure 2: Transport cost of natural gas technologies relative to distance (data extracted from literature,⁷ 1\$/GJ = 1.055\$/MMBtu)

Table 3: Fuel properties of natural gas at standard temperature and pressure (STP)⁸⁻¹¹ compared to those of LNG (-162 °C)^{3, 12-15}

Properties	Natural Gas (S.T.P)	LNG (-162 °C)
Molecular weight (g/mol)	19.5	16.043
Density (kg/m ³)	0.7 – 0.9	422.5
Energy density (MJ/L)	8.5 – 9.5	20.3 – 22.5
Boiling point(°C)	-161	-161
Viscosity (kg/m*s)	1.1 * 10 ⁻⁵	114 * 10 ⁶
Surface tension (N/m)	-	13.36
Specific heat (kJ/kg*K)	2.215	4.186
Thermal conductivity (W/m*K)	0.033	0.2015
Shelf life (days)	-	5 - 7

Table 4: Some key LNG projects worldwide¹⁶⁻²⁴

Project	Country	Capacity (mtpa)	Number of trains	Status
Darwin LNG	Australia	3.7	1	Operating
Brass LNG	Nigeria	10.0	2	Operating
Venezuela LNG	Venezuela	14.1	3	Operating
Trinidad & Tobago	Trinidad	15.7	4	Operating
North West Shelf	Australia	17.1	5	Operation
Arzew	Algeria	17.3	3	Operating
Bontang LNG	Indonesia	22.2	8	Operating
Nigeria LNG	Nigeria	22.2	6	Operating
Qatar gas 1 - 4	Ras Laffan	41.2	7	Operating
Gorgon Project	Australia	15.6	3	Operating
Wheatstone	Australia	25	2	Operating/Expansion - 2017
Gladstone LNG	Australia	7.2	2	Operating
Ichthys LNG	Australia	8.4	2	Under Construction - 2017
Yamal LNG	Yamal	16.5	3	Under Construction - 2018

Therefore the supply chain of LNG has been subject to significant developments in recent years as a result of rising energy production costs, increasing natural gas prices, rising gas import and concerns over increasing requirements on energy security.²⁵ The global LNG trade has grown from 73.62 billion cubic meters (bcm) [2.6 trillion cubic feet (tcf)] in 1990 to 283.17 bcm (10 tcf) in 2010 and is estimated to rise to 566.34 bcm (20 tcf) by 2040.²⁶ Another surge in the LNG trade is expected between 2015 –

2025 as major LNG projects in Australia are completed by 2020; closely followed by completion of projects in North America.²⁶ Table 4 presents some key worldwide LNG projects.

The profitability of LNG value chains have increased significantly,²⁷ due to technological advances and resulted in a reduction in cost of LNG value chains by 30 – 50% between 1980s and 2003.^{28, 29} The average cost breakdown for an LNG value chain is ~21% for upstream exploration and production, ~40% for liquefaction plant, ~20% for shipping facilities and ~18% for storage and regasification terminals.^{4, 30} Fixed values are dependent on different factors including trade volume, transportation distance and technology employed. The typical investment for an 8 mtpa LNG process is shown in Table 5. The upstream gas prices depend mainly on the reservoir while liquefaction costs depend on feed gas composition and liquefaction technologies in use. The shipping cost are based on the distance between seller and buyer while regasification prices are dependent on construction cost, regasification technologies and storage capacity in use.²⁹

Table 5: LNG value chain costs for a typical 8 mtpa process^{29, 31}

	Upstream	Liquefaction	Shipping	Regasification	Total
Gas use	Nil	10 – 14%	1.5 – 3.5%	1 – 2%	12.5 – 19.5%
Capital expenditure (billion dollars)	\$2 – 6	\$6 – 10	\$1 – 2.5	\$1 – 1.5	\$10 – 20
Miscellaneous (operating cost, maintenance cost etc.)	-	5% - 7% of capital cost	-	3% - 4% of capital cost	-
Unit cost per GJ (\$/MMBtu)	\$0.95 – 2.84 (\$1 – 3)	\$2.84 – 4.27 (\$3 – 4.5)	\$0.76 – 1.42 (\$0.8 – 1.5)	\$0.38 – 0.76 (\$0.4 – 0.8)	\$4.93 – 9.29 (\$5.2 – 9.8)

1.1.3 Life Cycle Performance of Natural Gas and LNG

The life cycle performance of coal (underground and surface mining),^{6, 32, 33} natural gas (conventional and shale gas),^{6, 32-34} oil (crude and oil sands)³²⁻³⁴ and biofuel^{6, 33-35}

energy systems for a period of 20 years is presented in Table 6. It can be seen that, of the total greenhouse gas (GHG) emissions in the life cycle assessment (LCA) of the energy systems, approximately 91, 95 and 79% for coal, oil and natural gas respectively are released during downstream combustion. Additionally, on average, emission during fuel production is 3% lower for oil and 21% higher for coal compared to natural gas. This is mainly due to the high emissions during the fuel combustion stages in coal system. It has also been noted that biofuels can be produced from numerous sources as a result, deriving an average emission comparison to that of fossil fuels is quite challenging.

Table 6: LCA of different energy sectors for a 20-year^a period^{6,32-35}

	Coal	Natural Gas	Oil	Biofuels
Fuel Produced ^b (g CO _{2eq} /MJ)	110 – 130	90 – 101	97 – 116	68 – 131
Electricity Produced ^b (g CO _{2eq} /kWh)	675 – 1,689	290 – 930	510 – 1,170	18 – 360
Transport ^b (g CO _{2eq} /km)	-	155 – 185	185 – 220	15 – 195
Total system levelised cost (\$/MWh)	100.1 – 135.5	65.6 – 130.3	-	111.0

^aThe 20 year period was chosen due to the global warming potential of the specified fuel sources within that time frame.

^bThe green-house gas emission is a summation of possible green-house gases released during the development of the infrastructure, during production/procurement of fuel and during the combustion of the fuel.

A similar trend is observed in the electricity production analysis, in which coal and oil on average produce more emissions than natural gas; biofuels had the least emissions compared to fossil fuels. It is important to note that the electricity production analysis for biofuels (Table 6) did not consider the carbon emissions from land use, and most biomass studies do not include the CO₂ emission from biomass plants with the assumption that CO₂ emission is equal to the CO₂ absorbed during the growth stages of the biomass plants.³³ Because the main area of biofuels is in transportation, biofuels have a low GHG emission per kilometre travelled in a passenger car, closely followed by natural gas, and then oil with the highest GHG emissions. Overall, the LCA in Table 6 shows that natural gas on average produces low GHG emissions for fuel

production, electricity production and transport use and costs less as a system compared to other fossil fuels; making it a very strong competitor in the world energy market. Even though biofuels have low GHG emissions compared to fossil fuels, the biofuels sector is still in its early stages and still has a long way to go to, before it can start making large contributions to the world energy market.

In comparison to pipeline gas, LNG results in ~50% increase of GHG emissions as results of additional liquefaction and tanker transportation, according to the LCA by Jaramillo et al.³⁶ presented in Table 7. It is important to note that emission due to leakages from pipeline transport method was neglected. To compensate for the increased emission due to LNG transportation; LNG value chain technologies have demonstrated increased energy efficiency ranging from 60 to 90%.^{31, 37}

Table 7: LCA of LNG vs. pipeline transport^a

Stages of life cycle	Emission intensity (g CO _{2eq} /kWh)	
	LNG	Pipeline (Natural gas)
Fuel Production	109	109
Liquefaction	68	N/A
Transport	27	N/A
Regasification	5	N/A

^aData were extracted from the study by Jaraillo et al.³⁶

1.2 Scope and Objectives

As natural gas demands continue to rise, it is crucial that risks in handling, storage and transportation of LNG are well understood. This thesis is therefore aimed at investigating, via means of mathematical modelling, LNG dispersion under various conditions. Below is a list of the main objectives of this thesis:

1. By utilising the ANSYS Fluent software, develop a CFD code for modelling LNG spill, pool formation and dispersion;
2. Investigate the effect of obstacles on the dispersion process of LNG vapour clouds;
3. To study the effect of sea surface and air temperatures on LNG spill, pool formation and dispersion;

4. To investigate the stability effect of sea and atmospheric dynamics on the dispersion process of LNG, following a spill and implications to Australian LNG transport.

1.3 Thesis Outline

This thesis is composed of a total of nine chapters (including this chapter); below is a brief summary of content covered in each chapter with a thesis map (Figure 3) to further illustrate the structure of the document.

- Chapter 1 contains the background, motives and objectives of this thesis.
- Chapter 2 reviews the LNG value chain, from production, liquefaction, storage, transportation and regasification; from which, the most likely source of hazards are identified and further discussed. Recent advances in the LNG production, spills, dispersion and safety are also gathered; from which research gaps are identified and forms the basis of this thesis.
- Chapter 3 summarises the methodology of the study from geometry creation, setting up the simulation to analysing the results.
- Chapter 4 summarises the main codes used to develop the direct CFD simulation method and simulation setup procedure. The results and discussion of the newly developed direct CFD simulation method benchmarked against experimental data and compared to conventional modelling methods is the presented. Finally the effect of impoundment on controlling LNG spill and vapour cloud dispersion is investigated.
- Chapter 5 validation of the newly developed direct CFD simulation method benchmarked against further experimental data is the presented. Followed by investigation on the effect of sea surface and air temperatures on LNG spill, pool formation and vapour cloud dispersion.
- Chapter 6 reports the effect of sea and atmospheric stability on LNG spill, pool formation and vapour cloud dispersion; followed by implications to Australian LNG transport.
- Chapter 7 concludes this thesis with the major findings and future work.

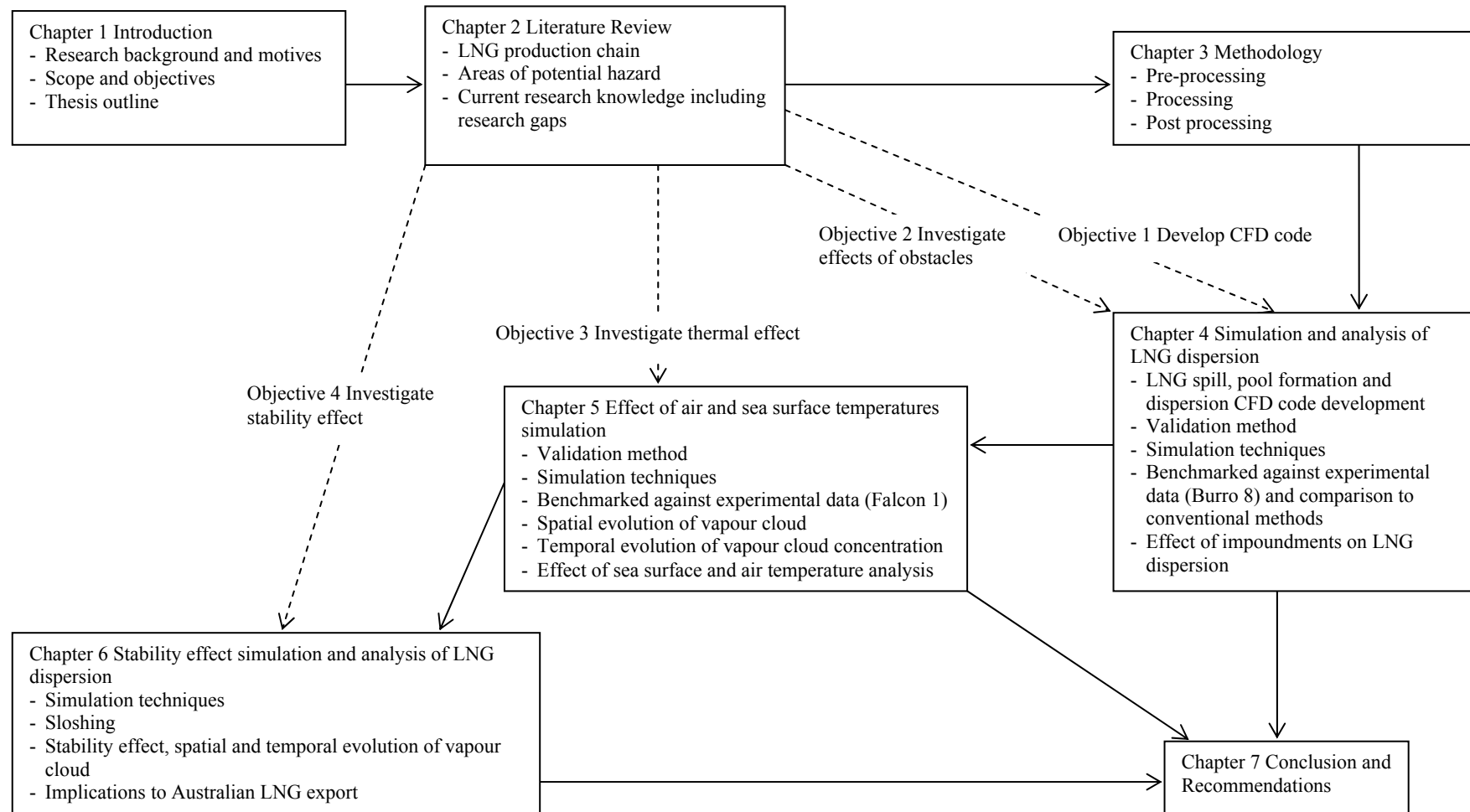


Figure 3: Thesis Map

2 LITERATURE REVIEW

2.1 Introduction

Considerable recent research has been conducted in developing efficient LNG value chains and managing the associated risks such as those in handling, storage and transportation of LNG. This has been largely driven by the increases in production and use of LNG, potential terrorist threats and public confidence in LNG safety.

The potential hazards include cryogenic tissue damage and embrittlement of material. Such hazards can be potentially caused by various physical and chemical interactions with LNG via direct contact, pressure from rapid phase transitions (RPT), asphyxiation, LNG pool fires, LNG vapour cloud fires, deflagration and detonations. Upon an LNG spill, an LNG pool forms on the substrate and vaporizes quickly to form a vapour cloud due to local mixing and heat transfer. Ignition of the LNG pool (LNG pool fire), or the LNG vapour cloud (vapour cloud fire) both affect the vaporization/dispersion process and causes thermal hazards.

Table 8 contains a summary of the recent reviews in literature on different aspects of the LNG value chain. From Table 8 it can be seen that the existing reviews relating to LNG production and events following an LNG spill were all done up to 2006. Therefore this literature review focuses on some of the recent research advances in LNG production, spill, dispersion and safety from 2007, although the classic earlier literature will also be covered in order to maintain a smooth connection to prior knowledge in a logical flow.

Table 8: Published review papers regarding different aspects of the LNG value chain

Reference	Literature covered	Years covered	Aspects covered
Wood ²⁵	Outlook of the global LNG trade	Up to 2012	Current status and future growth of global LNG
Lim et al ⁴	LNG plant designs	Up to 2012	Available LNG plant designs and implemented designs and their optimisations in practice based on costs.
Luketa-Hanlin ³⁸	Studies on large-scale LNG spills	Up to 2006	Behaviour of LNG spill including combustion and development of predictive models, concluding that experiments in order of 100 m ² are required.
Cleaver et al ³⁹	Summary of experimental data on LNG safety	Up to 2006	Behaviour of LNG spill, combustion and modelling issues, concluding that more experimental studies of RPT are required.
Koopman et al ⁴⁰	LNG safety research	Up to 2006	Behaviour of LNG from research performed by Lawrence Livermore National Laboratory; including dispersion model development.
Raj ⁴¹	LNG fires	Up to 2006	Some LNG fire experiments on land and water from 1970s to 1980s are reviewed, including fire hazard prediction models.
Havens and Spicer ⁴²	Problems with the United States LNG siting regulations	Up to 2006	Problems with determining and specifying exclusion zones for LNG spills.

2.2 LNG Production Chain

An LNG value chain transforms the raw natural gas into LNG as a carrier product for transport and distribution to end users. It consists of four main stages including upstream gas production and gathering, liquefaction, shipping and regasification. Below is a brief overview of these four stages including some recent research and development in these aspects.

2.2.1 Upstream Gas Production and Gathering

Fossil fuels are formed as the remains of plants, animals and microorganisms are compressed underneath the earth, under high pressures and temperatures for long periods of time. Based on the geological conditions, the carbon bonds in the organic matter are broken down to form natural gas, oil or coal, with more oil formed at lower temperatures but more natural gas formed at higher temperatures.⁴³ Natural gas is normally trapped under ground in a reservoir (conventional gas), by sedimentary rock (shale gas) and at times, interacts and is absorbed by coal (coal seam gas).⁴⁴ Natural gas can be found onshore or offshore, as associated gas or non-associated gas.²⁹ The non-associated gas can be dry, meaning that it is composed of mostly methane or it could be wet, containing hydrocarbons, such as butane, propane and other condensates. On the other hand, the additional expense of gathering associated gas is not deemed appropriate and as a result it is flared.²⁹ The typical composition of natural gas is listed in Table 9; the data was obtained from a sample taken from Qatar's North Field.⁴⁵

All forms of natural gas need to be treated to remove impurities (e.g. carbon dioxide, nitrogen, mercury and hydrogen sulphide) and/or heavier hydrocarbons (e.g. propane and butane), prior to the gas being sent to the liquefaction plant. The pre-treatment may consist of three main stages: acid removal, dehydration and mercury removal (Figure 4).⁴⁶ Impurities in the gas stream are referred to as acid gas; and can be removed by using an amine solvent mixed with water.⁴⁷ If significant hydrogen sulphide is present in the acid gas, then a separate stream is required for sulphur recovery.²⁹ Gas leaving the acid removal system is generally saturated and as a result is passed through a dehydration system.

Table 9: Typical composition of natural gas compared to LNG.⁴⁵

Component, mol %	Natural Gas	LNG
H ₂ S	0.96	-
CO ₂	2.45	-
N ₂	3.97	0.00 – 1.00
CH ₄	82.62	84.55 – 96.38
C ₂ H ₆	4.84	2.00 – 11.41
C ₃ H ₈	1.78	0.35 – 3.21
i-C ₄ H ₁₀	0.39	0.00 – 0.70
n-C ₄ H ₁₀	0.67	0.00 – 1.30
i-C ₅ H ₁₂	0.29	0.00 – 0.02
n-C ₅ H ₁₂	0.27	0.00 – 0.04
n-C ₆ H ₁₄	0.34	-
Others	1.42	-
Total	100.00	100.00

This is to prevent freezing when the gas reaches the liquefaction exchanger and is achieved by first cooling the gas with water, air or a refrigerant and then passing it through a molecular sized sieve.⁷ The final stage of gas pre-treatment is mercury removal; as mercury can corrode aluminium and since most of the components in the heat exchange is made from aluminium, it is crucial that this process is carried out.⁴⁷ Mercury removal is achieved by passing the feed gas through a sulphur-impregnated carbon bed, during which the mercury becomes non-volatile mercury sulphide.⁴⁷ From here the natural gas is sent to the liquefaction plant.

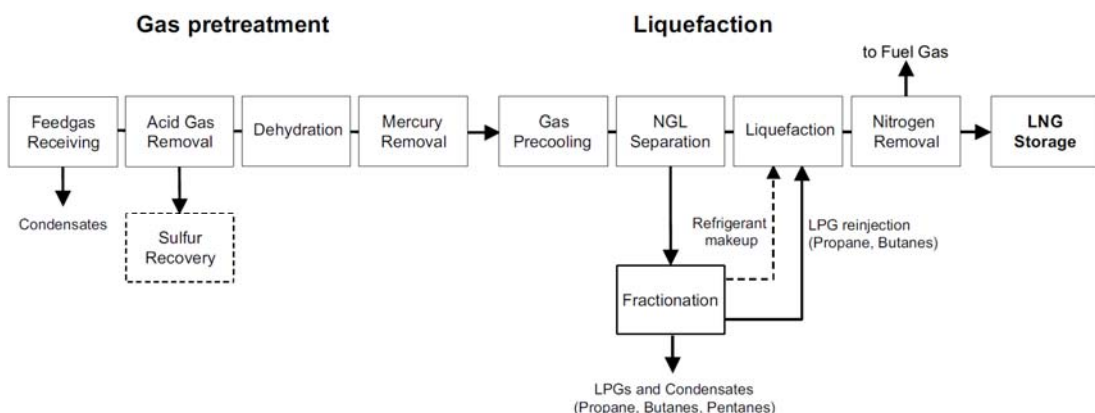


Figure 4: Natural gas pre-treatment and liquefaction diagram (adapted from the literature⁴⁶)

2.2.2 Liquefaction and Storage

Natural gas leaving the production facility is piped to a liquefaction plant, which can be located onshore or offshore (to date most have been located onshore) and may have a number of parallel systems (called trains) of heat exchanges and gas or steam turbines driving the compressor.²⁹ The natural gas is liquefied into LNG via cooling it to 112K,⁴⁸ reducing the volume of natural gas by a factor of 600. The LNG product is then stored in double-walled insulated tanks designed to maintain the low temperatures of the LNG. These storage tanks contain an inner cryogenic nickel/steel tank, surrounded by a layer of insulation and then followed by a prestressed concrete or mild steel outer tank (when mild steel is used a berm is constructed to contain the LNG in the case of a spill).²⁹

The rising demand of LNG has led to the development of gravity-based structures (GBS) and floating LNG (FLNG) terminals aimed at exploiting offshore natural gas reservoirs that are either too remote and/or not economically viable for onshore liquefaction facilities.⁴⁹ The GBS is an artificial island, intended for shallow waters where LNG production and storage will take place, such as the Adriatic LNG terminal.⁵⁰ Unlike the GBS, the FLNG is a floating, mobile system. The idea is that the structure will be constructed onshore and then sank to the seafloor at the desired location, such as Prelude FLNG. This technology has been applied to multiple oil and production facilities.⁴⁹ However, such LNG facilities also suffer from some undesired disadvantages, including large footprints, large construction costs, constant upgrading for existing onshore facilities, only applicable to a small range of water depths and potential safety risks (requiring a safe mechanism for LNG transfer to LNG tankers).²⁹

Various liquefaction processes have been developed by different companies as reviewed in a recent publication⁴ and also summarised in Table 10 and Table 11.⁵¹⁻⁷² The fundamental principles of these process can be found in other related publications by Barron,⁷³ Walker,⁷⁴ or Timmerhaus and Flynn.⁷⁵ As can be seen in Table 10 and Table 11, these processes have different single train capacity and efficiency (relative to cascade or C3MR) and deploy a range of refrigerants and heat exchanges for precooling, liquefaction and/or subcooling. The efficiency values

presented in Table 10 were reported in different studies, with each study claiming that a different process was the most efficient.

Table 10: Commonly used LNG liquefaction processes^a

Process	Developer(s)	Single train capacity (MTPA)	Efficiency relative to cascade	Efficiency relative to C3MR
Phillips' Optimized Cascade (POC)	ConocoPhillips	4 – 9	1.00	1.16
PRICO	Black and Veatch Pritchard	0.1 – 2.1	1.25	1.19
APCI Propane Precooled Mixed Refrigerant (C3MR)	APCI	0.5 – 6.1	1.15	1.00
Shell and APCI Dual Mixed Refrigerants (DMR)	Shell and APCI	0.5 – 8.4	N/A	1.03
IFP/Axens Liquefin	IFP/Axens	N/A	N/A	N/A
Parallel Mixed Refrigerant (PMR)	Shell	6 – 9	N/A	N/A
Gaz de France Integral Incorporated Cascade (CII)	Gaz de France	N/A	N/A	N/A
APCI AP-X	APCI	5.8 – 9	N/A	N/A
Statoil-Linde Mixed Fluid Cascade (MFC)	Linde in collaboration with Statoil	4 – 6.6	N/A	N/A

^aData were extracted from the study by Lim et al.⁴ that was based on the literature.⁵¹⁻⁷²

In addition, after liquefaction, LNG is stored in storage tanks at some point in the production chain, before being transferred to the LNG tankers for transportation. Compared to several conventional LNG storage models, a recent model⁹⁴ based on normal equations applied to non-linear parameter estimation has significantly improved the modelling accuracy for safe and economic managing of LNG storage sites (prevent stratification and rollover of LNG). The model also converges faster to a heat and mass transfer coefficient and can be used with level-temperature-density profiles (which can easily be obtained from gauges on the storage tanks) to obtain the required results.⁹⁴

Table 11: Comparison of refrigeration cycle configurations^a

Process	Refrigerant			Heat exchanger		
	(P)	(L)	(S)	(P)	(L)	(S)
POC	Propane	Ethylene	Methane	Plate fin heat exchanger (PFHE) or core-in-kettle	PFHE	PFHE
PRICO	MR	-	-	Cold box (PFHEs)	-	-
C3MR	Propane	MR	-	Core-in-kettle	CWHE	-
DMR	MR	MR	-	Coil-wound heat exchanger (CWHE)	CWHE	-
Liquefin	MR	MR	-	PFHE	PFHE	-
PMR	Propane or MR	Parallel MR	-	-	-	-
CII	MR	-	-	Heat-exchanger line (two PFHEs)	-	-
AP-X	Propane	MR	Nitrogen gas	Core-in-kettle	CWHE	CWHE and PFHE
MFC	MR	MR	MR	PFHE	CWHE	CWHE

^aData were extracted from the study Lim et al.⁴ that was based on the literature.⁵¹⁻⁷²

(P) = Precooling, (L) = Liquefaction, (S) = Subcooling

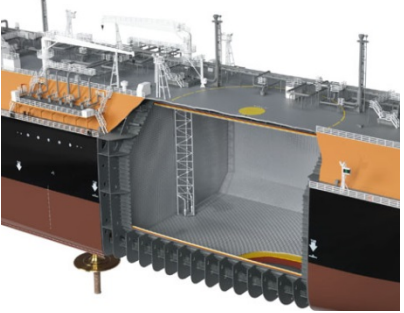
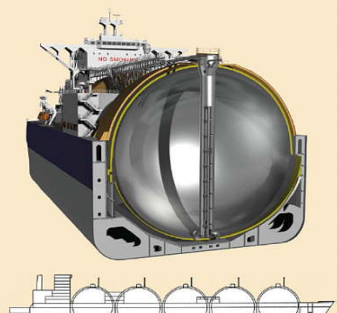
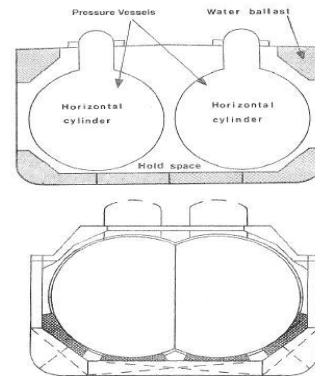
2.2.3 Shipping

After liquefaction and storage, the LNG is then loaded into ships for the long-distance transportation to the desired locations. The LNG ships (LNG tankers) are designed with double hulls for structural integrity, which also provides space for

ballast water to be stored, considering the light weight of the cargo. The cargo tanks are not part of the ship structure and are installed separately into the ship's holds.

Four main types of LNG tankers have been developed since the late 1960s; Table 12 lists the features and characteristics of these LNG tankers.⁹⁵⁻⁹⁸ The membrane type ships, one of the most common LNG tankers, ranging in size from 145,000 – 265,000 m³, utilize fully integrated rectangular tanks with reinforced polyurethane or plywood/perlite insulation.⁹⁶ Its close competitor, the moss type ships, range in size from 138,000 – 255,000 m³, are designed with spherical tanks, independent of the hull structure and utilise polyurethane insulation.⁹⁶ The preference for the membrane tankers, is mostly because of its capacity efficiency (use of the hull shape), with little to no void space between the storage tanks and the ballast tanks.²⁹ This makes a moss tanker of similar capacity as the membrane tanker, more expensive. The moss tanker however does have a higher resistance to sloshing and will most likely be considered for future offshore storage; especially in areas of bad weather. Next is the IHI SPB type ships that also use rectangular tanks with polyurethane insulation; however, unlike the membrane type tanks, the IHI SPB does not rely on the ship's hull for structural support.⁹⁷ The IHI SPB ships are also resistant to sloshing (due to its baffle technology) but its expensive design and small capacity (87,500 m³) compared to that of the Membrane or the Moss systems explains why only two ships are currently in-service. The last type is the Type C (cylindrical) system. The cylindrical shape of the Type C ships allows it to resist sloshing, while utilising polystyrene for insulation. These ships were designed specifically for cases where small cargo transportation is required (2,500 – 30,000 m³).⁹⁶

Table 12: A summary of various cargo containing systems for LNG⁹⁵⁻⁹⁸

Type	Membrane	Moss	IHI SPB	Cylindrical
Appearance	 Source: BG Group	 Source: LNG World Shipping	 Source: FLEX LNG	 Source: TGE Marine
Classification	Integrated tanks	Independent tanks (Type B)	Independent tanks (Type B)	Independent tanks (Type C)
Types	<ul style="list-style-type: none"> • GTT No. 96 • GTT Mark III • GTT CS1 • Membrane double row 	-	-	<ul style="list-style-type: none"> • Cylindrical design • Bilobe design
Designed vapour pressure	Less than 70 kPa	Less than 70 kPa	Less than 70 kPa	Greater than 200 kPa
Capacity	145,000 – 265,000 m ³ (4 – 5 cargo holds)	138,000 – 255,000 m ³ (4 – 5 cargo holds)	87,500 m ³ (4 cargo holds)	2,500 – 30,000 m ³ (2 – 4 cargo holds)

Self-supporting tanks	No (Reacts with hull structure)	Yes (Independent of hull structure)	Yes (Independent of hull structure)	Yes (Independent of hull structure)
Tank material	<ul style="list-style-type: none"> • 36% nickel steel (Invar) • Stainless steel 	Aluminium alloy of 9% nickel steel	Aluminium alloy of 9% nickel steel	<ul style="list-style-type: none"> • Aluminium alloy of 9% nickel steel • Stainless steel
Insulation properties	<ul style="list-style-type: none"> • 530 mm insulation plywood boxes filled with perlite • 250 - 270 mm reinforced polyurethane foam 	220 mm polyurethane foam	Polyurethane foam	300 mm polystyrene panels
Secondary barrier	Full secondary barrier	Partial secondary barrier	Partial secondary barrier	No secondary barrier
Ability of partial filling	Tanks are to operate at below 10% or above 80% of tank depth; to reduce sloshing	No limits as spherical tank shape prevent sloshing	No limits as centreline bulkhead prevents sloshing	No limits as tank shape prevent sloshing
Deck space	Flat deck space with chamfer	Very limited deck space	Plenty of deck space	Plenty of deck space
Maintenance on site	Poor accessibility to tanks and requires staging	-	Excellent accessibility to tanks	-
Ships in serves	~ 230 ships	~ 100 ships	2 ships in service	-

During transportation of the LNG, boil-off occurs daily (approximately 0.15% of the cargo²⁹). Since current LNG tankers are not constructed with on-board regasification facilities, the boil-off gas is captured and used as fuel to assist in propelling the tankers. Once at the import terminal, the LNG is unloaded, leaving behind a small amount of LNG, the heel, to keep the tanks cool in the ballast voyage.²⁹ To date there has been no LNG cargo lost or spilled during the shipping phase, and it is believed that with acceptable maintenance the LNG vessels can have a working life of 40 years or more.²⁹

2.2.4 Regasification Terminals

The LNG value chain ends at the regasification terminals. At each unloading berth, several unloading arms are employed for transferring LNG from the LNG tankers to the storage tanks. The main purpose of the storage tanks are to hold the LNG until it is ready to be vaporized for use as fuel. The storage tanks at the regasification terminals are exactly the same as those at the liquefaction plant.²⁹

The LNG is then passed through vaporizers, which warm the LNG to or above 5°C (41°F) by utilising either seawater, air, natural gas or an external heat source and consumes a significant amount of electrical energy. By utilising a new combined power cycle, that incorporates a gas turbine and an ammonia cycle with one pressure step, the efficiency can be improved from 44% up to 46%, while decreasing capital cost.⁹⁹ Boil-off also occurs in the storage tanks at the regasification terminal at a rate of 0.05% of tank volume per day or less. In order to decrease boil-off gas (BOG) it is believed that the number of stages (compression and reliquefaction) in the regasification system should be increased; because an increase in the number of stages leads to a decrease in BOG flow rate.¹⁰⁰ Although this will reduce the operation cost, it will also increase the total capital cost; therefore an optimum number of stages will need to be determined (via optimization using models, e.g. that developed by Liu et al.¹⁰⁰).

Cold is also an important energy source that is available during regasification. Innovative technologies such as a novel co-generation concept have been proposed to recover exergy from LNG for the generation of power (with overall system

efficiency of 52%).^{101, 102} There is potential for this novel co-generation concept to be improved by focusing on the gas-turbine power system, in order to improve efficiency, reduce environmental impact and improve cost.¹⁰³ Other innovative technologies utilising cold energy, consider the use of helium (49% efficiency),^{104, 105} ammonia-water mixture (48% efficiency),¹⁰⁶ and a combination of tetrafluoromethane and propane (23.5% efficiency)¹⁰⁷ as a working fluid, with some plants even able to achieve near-zero CO₂ emission.¹⁰⁸ The feasibility of using cold energy from LNG regasification in other industries such as deep freezing agro food industries, air conditioning facilities in supermarkets and hypermarkets has also been demonstrated in numerous literatures; with carbon dioxide as the preferred fluid for transferring the cold energy.¹⁰⁹⁻¹¹²

After LNG regasification and prior to any natural gas leaving the regasification terminal, it is metered, during which quality and pressure is regulated to meet customer requirements; at times the natural gas is also odorized in order to improve the chances of locating leaks in transportation systems or customer appliances, if there were to occur.²⁹

2.2.5 LNG Value Chain Potential Hazards

During the LNG process, some simple features/events can lead to a series of catastrophic event; with the most common been a LNG spill. Figure 5 below shows the likely series of even that can occur following an LNG spill. The factors and parameters that influence and control the spread of these events are not fully understood. These events can be categorised into three main sections: a) pool formation – understanding is needed on the key factors that affect the pool spreading, pool boiling, and the occurrence of rapid phase transitions; b) vapour dispersion – understanding is needed on what effect wind and obstacles have on the dispersion processes of the vapour cloud; and are there other governing factors; and c) combustion – understanding is needed on the characteristics of (and the key factors influence) the pool fire and vapour cloud fire formation and spread, how do the two different fires compare to each other. These types of questions have led to the use of experimentation and mathematical modelling to study LNG spills, with the aim of improving knowledge and further understanding the likely case of events following

an LNG spill and how it can be prevented and/or managed. Such knowledge and understanding are essential to maintaining and managing the safety of LNG.

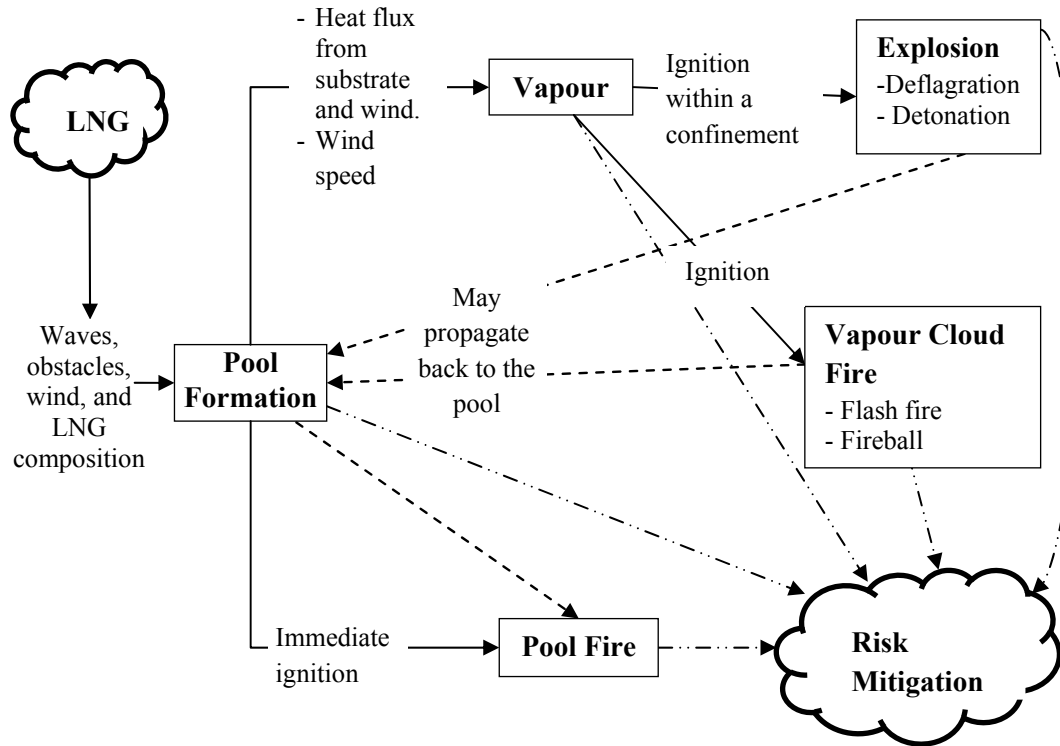


Figure 5: LNG spill events.

2.3 LNG Spill, Vapour Production, Dispersion and Combustion

From the early 1970s, lab and field scale experimental studies of LNG vapour production, dispersion and combustion have been conducted.³⁹ These studies were conducted with the aim of collecting data, that can later be used for benchmarking and the validation of computer models.^{113, 114} Extensive measurements were conducted considering various parameters including meteorological parameters (e.g. temperature, humidity, wind speed, turbulence, solar heat flux etc) and gas parameters (e.g. temperature, concentration and ground heat flux etc).³⁹ LNG spills on land or water can range from all sizes and at times the anticipated spill size or conditions cannot be replicated experimentally. This has prompted the use of mathematical models in order to simulate, study and understand the characteristics of an LNG spill leading to vapour production, dispersion and/or combustion. These mathematical models need to be validated, with existing experimental studies, to be confident in using them for further studies.

2.3.1 Pool Formation

Upon spilling on water, LNG spreads and boils due to the large temperature difference between the LNG, water surface and surroundings. Spills on confined, calm water can behaviour similarly to spills on land, due to the formation of ice which results in a decrease in evaporation rate over time. Vaporization rate is also important in that it influences the distance to the low flammability limit (LFL) and the burn rate of pool fires. Therefore, vaporization rate, including the size and shape of the LNG pool are key parameters influencing LNG pool formation.³⁸

2.3.1.1 LNG Spread on Water

In the literature, most of the experiments concerning LNG spreading on water were conducted prior to 2007. Those experiments were on small scales (with spill volume of approximately 3 m³ and less) and application of such experimental results to large-scale spills (with volumes of approximately 8 m³ and greater), are known to have technical uncertainties in terms of the dynamics of the front of the spreading pool and the heat transfer rate.³⁸ While efforts were made to deploy models for simulating bubble formation at large scales based on small-scale experimental data, the effect of waves and ice formation can introduce some more uncertainties in such prediction.³⁹ Therefore, large-scale experiments are certainly still in need.

2.3.1.2 Pool Boiling

Pool boiling occurs when LNG is spilled on water through three stages; namely, the nucleate boiling, transition boiling and film boiling. To date, research and development (R&D), on pool boiling of LNG leads to several major conclusions:^{38, 115} a) evaporation is a function of the molecular weight of the material (starting from the lowest); b) boiling does not take place at a constant temperature; c) the vaporization rate of LNG is very different from that of pure methane, the addition of ethane or propane results in a more rapid vaporization and increased boil-off rates by a factor of 1.5 – 2; and d) evaporation during the spill phase is also an important consideration as it may contribute to up to 20% of the overall evaporation.

2.3.1.3 RPTs

Rapid phase transitions (RPTs) are physical or mechanical expansions in which high-pressure energy is released and can occur when cold LNG comes into contact with water. RPTs occur primarily during experiments at laboratory scale.³⁸ The only large scale RPTs observed were during the Coyote test series, in which 6 of 13 spills

carried out resulted in RPTs. To date, R&D on this aspects has led to the following observations:³⁸⁻⁴⁰ a) RPTs at large scale behave differently to those small-scale counterparts; b) occurrence is significantly influenced by water temperature and depth of penetration; c) the strength of RPTs correlates with spill rate and d) RPTs can lead to an increase in the distance, to the LFL by up to 65%. Several theoretical models exist for studying RPTs, such as the superheat theory, the predictive empirical model and the CFD model.^{38, 39}

2.3.1.4 Modelling

Recent studies on LNG pools have focused more on modelling of the pool formation process rather than on experimental work. The numerical models used are mainly classified into two categories: the integral model or the Navier-Stokes model. There are numerous models for studying LNG pool formation, including Raj and Kalenkar,¹¹⁶ Opschoor,¹¹⁷ SOURCE 5,^{42, 118-120} GASP,^{121, 122} SafeSite3G,^{123, 124} PHAST,¹²⁵⁻¹²⁹ ALOHA,¹³⁰⁻¹³² ABS Consulting model,¹² LNGMAP^{12, 133, 134} and FLACS.^{135, 136} Of these models, the most commonly used are presented in Table 13.

The simpler of the two methods is the integral models which originated in 1980s. These models utilise algebraic equations to obtain solutions and are usually limited to modelling of circular pools, flat substrates and heat transfer only from the substrates. Table 13 contains some commonly used integral models for pool formation modelling. The LNGMAP^{12, 133, 134} is the most robust due to its ability to effectively incorporate real-time geographic information such as wind effects, current effect, atmospheric conditions etc., into the model.¹³³ PHAST,¹²⁵⁻¹²⁹ is an older model than LNGMAP^{12, 133, 134} and seems to be more widely used and will most likely continue to be, due to its ability to model spills both on land and water. PHAST,¹²⁵⁻¹²⁹ is also more superior to SOURCE 5^{42, 118-120} and GASP,^{121, 122} models due to its ability to account for non-circular LNG pool formation and inclusion of heat convection/radiation from sources other than the substrate. Navier-Stokes models are more complex and the most complete models. Modelling pool formation with Navier-Stokes models can be time consuming due to their complexity. As a result, researchers prefer to model pool formation with integral models and then transfer the data over to Navier-Stokes models for further analysis.¹¹⁸ A more in-depth description of the Navier-Stokes models is given in Section 2.3.2.4.

The current pool spread models (e.g the standard model of inertial-gravity spreading) are based on oil pools spreading, however it is important to note that oil and LNG behave differently.¹³⁷ This standard model is applicable for rapidly formed pools; to account for this, many assume that the spill of LNG from a tanker is due to quasi-steady gravity flow.¹³⁷ The pressure field is also assumed to be hydrostatic, which is not the case in the pool front. The spread of a LNG pool is treated as inviscid by the standard model; which is a reasonable assumption due to the occurrence of the Liedenfrost effect. Fay¹³⁷ carried out studies in which the properties of LNG spills were examined to suggest that a different model should be used and to compare the differences that would ensue from the use of an alternative model.

An alternative model, characterised by an asymptotic spreading law, called the supercritical model was also developed.¹³⁷ due to questions arising, based on the density ratio between the spill substances and the sea, the effects of the pool leading edge and the initial, and spill conditions. When the maximum radius and evaporation time of the supercritical model was compared to the standard model, a ratio (super to standard) of 2.51 was obtained for the maximum radius and 0.159 for the evaporation time.¹³⁷ Based on this, a supercritical model would result in a larger maximum radius and shorter evaporation time than the standard model. These findings were also verified by a Chian Lake experiment in which the supercritical model had a better fit to experimental data.

Table 13: Some well-known pool formation models for LNG pool modelling

Model	<i>LNG pool formation models</i>			
	SOURCES ^{42, 118-120}	GASP ^{121, 122}	PHAST ¹²⁵⁻¹²⁹	LNGMAP ^{12, 133, 134}
	Integral model	Integral model	Integral model	Integral model
Principles	<ul style="list-style-type: none"> Initiated in 1980s and simulates instantaneous or continues releases, pool formation and evaporation. 	<ul style="list-style-type: none"> Initiated in 1980s and simulates instantaneous or continues releases of a circular pool and vaporisation rate. 	<ul style="list-style-type: none"> Initiated in 2002 and simulates discharge, pool formation, evaporation, dense gas dispersion and fires. 	<ul style="list-style-type: none"> Initiated in 2005 and simulates instantaneous or continues releases of a circular pool, vaporisation rate and fires for marine spills.
Method	<ul style="list-style-type: none"> Algebraic equations, and in some cases are solutions of ordinary differential equations. Models bulk quantities as a function of time. 	<ul style="list-style-type: none"> Algebraic equations, and in some cases are solutions of ordinary differential equations. Models bulk quantities as a function of time. 	<ul style="list-style-type: none"> Algebraic equations, and in some cases are solutions of ordinary differential equations. Pseudo-component approach for mixtures. 	<ul style="list-style-type: none"> Discrete set of linked algorithms and a particle based approach. Fully-integrated geographic information system.
Accuracy	-	-	-	<ul style="list-style-type: none"> Can range from 1% – 38%, however no large scale experiments are available to be used for validation.
Validations	<ul style="list-style-type: none"> Unclear, although it might have been validated in the process of validating DEGADIS. 	<ul style="list-style-type: none"> Some validations were conducted during the development of the program but most was not published. 	<ul style="list-style-type: none"> Wind tunnel experiments. Kit Fox. Numerous field experiments. 	<ul style="list-style-type: none"> ABS Consulting and Sandia numerical simulation cases.

Advantages	<ul style="list-style-type: none"> • Output from SOURCE5 can be used as input to the DEGADIS dispersion code. • Can model LNG spreading on land, confinement by a simple shape bund/dike, instantaneous or continuous releases, drainage and permeable ground. • Can also model LNG spread on water for both instantaneous and continuous releases. • Accounts for heat conduction from substrate. 	<ul style="list-style-type: none"> • Can account for spills on land and water. • Can model LNG spreading on land, confinement by a simple shape bund/dike, instantaneous or continuous releases. • Accounts for smooth and rough ground. • Heat transfer from the sun, substrate and air are all included. 	<ul style="list-style-type: none"> • Can account for spills on land or water surfaces. • Accounts for instantaneous and continuous releases. • Effects of bund walls. • Can model heat conduction from the substrate, convection from the air and radiation. 	<ul style="list-style-type: none"> • Can model pool spreading, transport on water, evaporation from water and the transport in the atmosphere; either constant or time dependent. • Accounts for thermal effects of conduction and radiation.
Disadvantages	<ul style="list-style-type: none"> • Cannot model a rough or sloping ground. • Cannot model non-circular pools, channelled flows, or confinement by arbitrary shaped dikes. • Heat transfer from the sun, fires and air are all neglected. • Inability to account for mixing with air in a confinement. • Inability to account for expansion of the vapour 	<ul style="list-style-type: none"> • Permeable ground, sloping ground and drainage are not modelled. • Does not account for non-circular pools. • Radiative heat from fire are not included; but can be added as user-defined input. • Does not account for RPTs. 	<ul style="list-style-type: none"> • Cannot model non-flat ground. 	<ul style="list-style-type: none"> • Cannot account for RPTs. • Restricted to marine spills (spills on a water surface).

	volume due to heating above the boiling temperature.			
Scales	<ul style="list-style-type: none"> • Field. • Laboratory. 	<ul style="list-style-type: none"> • Field. 	<ul style="list-style-type: none"> • Field. 	<ul style="list-style-type: none"> • Field.
Applications	<ul style="list-style-type: none"> • LNG hazard assessment. 	<ul style="list-style-type: none"> • LNG Hazard assessment. 	<ul style="list-style-type: none"> • Hazard analysis (power plants, refineries, chemical plants, petrochemical plants, pharmaceutical facilities, oil rigs) 	<ul style="list-style-type: none"> • Hazard analysis (LNG ships and offshore platforms).
Code accessibility	<ul style="list-style-type: none"> • N/A 	<ul style="list-style-type: none"> • N/A 	<ul style="list-style-type: none"> • N/A 	<ul style="list-style-type: none"> • N/A

2.3.2 Vapour Dispersion

In the case of unconfined LNG spills on water, the LNG cloud travels at the wind speed prior to dispersion. Since the vapour forms at the boiling temperature of LNG, it will initially be denser than air. For land-based facilities, dense gas behaviour is advantageous because it can be easily controlled. However, this can also be a disadvantage since it takes longer to disperse. Most of large-scale LNG dispersion tests of spills on water were done prior to 2007, with the key experimental conditions being summarised in Table 14 by Luketa-Hanlin.³⁸ The spill volume, spill rate, vaporization rate, presence of obstacles and the atmospheric conditions are considered to be key parameters in determining the LFL.^{68, 70, 73} The recent research advance in LNG spill has been focusing on vapour dispersion, including experimental studies on the effect of water curtains, underwater releases and turbulence on vapour dispersion and modelling studies on the use and development of models for simulating vapour dispersion.

Table 14: LNG dispersion test on water³⁸

Experiment	Spill volume (m³)	Spill rate (m³/min)	Pool radius (m)	Downwind distance to LFL (m) (max)
ESSO	0.73 – 10.2	18.9	7 – 14	442
Shell	27 – 193	2.7 – 19.3	NA (jettisoned)	2,250 (visual)
Maplin Sands	5 – 20	1.5 – 4	~10	190 ± 20
Avocet (LLNL)	4.2 – 4.52	4	6.82 – 7.22	220
Burro (LLNL)	24 – 39	11.3 – 18.4	~5	420
Coyote (LLNL)	8 – 28	14 – 19	Not reported	310
Falcon (LLNL)	20.6 – 66.4	8.7 – 30.3	Not reported	380

2.3.2.1 Water Curtains

The water spray curtain is widely used as an inexpensive technique for controlling and mitigating many toxic and flammable vapours. Field tests¹³⁸⁻¹⁴³ have shown that water curtains can reduce concentration of LNG vapour clouds and are able to

interact with vapour clouds by imparting momentum, heat transfer and air entrainment. However, the effectiveness of different water curtains (with different flow configurations, drop sizes, coverage height and coverage width) for LNG concentration reduction and temperature increase is still largely unknown. Such knowledge is essential to developing structured engineering guidelines for the design of water curtains in practical applications.

Rana et al.^{144, 145} investigated the effectiveness of two different water curtains in dispersing LNG vapour cloud using an experimental setup consisting of LNG supplied by a tanker truck and discharged on a spill area (concrete pad), enclosed with wooden frames. The nozzles selected were a 60° full cone spiral and 180° flat-fan water curtain types which were placed downwind of the spill site. Forced dispersion from the water curtains led to a reduction in the LNG vapour concentration. However, by studying the strength and dilution ratios of both water curtains, it was evident that the full cone spray is more effective at creating turbulence and therefore increasing mixing with air. However, the flat-fan is effective in creating a solid barrier hence pushing the vapour cloud upwards and reducing ground level concentration. A further study by Rana et al.¹⁴⁶ involved the LNG been spilled on a water surface. A comparison between the vapour cloud motion from the two studies suggests that water curtains disperse LNG vapour clouds by air entrainment and mixing. From these studies, it is evident that the full cone water curtain is the most efficient (as shown in Figure 6 where the full cone spray resulted in a higher heat loss compared to the flat fan). However, a combination of different types of sprays will ensure sufficient mixing, heat transfer and momentum impact to disperse various size of LNG vapour clouds. Olewski et al.¹⁴⁷ also carried out water curtain dispersion experiments using a smoke trace in place of LNG for safety reasons. A flare was placed in front of an improvised wind tunnel. Two types of flat-fan sprays were tested with several water flow rates and fan speeds, totalling to 24 different tests. Experimental results reinforced the findings by other researchers as to the ability of water curtains to control vapour clouds by mechanical or momentum transfer effects.

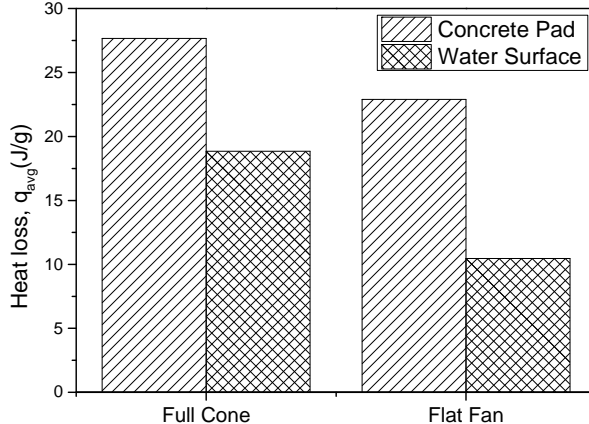


Figure 6: Calculated heat loss by water curtain (data were extracted from Rana et al.¹⁴⁶)

Kim et al.¹⁴⁸ carried out CFD simulation (on a similar experimental setup to that used by Rana et al.¹⁴⁵) of water curtains using ANSYS Fluent, as current models were not enough to draw a final conclusion on design parameters and the fact that heat transfer and well defined atmospheric dispersion was not included in most water curtain models. With broadly good prediction, the model simulation over-predicted the experimental data, which was desirable when trying to find the vapour cloud exclusion zone.¹⁴⁸ The added heat transfer effect was noted to induce distinct air-vapour mixture, resulting from the natural circulation within the air-vapour mixture. An increase in heat and/or mass transfer leaded to a reduction in the vapour cloud exclusion zone. Further CFD simulations by Kim et al.¹⁴⁹ aimed at determining key parameters (including droplet sizes, droplet temperature and installation configurations) for water curtain emergency system design. Even though further investigations are required, especially regarding turbulent effects of different sprays, there were several important conclusions: a) heat transfer rate increases with water flow rate; for droplet sizes ranging from 0.58 – 1.43 mm, a 0.94 mm droplet was noted to have the highest heat transfer rate per water flow rate; b) the higher the droplet temperature the better the dispersion; a 313 K droplet temperature was the most optimal, and any droplet temperature below this showed signs of potential hazards with the LNG vapour cloud flowing around the water curtain due to insufficient heat transfer; and c) the installation configurations have an optimal tilt angle with the wind (in that case 60° compared to other angles) and the closer the nozzles are to the source, the better the interaction and forced dispersion of the vapour cloud.

2.3.2.2 Underwater Releases

Little is known about behaviour of LNG following its release underwater and current models are not sufficient to quantify the potential hazards from such a spill. Using a concrete pit filled with water, Qi et al.¹⁵⁰ carried out tests at the Brayton Fire Training Field to understand the phenomena that occur from an underwater LNG release including the behaviour of the emanating vapour. LNG was released from a 2.5 cm (9.84 in) nozzle at a depth of 0.71 m (2.33 ft) below the water surface. There was no notable LNG pool formation on the water surface, most likely due to the high rates of evaporation and gas release. It is also possible that all the LNG was not vaporised underwater, but instead was thrown up with the rest of the vaporised liquid. The vapour cloud that emanated from the water surface was at a temperature below the dew point of air and as a result the vapour cloud was visible. The lowest temperature recorded for the vapour cloud was -1 °C, which explains why the vapour cloud was buoyant as the neutral buoyancy temperature of natural gas is -117 °C.

2.3.2.3 Effects of Turbulence

The rate of evaporation is necessary for the accurate prediction of the formation, growth and dispersion of vapour clouds. Typically it is assumed that the evaporation rate is constant, for example the detailed CFD study by Cormier et al.¹⁵¹ used a constant mean evaporation rate. However, it is known that at the spill point, as well as the leading edge of the pool, turbulence and evaporation rate are both elevated. Morse et al.¹⁵² focused on providing data regarding the evaporation rate of LNG from a water surface by controlling the turbulence. Small scale experiments were performed in a double-walled vertical cylinder, with a submerged turbulent jet, as shown in Figure 7. The water level was held at a constant level, and once the turbulence surface was established, the LNG was poured onto the water surface. The pressure in the cylinder as well as the temperature of the escaping vapour were recorded and used to calculate the evaporation rate. Morse et al.¹⁵² observed that for every 1cm (0.39 in) increase in LNG thickness, there was approximately a 10% increase in evaporation rate. On the other hand, if turbulence intensity doubles, then the evaporation rate will also double. Based on this it is clear that evaporation rate depends on turbulence intensity, and at a smaller level, the thickness of the LNG layer. However, this effect could be different at large scales.

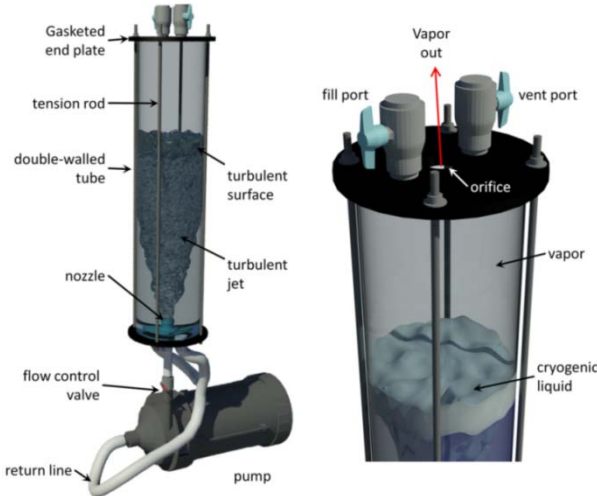


Figure 7: Small-scale experimental setup for measuring the evaporation rate of LNG from a water surface by controlling the turbulence (adapted from the study by Morse and Kytömaa¹⁵²)

2.3.2.4 Modelling

Since the 1980s, various numerical models have been developed for studying LNG vapour dispersion; with the main difference between models evident in their ability to completely simulate the dispersion process, their capabilities in different release processes, their ability of the model to describe process, the completeness in fields and data used, and the complexity of the terrain for which the model is situated in.⁴⁰ Other differences which are considered when looking at numerical models include the computational requirements such as power, speed and memory. These mathematical models can be classified as either box/top-hat models or Navier-Stokes models.¹⁵³

Box or Top-hat Models

There are two types of box or top-hat models: modified Gaussian models and similarity-profile models, depending on the complexity of conservation equations that must be solved.⁴⁰ The Modified Gaussian models are the simplest as Gaussian equation is used for the conservation of species, while neglecting or simplifying those for momentum and energy.¹⁵³ The similarity-profile models utilise simplified conservation equations with a mathematical complexity of one dimension.³⁸ Such simplicity is achieved via averaging the LNG cloud properties across the surface of the entire cloud or over the cross wind plane.^{38, 40} To regain the structural loss due to averaging, similarity profiles are used; therefore leading to quasi-three-dimensional

solutions. Examples of similarity-profile models include SCIPUFF,¹⁵⁴ TWODEE,¹⁵⁵
¹⁵⁶ SLAB,¹⁵⁷ HEGADAS,¹⁵⁸⁻¹⁶⁰ DEGADIS,¹⁶¹ ALOHA^{131, 132} and GASTAR.¹⁶² Of these models, the most commonly used are, SLAB, HEGADAS, DEGADIS and ALOHA (Table 15).^{131, 132, 157-159, 161} ALOHA seems to be the most widely used for safety engineering modelling applications in industry, due to its fast computational time and reasonable accuracy.¹³¹ On the other hand, the ease of use and fast computational time of DEGADIS and SLAB have led to them being used in both the public and private sectors.³⁸

Navier-Stokes Models

The Navier-Stokes models contain the most physically complete description of LNG dispersion process and are constructed from three-dimensional and time dependent conservation equations of momentum, mass, energy and species.^{118, 135, 136, 151, 163-167} Examples of Navier-Stokes models that have been used for denser-than-air modelling include FEM3, FEMSET, FLACS, HEAVYGAS, ZEPHYR.^{135, 136, 160, 168} Table 16 lists the key features and comparisons of four well-known Navier-Stokes models (FEM3, FLACS, FLUENT and CFX) for LNG vapour dispersion. It can be seen that recently Fluent and CFX numerical models have been the main Navier-Stokes models used for modelling. This is largely due to the key advantages of these models including robustness, multiple solving methods, high levels of accuracy and ability to add to the coding for specific simulations.¹⁶⁹ Although giving a more complete description of the physical processes available and performing better than box or top-hat models,³⁸ the Navier-Stokes models are more computationally expensive.¹⁵³

The recent developments in modelling are on four aspects including developments in models, modelling of complex geometries, modelling of complex scenarios (e.g. the effect of wind and ship motion) and evaluation of mathematical models. These advances are summarised below.

Table 15: Some well-known Similarity-Profile/Modified Gaussian models for LNG vapour dispersion

Model	Similarity-Profile Models/Modified Gaussian Models			
	SLAB ¹⁵⁷	HEGADIS ¹⁵⁸⁻¹⁶⁰	DEGADIS ¹⁶¹	ALOHA ^{131, 132}
Principles	<ul style="list-style-type: none"> Simulates the atmospheric dispersion of denser-than-air releases. 	<ul style="list-style-type: none"> Simulates the steady state or transient ground-level dispersion of a heavy gas cloud. 	<ul style="list-style-type: none"> Simulates a wide variety of denser-than-air gas releases. 	<ul style="list-style-type: none"> Simulates a wide variety of denser-than-air gas releases.
Method	<ul style="list-style-type: none"> Spatial averaging so as to treat the clouds as a steady state plume, transient puff or a combination of both. Conservation equations of mass, momentum, energy and species. 	<ul style="list-style-type: none"> Time dependent model uses a quasi-steady-state description by utilising ‘observers’. 	<ul style="list-style-type: none"> Lumped parameter approach. 	<ul style="list-style-type: none"> Gaussian and heavy gas dispersion models.
Accuracy	<ul style="list-style-type: none"> LFL was predicted to +/- 15% for LNG spills. 	<ul style="list-style-type: none"> The prediction of maximum downwind concentration is over predicted. However this prediction then becomes more accurate as the downwind distance increases. 	<ul style="list-style-type: none"> Downwind gas concentration decay is consistent with experimental data. 	<ul style="list-style-type: none"> Performed well for all validation tests.
Validations	<ul style="list-style-type: none"> Burro and Coyote series tests. Eagle series. 	<ul style="list-style-type: none"> Wind tunnel and laboratory experiments. Maplin Sands field tests. Thorney Island experiments. Goldfish 1 experiment. 	<ul style="list-style-type: none"> Burro and Coyote series tests. Maplin Sands. Thorney Island Phase I trials. 	<ul style="list-style-type: none"> Prairie Grass. Kit Fox.

Advantages	<ul style="list-style-type: none"> Typical dispersion simulations can be solved in a few minutes on a IBM-AT class computer. 	<ul style="list-style-type: none"> Simulation of instantaneous releases, time varying releases, and continuous releases. 	<ul style="list-style-type: none"> Simulation of instantaneous releases, time varying releases, and continuous releases. 	<ul style="list-style-type: none"> Models puff and plume, and heavy gas dispersion. Simulations can be conducted within a few minutes.
Disadvantages	<ul style="list-style-type: none"> Can't model complex terrain or flow around obstacles. 	<ul style="list-style-type: none"> Can't model complex terrain or flow around obstacles. Can't model elevated source flows. 	<ul style="list-style-type: none"> Can't model complex terrain or flow around obstacles. 	<ul style="list-style-type: none"> Can't model complex/changing terrain. Can't model particulate dispersion.
Scales	<ul style="list-style-type: none"> Laboratory. Field. 	<ul style="list-style-type: none"> Laboratory. Field. 	<ul style="list-style-type: none"> Laboratory. Field. 	<ul style="list-style-type: none"> Field.
Applications	<ul style="list-style-type: none"> Ground level evaporating pool, an elevated horizontal jet, a stack or elevated vertical jet and an instantaneous volume source. 	<ul style="list-style-type: none"> Dispersion downwind of a transient ground-level source or a vertical transition plane with a near field jet model. Heat and water-vapour transfer from substrate. Gravity slumping and dispersion. 	<ul style="list-style-type: none"> Prediction of concentrations in the low flammability range. 	<ul style="list-style-type: none"> Designed for people responding to chemical accidents. Emergency planning and training.
Code accessibility	<ul style="list-style-type: none"> N/A 	<ul style="list-style-type: none"> N/A 	<ul style="list-style-type: none"> N/A 	<ul style="list-style-type: none"> N/A

Table 16: Some well-known Navier-Stokes models for LNG vapour dispersion

Model	<i>Navier-Stokes Models</i>			
	FEM3 ^{164, 169}	FLACS ^{135, 136}	FLUENT ^{118, 165, 166}	CFX ^{151, 163, 167}
Principles	<ul style="list-style-type: none"> Initiated in 1973. Simulation of large heavier-than-air gas releases. 	<ul style="list-style-type: none"> Initiated in 1980s. Simulation of gas dispersion and subsequent explosion. 	<ul style="list-style-type: none"> Initiated in 1983. Simulation of various flow scenarios. 	<ul style="list-style-type: none"> Simulation of various flow scenarios.
Method	<ul style="list-style-type: none"> Modified Galerkin finite element method. Time-dependent equations of mass, momentum, energy and species. Reynolds averaged Navier-Stokes equations (RANS) for calculating the process of momentum. K-theory sub model for turbulence. 	<ul style="list-style-type: none"> Finite volume method. Time-dependent equations of mass, momentum, energy and species. k-ε for turbulence. 	<ul style="list-style-type: none"> Finite volume method. Time-dependent equations of mass, momentum, energy and species. Reynolds averaged Navier-Stokes equations (RANS) and Reynolds stress models (RSM) for calculating the process of momentum. Realized k-ε for turbulence. Multiple solving approaches. 	<ul style="list-style-type: none"> Finite volume method. Time-dependent equations of mass, momentum and energy. Reynolds averaged Navier-Stokes equations (RANS) for calculating the process of momentum. k-ε for turbulence. other mathematical models available for modelling processes such as combustion or radiation. Utilises a coupled solver.

Accuracy	<ul style="list-style-type: none"> Under prediction of peak concentrations values by a factor of 2. Predicts well the salient features in large instantaneous releases. 	<ul style="list-style-type: none"> 70% of the time it predicted values are within a factor of two of the observed experimental data. Can accurately predict down wash from large tanks. 	<ul style="list-style-type: none"> RSM predicted the turbulence kinetic energy to within 80% of the expected value; however reduced to 50% at ground level. Gas concentrations was within 80% of the experimental data. 	<ul style="list-style-type: none"> Over prediction of thermal impulses by a factor of two, however still acceptable from a safety point of view. Under prediction of concentrations at high elevations due to over assumption of gas behaviour.
Validations	<ul style="list-style-type: none"> Thorney Island Phase 1 trials. 	<ul style="list-style-type: none"> Prairie Grass. Kit Fox. EMU. MUST. 	<ul style="list-style-type: none"> Burro series field test. DEGADIS model. ADMS model. Falcon tests. 	<ul style="list-style-type: none"> Coyote series trials. Brayton Fire Field Tests.
Advantages	<ul style="list-style-type: none"> 3D Can model complex terrain and flow around obstacles. Can accommodate multiple instantaneous sources. 	<ul style="list-style-type: none"> 3D Can model complex terrain and flow around obstacles. Distributed porosity concept is used to characterise the geometry while not reducing calculation time as much as other models. 	<ul style="list-style-type: none"> 3D Can model complex terrain and flow around obstacles. Can create user defined functions. Can model temporal and spatial gas dispersion, including gravity slumping and time dependent effects. 	<ul style="list-style-type: none"> 3D Can model complex terrain and flow around obstacles. User interface that allows for customisation and automation.

Disadvantages	<ul style="list-style-type: none"> • Inappropriate K-theory submodel. • Can't model in homogenous vegetation cover all in the same computational domain. • Can't model jet releases, explosive sources and chemical reactions. 	<ul style="list-style-type: none"> • In the case of flat terrain simulations, Gaussian models can provide better accuracy than the FLACS model. 	<ul style="list-style-type: none"> • More complex than other specific models such as ADMS. • Long simulation times required. 	<ul style="list-style-type: none"> • More complex than other specific models. • Long simulation times required. • Single solver, unlike FLUENT.
Scales	<ul style="list-style-type: none"> • Field. 	<ul style="list-style-type: none"> • Field. • Laboratory. 	<ul style="list-style-type: none"> • Field. • Numerical. 	<ul style="list-style-type: none"> • Field.
Applications	<ul style="list-style-type: none"> • Modelling of gravity slumping and spreading, formation of doughnut-shaped cloud and cloud bifurcation in the case of LNG spill. • Submodel for treating aerosol effects in pressurized NH₃ spills. • Phase-change model for humidity. • Tool for emergency response planning for liquid Cl spills. 	<ul style="list-style-type: none"> • Primarily designed to model explosions in offshore oil platforms. • Can model dispersion and ventilation in complex geometries. 	<ul style="list-style-type: none"> • Design and optimisation of most industrial applications. • Modelling of complex flows including turbulence, heat transfer and radiation, chemical reactions, combustion, multiphase flows and moving geometries. 	<ul style="list-style-type: none"> • Modelling of complex flows including turbulence, heat transfer and radiation, chemical reactions, combustion, multiphase flows and moving geometries.
Code accessibility	<ul style="list-style-type: none"> • N/A 	<ul style="list-style-type: none"> • N/A 	<ul style="list-style-type: none"> • Accessible through user defined functions. 	<ul style="list-style-type: none"> • User interface that allows for customisation and automation using session files, scripting and the CFX expression language.

2.3.2.4.1 Developments in Models

Federal Energy Regulatory Commission (FERC) developed a box/top hat type model that uses the model developed by ABS Consulting¹² for source term modelling and DEGADIS for vapour dispersion modelling. The FERC model was successfully used for a comprehensive sensitivity analysis on the effect of tank (25,000 m³) conditions, release scenarios, and environmental conditions on LNG spill, spread and dispersion.¹⁷⁰ Table 17 summarises the main conclusions of the simulations, considering key parameters such as breach diameter, ullage pressure, weather conditions and surface roughness on LNG spill and dispersion.¹⁷⁰ It was concluded that breach size and ullage pressure are important parameters that have significant effect on LNG spill duration, pool size and dispersion. LNG spilled from a spherical tank always has a higher spill rate.

Table 17: The effect of hole size and breach diameter on spill and dispersions using the FERC model^a

Time to empty	Decreases dramatically with increase in hole size, pool radius also increase (asymptotes at 5m hole size)	Decreases with increase in ullage pressure, pool radius also increase size
Vapour dispersion	Decreases dramatically with increase in hole size, pool radius also increase (asymptotes at 5m hole size)	-
LFL	-	Increases with increase in ullage pressure (not affect for ullage pressure > 13.79 kPa)

^aData extracted from the study by Qiao et al.¹⁷⁰

The most recent SafeSite_{3G}TM model is also a box/top-hat type model that was developed to predict the dynamic effect of LNG discharge and pool ignition on the pool spread process.¹²³ The model was utilised for the dynamic analysis of an LNG tank (25,000 m³) release conditions, LNG spread, dispersion and combustion. It was found that the bevelled cross-section of a membrane tank can easily be replaced with a rectangular cross-section and still obtain a high degree of accuracy (discharge rate vs. time). The analysis showed that when the average pool depth is above a minimum, both burning and non-burning pools spread at the same rate but the evaporation flux of the discharged LNG is dependent on turbulence generated during the spill.¹²³ SafeSite_{3G}TM was also able to capture and show, that for a period of

constant discharge rate, the discharge rate would be greater than evaporation rate; this effect was also noted by Johnson et al¹⁷¹ by using the consequences analysis methodology developed by FERC.

LNGMAP is another box/top-hat type model that uses a discrete set of algorithms within a geographic information system framework for studying LNG releases and transport for marine spills,¹³³ overcoming a series of limitations of existing models.^{172, 173} The model predicts time-dependent release, spreading and transport of LNG on water surface, LNG evaporation from the water surface (effect of current and waves), LNG transport and dispersion in the atmosphere, and the burning and associated radiant fields of LNG fires.¹³³ The model was validated by carrying out simulations presented in the ABS Consulting¹² and Sandia reports.¹³⁴ Compared to the Sandia cases, LNGMAP predicted the distance to the thermal radiation contours being larger for small holes sizes and lower for the largest hole size (see Table 18). LNGMAP was successfully used to simulate three emergency LNG tanker cases (both with and without ignition of the LNG pool): a tanker continuing on course at 7.5 m/s (24.61 ft/s), a tanker stopping within 3 min and a tanker changing direction and heading to the nearest location to ground.

Table 18: Comparison of LNGMAP to Sandia predictions^a

	Hole size 1 and 2 m²	Hole size 5 m²
Pool diameter (m)	~ 15 – 23% larger	~ 15% lower
Spill duration (min)	~ 1% larger	0% difference
Distance to thermal radiation contours (m)	~ 10 - 20% larger	10 - 38% lower

^aData were extracted from the study by Spaulding et al.¹³³

Vilchez et al.¹⁷⁴ devised a “dispersion safety factor” (DSF) based on the concept that when LNG is spilled on land or on water, the visible cloud formed is due to the air reaching the dew point temperature of water resulting in condensation. DSF can be calculated based on a relationship between the downwind length of the flammable cloud at LFL, X_{LFL} (m), and the downwind length of the visible cloud, X_{VIS} (m): $DSF = X_{LFL}/X_{VIS}$. With the help of DEGADIS, DSF was validated against the experimental

data of Maplin, Burro and Coyote tests. As humidity increases, DSF decreases, which leads to the flammable region falling within the limits of the visible cloud (safer situation). If humidity decreases, DSF increases, which leads to the flammable region extending beyond the limits of the visible cloud (more dangerous). If X_{VIS} is known, X_{LFL} can be determined via gathering significant sets of data.

2.3.2.4.2 Modelling of Complex Geometries

Most field studies, with the exception of the Falcon trials, of LNG dispersion are in unobstructed conditions. In practice, in the event of an LNG spill onshore, the receiving terminals are designed to direct the spill towards a sump or impoundment area where an LNG pool is formed.¹⁷⁵ In order to study the dispersion of natural gas clouds evolving from LNG pools in trenches, Melton et al.¹⁷⁶ deployed a fire dynamics simulator, a CFD model originally developed from modelling thermally-driven fluid flow behaviour during fires in a 450,000 m³ capacity LNG import terminal. The focus was on the effect of the substrate material and the terrain, via varying the combination of medium density concrete, spill into trench and flowing to impoundment and direct spill into impoundment. It was evident that the inclusion of terrain effects increases turbulence and mixing, resulting in shorter dispersion distances (but not always being the case). It is important to define where the LFL is measured from as a “pocket” or isolated volume of cloud can result in a larger LFL - an increase of 10% - 30% identified in the study.

Gavelli et al.¹⁷⁷ also investigated LNG dispersion from the trench, using a hydraulic model (not accounting for decrease in mass flow rate) to analytically calculate the evolving LNG flow and vaporization rate along the trench. This was then imported into CFD Fluent to calculate the dispersion of the vapours. For cloud dispersion from a trench with perpendicular wind flow direction (relative to the trench), the ½-LFL extended 65m (213.25 ft) downwind of the trench and receded before the 10 min spill duration was over as results of the decreases in heat transfer from the trench. When wind direction was parallel to the trench, ½-LFL was in the order of 100 m (328.08 ft). However, the inclusion of a vapour fence had little effect in containing the cloud; instead it increased turbulence and mixing, increased the dissipation and decreased the LFL by 30 m.

Considering LNG spill and dispersion into a sump or impoundment, Ponchaut et al.¹⁷⁵ solved the shallow water equations (SWEs). Unlike the integral models, SWEs account for the pool thickness distribution and the growth of the pool with time, using one-dimensional Fourier conduction equation for modelling the heat transfer. The SWEs account for pool thickness and hydraulic jump, which cannot be modelled by integral models. The pool was predicted to reach the sump wall in 6s via SWEs, instead of 9s via PHAST that is a common integral model. This resulted in a slightly lower vaporization rate in the PHAST model. The effects of elevation of the spill source and the effect of sump floor shape (conical vs. flat) were also considered. An increase in the spill source elevation led to a higher peak vaporization rate. However, a conical sump floor would be more favourable in the case of hazard mitigation in cases where the sump floor is close to property boundaries, as peak vaporization was reduced.

2.3.2.4.3 Modelling of Complex Scenarios

The use of SOURCE5 and DEGADIS is not accurate for predicting flammable vapour dispersion from LNG spills into impoundments because vapour entrainment by wind is not considered. More accurate CFD package Fluent was used for such prediction, validated using Flacon test data.¹¹⁸ The comparison between the CFD simulation results and the experimental data clearly showed that the general shape of the cloud captures the stable stratification that was measured in the experiments. Even though there were some discrepancies, the CFD predictions showed good agreement with the experimental data in terms of gas concentration profile. The effect of the impoundment and source turbulence were also studied. As expected, the impoundment partially contained the spill and limits its spread in the downwind and lateral direction, while a decrease in source turbulence led to highly stratified and undiluted with vapour cloud within the impoundment. Therefore, mixing seems be dominated by the turbulence generated by the spill and that the turbulent-driven entrainment affects the rate at which the gas is dispersed and as a result the downwind concentrations.

Considering the effect of wind at a -9.3° wind direction, Giannissi et al.¹⁷⁸ simulated the Falcon test series to study the effect of a two-phase jet release, using ADREA-HF that is a three-dimensional CFD code developed for pollutant and hazardous gas

dispersion studies.¹⁷⁹⁻¹⁸¹ The simulations considered two cases, the first was a two-phase release and the second involved a mass flux from the water pond surface, similar to that of Gavelli et al.¹¹⁸ Both source modelling techniques were in good agreement with the experimental data. However, the two-phase case was better at predicting the maximum concentration and arrival time and the mass flux case resulted in longer vapour cloud hold up within the impoundment when compared to the two-phase jet case. This is most likely due to the more realistic/accurate representation of the effect of turbulence generated by the two-phase source as the LNG impacts the water surface. The effect of a -9.3° wind direction was noted to have a large impact on the vapour cloud for the mass flux case as compared with the two-phase release case. This agrees with Gavelli et al.,¹¹⁸ that under low wind and stable atmospheric conditions source turbulence will dominate the mixing and dispersion process. Modelling the spill as a two-phase jet release appears to give a more realistic simulation and more accurate results.

Qi et al.¹⁶³ utilised the CFD code ANSYS CFX to simulate an environmental setup similar to that used in the Falcon series trials, with additional experimental data in the Brayton Fire training Field (BFTF) where no upwind obstacle was used. It involved spilling LNG unto a water surface in an impoundment. The physical behaviour of the LNG vapour cloud was well captured. Unlike the studies conducted by Gavelli et al.¹¹⁸ and Giannissi et al.,¹⁷⁸ it was clear that both wind velocity and turbulence were dominant in terms of vapour dispersion. This is because that in the experimental work of Qi et al.,¹⁶³ the wind velocity was higher and the spill rate was lower (Table 19) than that of Gavelli et al.¹¹⁸ and Giannissi et al.¹⁷⁸ This would result in lower source turbulence, allowing the wind to dominate the flow process. The simulation results from ANSYS CFX were in reasonable overall agreement with the experimental data (as shown in Table 20); however, it under-predicts ground level gas concentration, while underestimating downwind gas concentrations at higher elevations. This suggests that CFX overly assumes the slumping behaviour of the gas and takes less into account the buoyancy change. Qi et al.¹⁶³ believed that this might be due to incomplete description of the heat transfer process during the simulation setup and other sources of uncertainty such as mesh size and source term turbulence. The cruciality of a sensitivity study in model validation was demonstrated by

decreasing the maximum mesh spacing, which changed the results from underestimated to actually matching the experimental results.

Table 19: Test conditions for spills into impoundments followed by dispersion.

	Wind speed (m/s)	Spill rate (m^3/min)
Qi et al. ¹⁶³	1.8 – 2.2 m/s	0.265 – 0.75 m^3/min
Gavelli et al. ¹¹⁸	1.7 m/s	28.7 m^3/min
Giannissi et al. ¹⁷⁸	1.7 m/s	28.7 m^3/min

Table 20: Comparison of the distance to LFL for LNG dispersion in BFTF^a

	LFL (5% v/v concentration of LNG)	
	At 0.3 m (height)	At 1.22 m (height)
Experiment	8.69 – 13.53 m	6.09 – 13.47 m
ANSYS CFX Simulation	9.80 m	13.47 m

^aData were extracted from the study by Qi et al.¹⁶³

Spaulding et al.¹³³ found that compared to the stationary case, the moving motion of the vessel leads to much lower concentrations of LNG vapour distributed over a much wider area. This is because as soon as the vessel stops, the LNG pool will be restricted, reaching a maximum pool area and for a longer duration, therefore resulting in a higher vapour cloud concentration than if it continues moving. A similar conclusion was also deduced for an ignited LNG pool, in which an earlier stop of the vessel results in a more isolated thermal radiated area, which lasts for a longer time. The modular algorithm based design of LNGMAP makes it able to incorporate new algorithms. Currently, LNGMAP is more computational efficient than CFD models, and with further advancement might be confidently used to provide more realistic spill consequences.

There has been little focus on the effect of a substrate temperature to the vaporization of LNG; especially for LNG spills on water. Vesovic¹⁸² investigated the rate of vaporization of LNG, by developing a model for heat transfer from water to the LNG, with the assumption that LNG is released instantaneously and the spreading pool forms a cylindrical shape. The spreading occurs in the gravitational-inertial regime, in which the height of the pool provides the driving force, while the inertia of

the ambient water provides the resistance to spreading.¹⁸² Two scenarios were considered; firstly water temperature remains constant and secondly heat arrives to the water surface by conduction only. It was found that the maximum evaporation time is proportional to the forth root of the initial mass spilled. The derived expression is similar to that of Raj and Kalelkar¹¹⁶ and Opschoor.¹¹⁷ However, the results are 10% higher, most likely due to the different assumptions and models used. In the second case which heat transfer was assumed to be by conduction, the results showed that rate of vaporization of LNG depends not only on its composition but also on the dynamics and surface temperature of the water. Initially the thermal inertia of the thin vapour film governs the heat transfer, and 10 – 15 s after the spill the transition boiling will start, leading to the thermal inertia of the growing ice layer governing the heat transfer.

2.3.2.4.4 *Evaluation of Models*

Various models for simulating LNG dispersion relied on different assumptions and empirical constants which can cause uncertainty. The uncertainty due to lack of knowledge (i.e. epistemic uncertainty) can be reduced over time as more data are available while the uncertainty due to variability within a model's variables (i.e. aleatory uncertainty) cannot be reduced. Siuta et al.¹⁸³ showed that two respective methods can be used to evaluate the uncertainty of models, i.e. the fuzzy sets (FS) theory for analysing epistemic uncertainty and the Monte Carlo (MC) simulation for analysing the aleatory uncertainty. These techniques have been successfully applied to evaluate the prediction from the Classical model (developed by ABS Consulting),¹² Gaussian dispersion (GD) model and Britter-McQuaid¹⁸⁴ (BMQ) model for the Maplin Sand and Coyote field experiments (see Table 21).

Table 21: One of the test cases comparing the addition of the fuzzy and MC methods to the source term modelling of the Classical model^a

Fuzzy/MC compared to Classical model	
Maximum release rate	~ 20% lower
Spill duration	15% higher
Maximum pool radius	12.5 – 20.7% lower
Maximum evaporation times	8.5% lower

^aData extracted from Siuta et al.¹⁸³

Ivings et al.¹⁸⁵ proposed a comprehensive model evaluation protocol (MEP) for evaluating the accuracy of various models. The MEP was devised for the National Fire Protection Association (NFPA) Standard 59A. Four main pillars were considered: a model evaluation questionnaire for collecting essential information needed for model assessment; a model validation database with sufficient information for verification and validation (following the method developed during the SMEDIS project¹⁸⁶⁻¹⁸⁸); a set of qualitative and quantitative model assessment criteria (stated in MEP¹⁸⁹) for qualitative assessment against statistical performance measures; and a comprehensive model evaluation report as key output of the MEP. MEP has been fully used and published for a CFD model by Hansen et al.¹⁹⁰ and for the evaluation of the integral model PHAST that has now been approved for use in LNG siting applications in the USA.

2.3.3 Combustion

2.3.3.1 LNG Poll Fire and Vapour Cloud Fire Experiments

A variety of LNG fire tests were conducted over the past three decades. These fire tests can be classified as fires of LNG pool and vapour cloud on land or fires of LNG pool and vapour on water, with the differences mainly in the burn rate and the resulting flame height.³⁸ Compared to land LNG pool fires, fires on water has a higher burn rate and flame height by as much as a factor of two, as results of additional heat flux from the water.³⁸ On the other hand, surface emissivity power for both water and land tests, has been found to be similar for LNG pool diameters up to 15m (49.21 ft).^{38, 41} Table 22 lists the up-to-date large tests for LNG pool and vapour cloud, summarised by Luketa-Hanlin³⁸ and extracted from previous studies.¹⁹¹⁻¹⁹⁹ It was also found that pool fires are affected by wind and can be influenced by the shape of any surrounding bunds; whereas surface emissivity is affected by pool size.³⁹ The area of burn is also dependent on the type of ignition.⁴¹

There have been limited recent research on LNG combustion tests which focused on the properties/governing factors of pool fires and vapour cloud fires. Lowesmith et al.²⁰⁰ investigated the nature of two-phased oil and gas jet fires, considering the effects of confinement on jet fires and their behaviour with water deluge for simplifying hazard assessment. Correlations and guidance for assessing jet fires were

successfully developed based on experiments from various studies including those conducted by Advantica Limited, SINTEF and Shell since 1980s.

Studer et al.²⁰¹ studied the properties (such as flame visible length, radiation flux and blowout) of large-scale methane/hydrogen jet fires. The CAST3M code was in good agreement with the experimental results and later used to calculate some safety related quantities. It was found that right after ignition, a flame ball formed, and flame length was noted to decrease with time due to a decrease in the mass flow rate. A set of correlations were then developed for estimating the flame length.²⁰¹ However, the predictions using these correlations are ~15% lower than those predicted by the correlations developed by Lowesmith et al.,²⁰⁰ mainly because the released power of the experiments in the study by Studer et al.²⁰¹ is at the lower limit of the correlation.

Advances have also been made to develop blowout stability (flame stability) diagrams for different fuels. For example, Wu et al.²⁰² carried out a study that developed a blowout stability diagram of hydrogen flame diameter vs. atmospheric pressure. Lowesmith et al.²⁰⁰ developed one for natural gas flames. When blowout of the Studer et al.²⁰¹ experiment was imposed onto the flame stability diagrams of Wu et al.²⁰² and Lowesmith et al.,²⁰⁰ good agreements have been reached. It is clear that the phenomenological model developed by Studer et al.²⁰¹ is capable of predicting flame length, blowout velocities and radiant fluxes while Lowesmith et al.²⁰⁰ have presented good background and correlations for jet flame hazard assessment.

2.3.3.2 Deflagration/Detonation Experiments

Explosion from fuel combustion can be classified as deflagration or detonation. In deflagration the fuel-air mixture burns slowly at speeds in the order of 1 m/s; whereas in detonation the flame front travels at a shock wave at speeds in the order of 2,000 – 3,000 m/s (6,561.68 – 9,842.52 ft/s) followed by a combusting wave that supplies it with energy.^{38, 39} Since the reviews published in 2007, no significant deflagration/detonation experiments have been performed. As concluded previously, detonations are very difficult to achieve in LNG fires because the primary component methane has a low reactivity; and deflagrations can transition into a detonation explosion if there is a confinement or blockage.^{38, 39}

Table 22: LNG fire tests on water and land^a

Study	Spill terrain	Spill volume (m ³)	Spill rate (m ³ /min)	Pool diameter (m)	Flame length (m) (L/D)	Surface emissive power (kW/m ²)		Burn rate 10 ⁻⁴ m/s or (kg/m ² s)	Flame speed for vapour cloud fires (m/s)
						Pool fire	Vapour cloud fire		
U.S.CG China Lake Tests ¹⁹¹⁻¹⁹⁴	Water	3 – 5.7	1.2 – 6.6	~15 (effective)	25 – 55 (2.8 – 4.4)	210 ± 30 (narrow) 220 ± 50 (wide)	220 ± 30 (narrow) 200 ± 90 (wide)	4 – 11 (.18 – .495) (calculated)	8 – 17 (relative to cloud)
Maplin Sands ^{196, 198}	Water	5 – 20	3.2 – 5.8	30 (effective)	80 (2.6)	178 – 248 203 (avg)	137 – 225 174 (avg)	2.1 (.0945) (calculated)	4.5 – 6.0
Coyote ¹⁹⁷	Water	14.6 – 28	13.5 – 17.1	Not measured	Not measured	Not measured	150 – 340	Not measured	30 – 50 (near ignition sources)
Maplin Sands ¹⁹⁵	Land	Not reported	NA	20	43 (2.15)	153 (avg) 219 (max)	NA	2.37 (0.106) (measured)	NA
Montoir ¹⁹⁹	Land	238	NA	35	77 (2.2)	290 – 320 (narrow angle) 257 – 273 (wide angle) 350 (max)	NA	3.1 (0.14) (measured)	NA

^aData were extracted from the study Luketa-Hanlin³⁸ that was based on the literature^{191-194 195-199}

2.3.3.3 Modelling

An LNG pool fire can transmit significant radiant heat to an object outside the fire, with the heat flux strongly dependent on various parameters including the properties of fire (e.g. size, shape and geometry), surrounding atmosphere (e.g. transmissivity) and the object (e.g. location, orientation).⁴¹ Technical issues that arise when modelling LNG pool fires are usually due to the scale of the fire. As pool fires become larger, physical phenomena such as oxygen starvation in the centre of the pool fire, smoke generation and a reduction in the emissivity power become more important.³⁹ Extrapolation from small fires can lead to misleading results so that developing modelling techniques are in great need for studying large scale LNG pool fires.

Typically, there are three approaches to modelling LNG fires: the point source method (simplest), solid flame method (next level of complexity) and field (or Navier Stokes) method (most complex/complete) as shown in Table 23. The point source model can easily produce result, however the assumptions taken, such as neglecting wind and obstacle effects, assuming that all heat is radiated at ground level, can lead to questionable accuracy.¹⁹⁴ On the other hand the solid flame model accounts for wind and atmospheric conditions, however the cylindrical flame modelling approach can at times lead to inaccurate results.^{194, 203-208} Navier-Stokes models as previously discussed in Section 2.3.2.4 are the most complete and robust able to provide the most accurate results.^{118, 167, 194} The same conclusion stated in Section 2.3.2.4 applies here. Fire modelling can only be improved if further evaluation studies are carried. In doing so, issues such as the effects of radiation, surface emissivity, flame interaction with objects, and the effect of pool fire size need to be studied extensively at the field scale in order to generate data for model evaluation/validation.

2.3.3.3.1 Overpressure from LNG vapour Cloud Ignition

Previous studies for LNG facilities focused on overpressures from ignition of vapour clouds or pool fires from an LNG spill. These analyses were usually performed with simple methods such as TNO-Multi Energy Method (MEM) or the Baker-Strehlow-Tang (BST) method.²⁰⁹ However these models are inadequate for near field calculations, are not sensitive to degree of congestion, and cannot account for

obstacles. Gavelli et al.²⁰⁹ used the advanced modelling tool FLACS to study LNG vapour cloud explosions in two spill scenarios (a worst case and a realistic case) occurred from a 140,000 m³ Moss-type LNG vessel moored at an offloading pier. In the worst case scenario, 23,000 m³ of stoichiometric gas cloud was spilled, and in the realistic scenario (one of many possible encounters) LNG was spilled at the loading rate of 5,000 m³/h for 10s and then dispersed for 3 mins by wind. In both cases, the resulting overpressure was well below the minimum threshold for human injury (16.54 – 20.68 kPa) or facility damage (101.35 kPa).²⁰⁹ Clearly, the low reactivity of methane results in overpressures although such overpressures appear to occur within a safe range even at an applied safety factor of two for accounting for uncertainties in modelling.

Abe et al.²¹⁰ studied the blast effects of liquid oxygen/LNG fuel mixture using the hypercode ANSYS AUTODYN, considering four cases including two large scale liquid fuel explosion of 17 and 5 tonnes, two equivalent scale gas explosions (~13 and 3.9 tonnes), and 5.8 grams gas explosion. Assumptions such as wind-free and a static state environment were assumed. From the large scale simulations, it is clear that overpressures are generated. A secondary shock wave was also noted (believed to be the reflection of the shock wave from the ground). As the overpressure moved further away, the constant volume combustion pressure profile formed is nearly identical to that of a detonation. For the liquid case, blast effects were noted to be 40 – 50% higher at any distance than those for the gas cases. The properties of the blast wave at relatively long distances were also believed to be independent of ignition conditions. The maximum overpressure recorded was ~65 kPa (9.42 psig) at 100m from the explosion point, which is well above the safety thresholds for human (16.54 – 20.68 kPa), but below that for facilities (101.35 kPa). However, it is important to note that the study did not consider wind disturbances and weather conditions that can have significant effect on the energy of the overpressure.

Table 23: Some well-known models for LNG fire modelling

Model	<i>LNG Fire models</i>		
	Point Source ¹⁹⁴	Solid Flame ^{194, 203-208}	Navier-Stokes ^{118, 167, 194}
Principles	<ul style="list-style-type: none"> Initiated prior to 1970s and simulates pool fire as a point at ground level. 	<ul style="list-style-type: none"> Initiated in prior to 1970s and simulates fires as a geometric shape, usually based on wind condition. 	<ul style="list-style-type: none"> Initiated in the 1970s and simulates any type of fire with any shape.
Method	<ul style="list-style-type: none"> Semi-empirical approach. Inverse square law of radiation 	<ul style="list-style-type: none"> Semi-empirical approach. Representation of fire as a geometric shape, usually cylinder. 	<ul style="list-style-type: none"> Finite volume method. Time dependent equations of motion. $k-\varepsilon$ for turbulence. Combustion and soot models can be incorporated.
Accuracy	<ul style="list-style-type: none"> Provides a reasonably good agreement with experimental data, which is variable due to the assumption made. 	<ul style="list-style-type: none"> Provides a reasonably good agreement with experimental data, which is variable due to the assumption made 	<ul style="list-style-type: none"> Provides good agreement with experimental data if the correct physics is applied.
Validations	<ul style="list-style-type: none"> Different correlations and related factors have been developed based on findings from experimental work; and are selectively been used based on the modelling taking place. 	<ul style="list-style-type: none"> Different correlations and related factors have been developed based on findings from experimental work; and are selectively been used based on the modelling taking place. 	<ul style="list-style-type: none"> Via experiments such as the Esso tests, China Lake tests, Maplin sands tests, Gaz de France and many more.
Advantages	<ul style="list-style-type: none"> Simple and can easily produce results. 	<ul style="list-style-type: none"> Can account for interactions with water vapour and carbon dioxide in the atmosphere. Effects due to wind, such as flame tilt can be modelled. 	<ul style="list-style-type: none"> Can capture complex flame shapes and interaction of flames with objects. Can model pool fires, vapour cloud fires and fireballs.

Disadvantages	<ul style="list-style-type: none"> • Energy radiated depends on a number of factors and is not an intrinsic property of combustion. • Assumes that all radiant energy freed at ground level. • Assumes that the fire is small element at ground level. • Cannot account for wind and obstacle effects. 	<ul style="list-style-type: none"> • Flames with complex shapes, especially those arising from irregular shaped pools cannot be modelled. • Cannot account for flame zones in with object interaction. 	<ul style="list-style-type: none"> • Main disadvantage is the computational requirement compared to other models. • More complex compare to the other models.
Scales	<ul style="list-style-type: none"> • Field. 	<ul style="list-style-type: none"> • Field. 	<ul style="list-style-type: none"> • Field. • Laboratory.
Applications	<ul style="list-style-type: none"> • Fire hazard assessment. 	<ul style="list-style-type: none"> • Fire hazard assessment. 	<ul style="list-style-type: none"> • Fire hazard assessment.
Code accessibility	<ul style="list-style-type: none"> • N/A 	<ul style="list-style-type: none"> • N/A 	<ul style="list-style-type: none"> • Some Navier-Stokes models e.g. Fluent and CFX have accessible codes.

2.3.3.3.2 LNG, LPG and Gasoline Modelling

The consequence analysis methodology developed by Federal Energy Regulatory Commission (FERC) has become the standard method of modelling LNG releases, spread and pool fires.¹⁷¹ Vaporization can occur from two mechanisms: heat transfer from the spill surface and heat transfer from a flame. In both cases FERC methods assumes constant heat flux, i.e. 85 kW/m² (0.167 kg/m² s) for a non-burning LNG pool and 143 kW/m² (0.282 kg/m² s) for a burning LNG pool. On the other hand, radiation from a flame is modelled by means of the solid flame model.

Johnson and Cornwell¹⁷¹ performed studies to evaluate the effectiveness of the FERC method in simulating spills, vaporization and pool fires of material other than LNG (such as LPG and gasoline), considering two release scenarios. In the first scenario of an equal release volume of all three liquids, the burning gasoline pool reached the largest diameter, mainly due to its low vaporization rate, although the impacts from an expanding burning pool were nearly identical for all liquids. In the second scenario of the respective ship containment system of the different liquids, the gasoline pool was still larger than the LNG pool although the total volume of LNG spilt was five times larger. Therefore, an LNG release and ignition will not necessarily produce a significantly larger radiant impact than a smaller release of a less volatile material, such as gasoline for typical cargo containers under similar releases conditions. The FERC spill, vaporization and burning modelling method for LNG can also be used for other material such as LPG and gasoline if the correct material properties and physical data are used.

2.4 Safety

Accidental release to the environment poses a risk and requires special care when handling. Marine vessels, unloading facilities, land storage tanks and processing facilities are considered to be the key areas where risks are to be quantified.²¹¹ The key issues of siting LNG terminals include: a) no exclusion zone sitting for spills on water; b) misleading or erroneous specifications of input parameters for exclusions zone modelling; c) the use of unreliable models for exclusion zone calculations.⁴² While there have been no major incidents in this industry with the use of the current system, recent studies have focused on safety measures for human, LNG facilities

and ships, due to rapid increases in production and use of LNG, potential terrorist threats and public confidence in LNG safety.

2.4.1 Facilities

In the past, the relatively low demand for natural gas storage made it possible to locate such installations away from densely populated areas. However, it has become clear that there are advantages in bringing storage facilities closer to points of use. When studying the risks involved in an LNG facility, it is therefore crucial to deal with scenarios that are:²¹⁷ a) feasible in the course of operation; b) feasible by interaction with the surroundings; c) highly improbable, but theoretically possible; and d) intentional damage to the installation with a view of restricting the functions or endangering the surroundings. However, most safety and security documentation barely cover these scenarios. Scenarios *a-c* can be simulated using typical mathematical models while for scenario *d*, modelling of the entrance, including the influence of protective measure should be taken into account. As a result, Bernatik et al.²¹⁷ devised a method adapted from the critical evaluation for national monuments under the National Infrastructure Protection Plan,²¹⁸ and applied it to an LNG facility. This safety assessment method, allows for a simple mathematical equation that considers type of infrastructure, the casualties, economic impact, length of outage, impact on other sectors and environmental impact that would ensue from an LNG hazard. Coupled with a logical flow process (which involves setting security goals, identifying assets, risks to assets and implementing protective programs), this method can determine the effectiveness of a protective measure for an LNG facility.

2.4.1.1 Accident Modelling/Mitigation

Continuous monitoring and implementation of appropriate actions are essential to prevent, control and mitigate unfavourable consequences of LNG production and use. LNG facilities have a good safety record and as a result failure data on LNG systems are sparse. Due to this limitation in failure data for risk analysis, Yun et al.²¹⁹ devised a Bayesian-LOPA (layer of protection analysis) method for obtaining risk with less effort and time compared to most other methods. The Bayesian estimation allows for generic failure data (fire or explosion) from other industries, to be coupled with likelihood information from LNG industry, in order to determine failure data to be used in the risk analysis. HAZOP (Hazards and Operability Study) was incorporated, including gamma and Poisson distribution for prior and likelihood

information. This methodology was validated against existing data and studies to show that it is a powerful method especially for an industry (such as the LNG industry) where failure data is sparse.

Considering the cryogenic properties and flammable/explosive behaviour of LNG, Rathnayaka et al.²²⁰ recently developed and validated a new accident modelling approach that also incorporates HAZOP based on system safety identification, protection and prevention (i.e. SHIPP) for applications to an LNG facility. SHIPP is a safety assessment methodology that describes the steps of process safety assessment and provides a guide to possible improvement at every step of the accident process. Following the process accident scenarios identified using HAZOP, the accident process follows three steps: initiation, propagation and termination. To develop a predictive model for the occurrence of abnormal events, a Poisson probabilistic distribution was incorporated. This method was tested to be reasonably effective using realistic data from an LNG facility,²²⁰ with an overestimation up to 14% for the first three time intervals and then underestimations (with decreasing accuracy) as time intervals increases.

On the other hand, Parihar et al.²²¹ devised a method for consequence analysis at deep-water facilities. The method consists of the use of analytical models to describe the dynamics of unconfined spills; semi-empirical models for pool fires; and CFD for vapour cloud dispersion (this information was previously discussed). Such information is routinely needed for independent risk assessment studies of proposed facilities and the methodology has been validated and scrutinised against test data.

Li and Huang²²² developed a more mathematical based approach for assessing the level of risk and damage to facilities and humans at different radii from an LNG fire or explosion. The analysis consists of using the DOW method for fire risk analysis and a vapour cloud explosion (VCE) model. It is generally accepted that the likelihood of a boiling liquid expanding vapour explosion (BLEVE) occurring in an LNG tank during an LNG pool fire is low due to safety measures currently in place.²²³ However, BLEVE should not be disregarded as one BLEVE event did take place in Spain (June 2002), involving a road LNG tanker accident.²²⁴ The BLEVE event is usually followed by a fireball from which ~one-fourth of its energy is

releases as radiation.²²⁵ Li and Huang²²² included BLEVE for risk analysis by making use of the BLEVE model proposed by International Labour organisation.

In the event of a leakage or emergency, emergency shutdown (ESD) systems in the LNG plants can be used for stopping pumps etc. and isolating the leakage automatically.²²⁶ Therefore it is crucial that this ESD system is reliable and always operational in order to mitigate hazards and prevent escalation. Cheng et al²²⁷ devised a method in which fault tree analysis coupled with intuitionistic fuzzy set can be used to assess the reliability and find the component/s of the ESD that requires the most attention. Even though human expertise and knowledge of operations and maintenance of the ESD is required to collect failure information; this method has proven to be able to locate equipment whose improvements will greatly increase the reliability of the ESD, and resulting safety of the facility.

Looking from a different perspective, shutdowns are also periods during which maintenance takes place. To prevent loss of potential revenue during routine shutdowns, Keshavarz et al.²²⁸ determined a risk-based shutdown strategy to minimise the number of shutdowns, while maintaining minimal risk for the expected life time of the plant. This method is superior to traditional methods as it uses the Weibull distribution rather than linear failure probability methods; and can therefore accurately and easily use failure history data. The method can be used on both standby and redundant systems and takes account of numerous parameters including the current costs of the product. It was successfully tested on an APCI's PPMR process, showing that active redundancy reduces the risk for most short goal times. However, as the goal time increases there is a shift towards the standby strategy for reducing risk, suggesting that standby, active redundancy and preventative maintenance is crucial to preventing operational risks.²²⁸

In the case that a pool fire occurs, expansion foam, particularly high expansion (HEX) foam, can be effective in controlling LNG pool fire²²⁹ by blanketing the LNG pool surface, as a result preventing oxygen reaching the fire and also acting as an insulator by reducing fire radiation from the pool fire. An HEX foam application rate of 10 L/(min m²) is the most applicable and the fire control time can be reduced with an increase in application rate. The location of foam generation units and design are all crucial factors that should be considered; it is also important that the units are

available and operational at all times. Further investigation²³⁰ showed Foamglas is also able to significantly suppress LNG pool fires and is comparable (if not more effective) than expansion foams. However, Foamglas is not effective at LNG vapour mitigation.

Mitigation is also possible via CFD-based dynamic simulations of hazard consequence reduction. Sun et al.²³¹ examined both vapour dispersion by water curtains and fire mitigation by HEX foam using CFD validated against the well-known Falcon tests for vapour dispersion and the Montoir tests for pool fire radiation. Water curtains can reduce vapour cloud distance by approximately 61 – 84% while HEX foam application leads to a fire control time (time to reduced heat radiation by 90%) of 130s and 55s, which are comparable to 100 s and 60s from the respective experiments.²²⁹ This clearly demonstrates the great capability and applicability of CFD to hazard mitigation studies.

2.4.1.2 Other Safety Considerations

The historical safety record of LNG facilities has been excellent, mainly due to the international standard NFPA 59A design codes followed by the designers, constructors and operators. Taylor²³² presents a summary of the processes (NFPA 59A) that would be followed for site location and equipment placement. On the other hand, Raj and Lemoff²³³ discusses the risk evaluation approach of the 2009 edition (latest edition) of the NFPA 59A, compares it with the risk process of Europe and presents an example of how the NFPA 59A can be used. However, the NFPA is still lacking especially on criteria regarding radiant heat. It is clear that with the inclusion of consequence modelling, the process of determining the most cost effective and safest LNG plant can be accelerated.

Downstream safety in design is for chemical and refinery plants and follows a deterministic approach; while upstream is for offshore platforms and follows a risk based approach considering all risks. LNG plants are categorized as midstream. Due to increasing number of developments, the modularization concept is being widely applied to onshore LNG plant, leading to the plant design features becoming similar to that of offshore plants. Tanabe and Miyake²³⁴ compares the two approaches and

proposes a safety design approach for LNG plants, concluding that the most efficient way to ensure the safety integrity of the design is to have a good design basis and minimise uncertainty. Due to less flexibility of the module design, a deterministic approach appears to be more applicable for onshore modularized LNG plant and the approaches of using ‘Safety Criteria Design Basis Matrix’ and a ‘Hazard-Design Logical relation Tree’ are effective.²³⁴

Safety measures which are not usually fully developed at the early stages in current design practises are the emergency systems, the modularized plant and layout, and the tank selection. Due to this, Tanabe and Miyake²³⁵ discusses an approach to enhance safety design application at the concept definition phase. The proposed method is a combination of a ‘deterministic and risk based’ approach, which can overcome difficulties and restrictions due to limited information at the early stages of a project and will yield schedule and cost benefits.

2.4.2 Ships

Ships are the major carrier of LNG and the current world fleet consists of ~400 ships in size of 120,000 – 250,000 m³.²³⁸ There has been considerable interest in the use of LNG for ship propulsion,²³⁹ such as the dual-fuel steam turbine mechanical (DFSM) propulsion, dual-fuel gas turbine electric (DFGE) propulsion, dual-fuel diesel electric (DFDE) propulsion, and diesel mechanical propulsion with reliquefaction (SFDM+R).^{240, 241} Traditionally the DFSM propulsion has been the main system used but of low efficiency,²⁴⁰ with increase in LNG carrier size more suitable propulsion systems such as DFGE propulsion system is required. However, assessment on the applicability, availability and safety of these systems requires the considerations of numerous factors. For example, in terms of LNG vapour hazards for a gas leak in the DFGE compressor room, CFD simulations (using FLACS) showed that moving gas detectors to within the compressor room will eliminate a 50 s delayed detection time.²⁴⁰ It was also concluded that there is no benefit in having a second ventilation fan within the compressor room for leaks larger than 1.27 cm; and equipment outside the compressor room will not be affected by any fire that breaks out, unless the equipment is on the roof of the compressor room.²⁴⁰

The major contributors of risk associated with LNG shipping can also be determined via high-level risk assessments for LNG carriers. One approach is based on historical data of LNG accidents, published damage statistics and expert judgments for events such as collision, grounding, contact, fire and explosion and other events during loading and unloading.²³⁸ It was found that collision, grounding and contact was noted, together to account for 90% of the total incidents while LNG containment failure appears be amongst the highest contributors to risk (Table 24).²³⁸ Therefore, given the good safety record of LNG shipping, it is reasonable to focus more on ensuring that the LNG containments systems are designed to an acceptable standard; with cryogenic reliability and high thermal insulation performance for safe and efficient transport of LNG.

Table 24: Distribution of known relevant LNG accidents²³⁸

Accident category	Accidents (#)	Frequency (per shipyear)
Collision	19	6.7×10^{-3}
Grounding	8	2.8×10^{-3}
Contact	8	2.8×10^{-3}
Fire and explosion	10	3.5×10^{-3}
Equipment and machinery failure	55	1.9×10^{-2}
Heavy weather	9	3.2×10^{-3}
Events while loading/unloading	22	7.8×10^{-3}
Failure of cargo containment system	27	9.5×10^{-3}
Total	158	5.6×10^{-2}

2.4.2.1 Structure

Transportation of LNG is highly dependent on LNG tanker technology. As discussed in Section 2.2.3, the two mainstream tank systems are the membrane and the spherical tank systems (see Table 12) and recently the membrane tank system has been widely adopted due to its large capacity. The membrane system has a thermal insulating layer and a metallic membrane covering to maintain liquid-tightness without any leakage (as shown in Figure 8). The load of the LNG cargo is transmitted to the thermal insulating layers through the membrane (primary barrier).

It is likely that increased sloshing load in large-capacity LNG cargo containers may lead to failure of the corrugated section of the membrane.

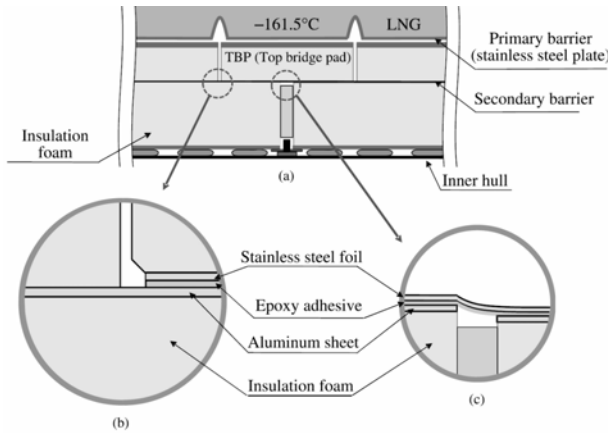


Figure 8: Schematic diagrams of LNG cargo containment system composed of primary and secondary barriers: a) overall drawing; b) enlarged view of the corner of top bridge pad; and c) insulation panels with level difference (adapted from the study by Bang et al.²⁴³)

Chul Kim et al.²⁵⁰ employed both experimental methods and finite element analyses (ABAQUS V6.7) to evaluate the pressure resistance of the conventional stainless steel membrane, via applying pressure loads to a 304L stainless steel corrugated membrane that is in most membrane tanks of Mark-III. Chul Kim et al.²⁵⁰ found the local yielding and plastic buckling loads of the three types of corrugations (the large corrugation, small corrugation and the large corrugation with reinforcing ribs) under the conditions of both symmetric loading and asymmetric loading (Figure 9). The addition of reinforcing ribs only seems to move the stress concentrations towards the ribs and results in larger deformations than the standard corrugations without ribs. Therefore, a new reinforcement method was then developed that inserts 2 mm thick 6061-T6 aluminium pipes into the corrugations. With testing it was confirmed that this new reinforcement method resulted in no permanent deformation of the corrugations or membrane; as a result increasing the pressure resistance of the membrane without compromising flexibility.

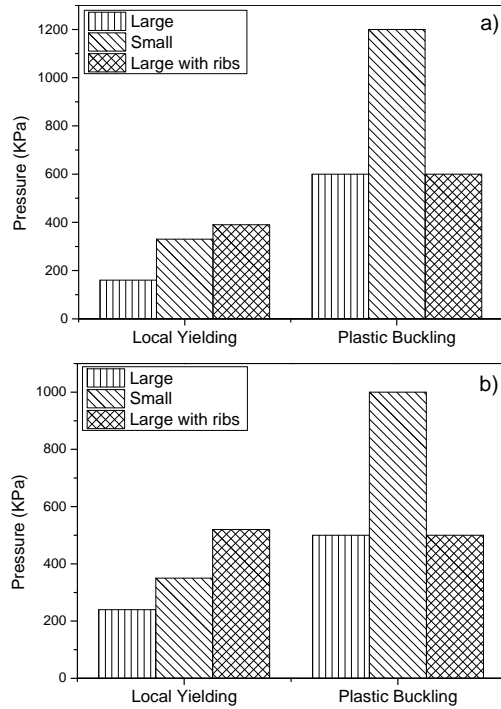


Figure 9: Yielding and buckling pressures of corrugations under symmetric loading a) symmetric loading b) asymmetric loading (data were extracted from the study by Chul Kim et al.²⁵⁰)

In addition to membrane with rigid supports (rigid membrane), it is also important to model the membrane with flexible supports in both static and dynamic cases. Finite element analysis (software ABAQUS) for such cases showed that the responses from the dynamic case significantly exceed those of a rigid supported insulation, demonstrating the need to include both the flexibility and dynamic loading conditions in analyses for LNG membrane systems.²⁵¹ This is particularly important because sloshing flow in ship containment systems is excited by ship motion and the sloshing motion itself can also affect the ship motion. However, up to date, most studies are limited to linear studies of both ship motion and/or sloshing. An example is the study of Pistani and Thiagarajan²⁵² in which impact pressures from a sloshing experiment was measured for a two-dimensional tank, with discussion on the problems that would be encountered in sloshing experimentation and how to overcome those problems. Mitra et al.²⁵³ developed an analysis method coupled both finite difference and time domain panel approaches for 3D sloshing and ship motion, capable of predicting both sloshing heights and the hydrodynamic pressures on the containment walls for further analysis. The method was verified against the data from existing scaled experiments. As expected, that the sloshing height increases

with wave height; and the waves, current and wind acting at 90° to the direction of ship motion results in the highest sloshing values. However, the effects of the waves were significantly more dominant (by up to 33%) than that of the wind and currents. The study further illustrates the need to include dynamic effects on studies of sloshing within LNG ship containment systems.

2.5 Conclusion and Research Gaps

The increasing demand of LNG as an energy source has led to increasing research interests regarding the risks involved in LNG storage, handling and transportation. Major conclusion in research gaps are briefly summarised below.

2.5.1 LNG Spill, Vapour Production, Dispersion, and Combustion

In spite of significant research advances, further research is required to better understand the hazards following an LNG spill. Particularly, there is a lack of experimental data from large-scale spills; under the circumstances where large-scale experiments are not feasible, specially-designed small-scale experiments need to be carried out for validating mathematical models.

Pool formation. The effect of sea waves on LNG pool formation and spread is not well understood. A major assumption so far is that the surface of the sea is flat while in reality it is dynamic and turbulent. The effect of currents associated with the waves can also have a large impact on the dynamics of the LNG pool and should be considered in future studies. Future research is also need to investigate the influence of the surface temperature of the substrate on LNG pool formation, especially ice formation from LNG spill on water due to the cryogenic temperatures of the LNG.

Vapour dispersion. There are various factors affecting LNG vapour clouds such as method of release (above water verse under water), spill rate, wind speed, atmospheric stability, rapid phase transitions, vaporization rate, obstructions and terrain. Recent studies have added to our knowledge by showing that water curtains are effective methods of controlling LNG vapour dispersion by imparting heat and momentum to the vapour cloud. Any increase in the turbulence of the substrate (spill on water) will lead to an increase in the evaporation rate of the LNG. Obstacles also result in a decreased lower flammability limit and terrain effects can lead to an

increase in turbulence. Therefore, the use of vapour fences for LNG dispersion control can be effective. However, new hazards can develop due to the build-up of vapour within the vapour fence. The past studies were also on small scales so that future experimental investigations are required at medium/intermediate scale experiments (200 m^3) for reducing epistemic and aleatory uncertainties. In addition, the scientific basis of many models have been questions especially integral models so that vapour dispersion simulation utilising field models (Navier-Stokes models) is highly desired because these models provide the most complete representation of the fundamental fluid dynamics.

Combustion. There have been several studies on LNG fires with the aim of determining the thermal radiation, burn rate and flame speed. Recent studies have shown that in the case of LNG vapour cloud ignition, the low reactivity of methane (the main component of LNG) results in overpressures within a safe range but the likelihood of high overpressures should not be neglected. It is also concluded that LNG releases and ignition will not produce a significantly large impact than a smaller less volatile material such as gasoline or LPG. A key gap in the field is the lack of large-scales LNG fire experiments, which should be well designed and conducted with correct instrumentation in a controlled environment, enabling easier determination of the key parameters affecting the flame's behaviour. Such more experimental data are essential to the validation of flame model.

2.5.2 Safety

The majority of studies on LNG deal with safety, with some focusing on the effects of LNG hazards on personnel or facilities. Various modelling techniques have been developed for safety assessment and may be effect for studying realistic scenarios. Mitigation techniques such as ESD, routine shutdowns, and the use of HEX and Foamglas have also been studied with the aim of improving safety in the most cost-effective way. In regards to LNG carriers, the flame treatment of the aluminium sheets in the insulation barrier of LNG ship containment systems is now known to lead to best bond strength. With the assistance of stud welding of support plates, adaptive curing of the adhesive, and glass reinforced fibres, the insulation foam is believed to provide the best crack retardation ability, leakage prevention and thermal insulation.

There are at least several aspects that require future R&D. First, it is still unclear whether the current criteria for exposure to a radiant heat flux of 5 kW/m² is suitable to prevent 2nd degree burn injuries. Therefore, further research that also considers duration of exposure and the physical, thermal and physiological properties of the receptor need to be conducted to determine whether this radiant heat flux range is suitable. Second, assessments of LNG safety issues need to integrate the credible inputs from the predictions of modelling with relevant complex conditions and geometries tailored to the underlying applications. Third, further improvements are required in the methodology of studying the LNG containment systems of ships. Particularly, the use of dynamic simulations/studies is highly recommended because the effect of dynamic loading (such as sloshing) can exceed those of static loaded cases.

2.6 Research Objectives of Current Study

Numerous research gaps in the LNG value chain have been identified from the literature review, as listed in Section 2.5. The scope of the thesis focuses on the downstream side of the value chain, notably LNG spill, pool formation and dispersion modelling. The main objectives of the study are listed below:

- (1) To develop a CFD code for modelling LNG spill, pool formation and vapour cloud dispersion;
- (2) Investigate the effect of impoundments, such as vapour fences, on LNG spill, pool formation and vapour cloud dispersion;
- (3) To examine the effect of air and sea surface temperatures on LNG spill, pool formation and vapour cloud dispersion;
- (4) To investigate the effect of atmospheric and sea stability on LNG spill, pool formation and vapour cloud dispersion; and the implications of the finds on Australian LNG export.

3 METHODOLOGY

3.1 Introduction

The aim of this study is gain a clearer understanding of LNG spills, pool formation and dispersion. To achieve this, the popular and commonly used ANSYS Fluent CFD program was utilised to conduct an in-depth analysis of LNG spills, pool formation and dispersion modelling. A series of three-dimensional simulations were carried out, so that the evolution of natural gas vapour cloud following an LNG spill can be monitored. This chapter details the methodology used to setup and run conduct the various studies.

3.2 Pre-Processing

The pre-processing section is the first stage of fluid modelling. In this stage the domain is created, meshed, initial conditions and boundary conditions applied, and simulation controls are set.

3.2.1 Geometry

Fluent uses Gambit, an industrially recognised geometry and meshing program for its applications. Most geometry can be built in Gambit or imported from another computer aided design system. Imported geometries are converted into suitable domains by virtual tools, in preparation for analysis by Fluent. As the geometries for this study are relatively simple, all geometry generation were conducted in Gambit.

3.2.2 Meshing

As mentioned previously, meshing is also conducted via Gambit. The following meshing techniques are automatically created by Gambit.

For 2D cases the following meshing types can be selected:

- Quadrilaterals
- Triangles

While 3D domains utilise the following meshing types:

- Hexahedra
- Tetrahedral
- Prisms
- Pyramids

3.2.3 Controls

Once the geometry has been created and meshed, it is ready to be opened in Fluent. When Fluent is opened it is crucial that the mesh is scaled to ensure that the appropriate dimensions are transported over. It is also very important to check the mesh using Fluent to ensure that no errors are evident which could cause problems when the simulation is running.

Once the mesh has been checked and scaled the model is ready to be finalized for simulation. In this stage the following steps must be defined and inputted:

1. Define the models and solver controls
2. Define the material properties
3. Define the operating conditions
4. Define the boundary conditions
5. Solver residuals
6. Solver initialization
7. Solver iteration

In Step 1 the models and solver controls need to be defined. For a transient buoyancy and velocity driven flow (as is the case in the current study), a pressure based solver with continuity models, energy equation models, turbulence models, multiphase models, mass transfer models and species transport models are needed; and as the study progresses to Chapter 6, wave modelling is also required.

In Steps 2 to 4, the material properties, operating and boundary conditions are defined.

In Steps 5 to 7, the simulation controls are set. These include the Solver initialization in which initial simulation values are set; Solver residuals, in which a means for monitoring convergence is set; and Solver iteration, in which simulation iteration step sizes and run time is set.

3.3 Processing

The computational grid (mesh) is the core of the CFD calculations. The mesh divides the domain into a great deal of tiny cells (finite volumes) and calculations are conducted at the nodes of each of these tiny volumes. Unstructured grid technology is used by Fluent, meaning that the grid can consist of multiple meshing types. This combination of complex modelling and unstructured meshing allows Fluent to

accurately model and analyse laminar and turbulent flows, with and without heat transfer, reactions or phase change.

To reduce the computation time of modelling, Fluent can utilise a non-iterative time advancement scheme and/or parallel processing. The non-iterative time advancement scheme reduces the time it takes transient simulations to obtain a solution, whereas the parallel processing capability involves distributing the work load dynamically among multiple computers in a network to solve a simulation, effectively reducing the simulation time.

3.4 Post Processing

This is the final stage of fluid modelling, in which the data is analysed. Fluent uses a wide range of post processing tools including:

- Shaded/transparent surfaces
- Fluid pathlines
- Scene reconstruction
- Contour and vector plots

The solutions will be exported to CFD-Post, an independent program for analysing the simulation data. A wide range of post processing tools are utilised by CFD-Post which include:

- Overlaying the model with plots including contour, X-Y plots and sketches.
- The ability to dissect models to observe internal flow patterns. These can be captured in screenshots and later animated.
- Being able to obtain data about the flow conditions at different points of the model.

Concentration contours were the main method of analysing data in this study of LNG spills. Firstly, concentration contours developed in Fluent were visually analysed by focusing on the flow behaviour and distance to the lower flammability limit (LFL). After the visual analysis, time-variant concentration profiles (change of temperature with time) at fixed locations were obtained to analyse the dispersion behaviour of the vapour cloud within the flow domain. Based on the LFL and the time-variant concentration profiles, a clearer understanding of LNG spill and vapour cloud dispersion in different conditions can be understood.

3.5 Utilisation of Methodology

This section contains a summarised description of how the above methodology is utilised within Chapters 4, 5 and 6.

In Chapter 4 the direct CFD simulation method is developed. To validate the model, geometry replicating the Burro 8 spill terrain was created and meshed. The Burro 8 spill boundary and initial conditions were then applied and a simulation was conducted. The validated direct CFD simulation method was then used to study the effect of impoundments. During this simulation the geometry including meshing, boundary and initial conditions were also set to replicate that used in the Burro 8 spill; however an impoundment was also created around the spill pond.

In Chapter 5 further validation tests were carried out against Falcon 1 spill tests. This was achieved by creating geometry to replicate the spill environment of the Falcon 1 tests. The Falcon 1 spill boundary and initial conditions were then applied and a simulation was conducted. The validated code was then used to study the effect of sea surface and air temperatures. This was achieved by first constructing an LNG tanker on the sea surface, with a breach on the side of the LNG tanker just above sea level; the domain was then meshed. Boundary and initial conditions were set and a simulation of LNG spill, pool formation and dispersion was conducted.

In Chapter 6, the effect of sea surface and atmospheric stability on LNG spill, pool formation and vapour cloud dispersion was investigated. To carry out this study, wave modelling techniques were coupled with the direct CFD simulation method. The same LNG tanker geometry used in Chapter 5 was also used in this chapter. Boundary and initial conditions were set to investigate the effect of stability, and the simulation was conducted with the subsequent results analysed.

4 A CFD MODEL FOR THE SIMULATION AND ANALYSIS OF LNG DISPERSION

Based on the literature review in Chapter 2, it is clear that there are still numerous research gaps surrounding the LNG value chain. In Section 2.2.5, we showed that from the complete LNG value chain, the most likely cause of catastrophic events would be an LNG spill. Therefore the aim of this study is to gain a clearer understanding of factors affecting LNG dispersion process, following an LNG spill. To achieve this, the popular and commonly used ANSYS Fluent CFD program is deployed to develop a CFD code with the aim of been able to more accurately model LNG pool formation and dispersion process.

4.1 Direct CFD Simulation Method Development

4.1.1 Introduction

The spill and dispersion behaviour of LNG have been investigated via numerous experimental studies, such as the Burro Series,^{113, 114} Coyote Series,^{254, 255} Falcon Series,²⁵⁶ Maplin Sands tests,²⁵⁷ Esso tests,²⁵⁸ Shell jettison tests,²⁵⁹ Avocet²⁶⁰ and BFTF.¹⁵¹ However, due the difficult, risks and high cost associated with such large scale experiments, computational modelling of LNG spill and dispersion is strongly favoured.

As mentioned in Section 2.3.2.4 there are three categories of computational methods for modelling LNG spill and dispersion. The integral models, Box or Top-Hat models and Navier-Stokes models; of which the Navier-Stokes models such as computational fluid dynamic (CFD) models are been favoured for LNG spill and dispersion studies due to their accuracy and completeness.^{118, 163, 178, 261} However, in most CFD modelling of LNG dispersion different assumptions and estimates are made, such as; a) simplifying and combining the LNG spill, pool formation and vaporization is simplified to a natural gas mass flux source term; such as using the water pond surface in the Burro and Falcon series tests as the natural gas source term.^{118, 165} b) The vaporization rate is also often fixed to a constant value such as 0.029 and 0.195.^{118, 165} These estimates are derived from previously published

experimental data of LNG spills,³⁸ such an approach is not desired because the pool radius and vaporization rate for an LNG spill are not constant.^{123, 133, 183} During an LNG spill, the pool starts forming and as LNG evaporates due to heat transfer from the substrate, the vapour cloud forms. If the LNG spill rate is lower than the vaporization rate, the size of the pool will decrease and subsequently the evaporation of LNG; this results in a decrease of vapour cloud formation. Neglecting the pool formation process via a mass flux source term and fixing the vaporization rate to a constant value does not reflect the actual physical process. A two-phase jet model¹⁷⁸ was developed for LNG dispersion modelling; however the flash vaporization assumptions made, resulted in the LNG inlet conditions been set primarily as a vapour inlet condition (98.04% vapour volume/total volume), therefore restricting the models ability to demonstrate pool formation/spread modelling. Furthermore, it is believed that the CFD model should be able to capture the whole process including flash vaporization (if it occurs), based on the inlet and given conditions and in particular more accurately capture the turbulence generated during the spill. Therefore, the objective of this section is to develop a detailed CFD model which captures the spill, pool formation and dispersion of LNG, with the validation using experimental data from a Burro series test.

4.1.2 The Burro Series Test

The Burro series tests were conducted in conjunction by the Lawrence Livermore National Laboratory (LLNL) and the Naval Weapons Center (NWC) at the China Lake, California in 1980.^{113, 114, 262} Sponsored by the U.S. Department of Energy, the Burro series tests consist of eight LNG spills and one liquid nitrogen spill. The LNG was released through a 0.25m diameter pipe straight downwards at the centre of the water pond that had an average diameter of 58m (see Figure 10).

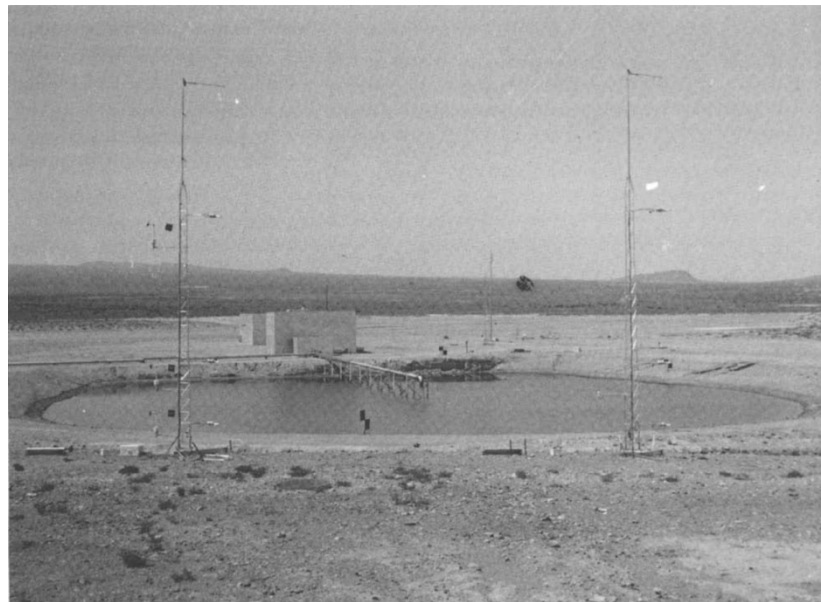


Figure 10: Spill facility and water pond.²⁶²

The spill volume ranged from 24 to 39 m³, the spill rate from 11.3 to 18.4 m³/min, the wind speed from 1.8 to 9.1 m/s, and the atmospheric stability from unstable to slightly stable. Twenty-five gas sensor stations were arranged in arcs, in the downwind side of the pool at distances of 57, 140, 400 and 800 m, respectively. Five turbulence stations and 20 wind field stations were arranged both in the upwind and downwind directions (see Figure 11). In this study, Burro 8 was selected to validate the model simulations because it was the most stable of the entire Burro series tests which resulted in a gravity driven dispersion process. The experimental data of the Burro 8 test is presented in Table 25.^{113, 114, 262}

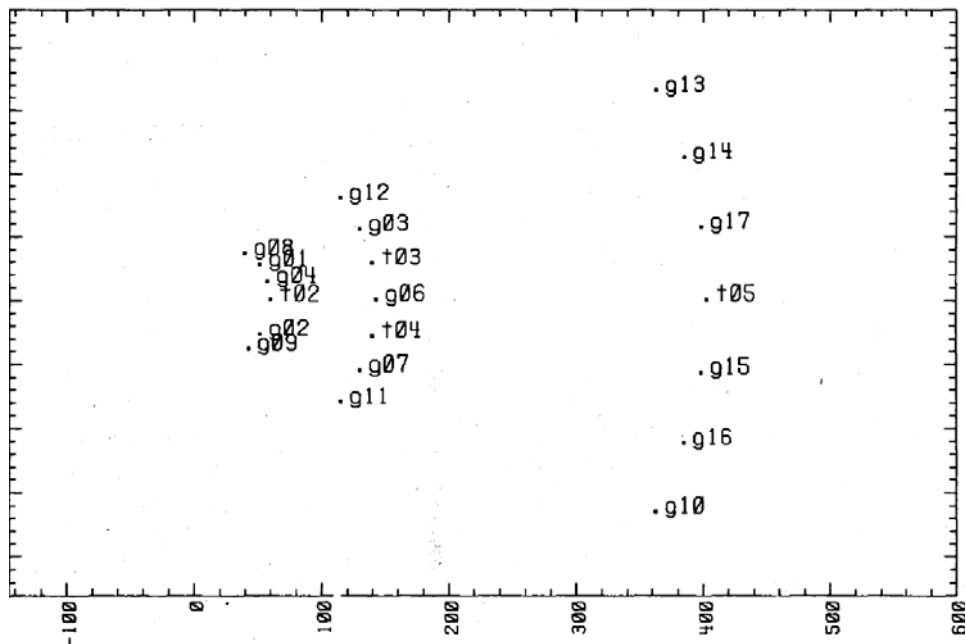


Figure 11: Gas sensor stations arrangement.^{113, 114}

Table 25: Burro 8 Spill: Atmospheric and Boundary Layer Conditions.^a

LNG composition (%)	Methane – 87.4 Ethane – 10.3 Propane – 2.3
Spill temperature (K)	111.7
Water pond diameter (m)	58.0
Spill rate (m^3/s)	16.0
Spill duration (s)	107
Spill volume (m^3)	28.4
Wind speed (m/s)	1.8 (-9.8° , wind direction)
Relative humidity (%)	4.6
Ambient temperature (K)	306.25
Atmospheric stability	Slightly stable (Class E)
Friction velocity, u_* (m/s)	0.075
Dynamical temperature ^b , T_* (K)	0.029
Surface temperature, T_0 (K)	310.76
Monin-Obukhov length (m)	15.1
Roughness height (m)	0.0002

^aData extracted from Koopman et al.^{113, 114, 262}

^bDynamic temperature also known as potential temperature is the temperature a parcel of air would have if it were expanded or compressed, adiabatically to standard pressure.

4.1.3 Mathematical Formulation

The direct CFD simulation method (DCSM) has been developed in ANSYS Fluent for predicting the spread and dispersion of natural gas by combining the Reynolds averaged Navier-Stokes (RANS) equations and Reynolds stress models (RSM) for process calculations. The major flow equations include the momentum, continuity, energy, turbulence and species equations,²⁶³ which are presented below. These flow equations are then closed by including a mass transfer model to incorporate phase change; while interaction between phases are considered via drag, slip velocities and surface tension modelling.

Continuity equation

$$\frac{\partial \rho}{\partial t} + \nabla \cdot (\rho \vec{v}) = 0 \quad (1)$$

where ρ is the density of the vapour cloud and \vec{v} is the three dimensional velocity vector. In the case of a multiphase flow, the continuity equation needs to integrate the mass transfer terms between phases and therefore Eq. (1) is modified as shown below, where m_{lg} is the mass transfer rate from liquid to gas phase, while m_{gl} is the inverse.

$$\frac{\partial \rho}{\partial t} + \nabla \cdot (\rho \vec{v}) = m_{lg} - m_{gl} \quad (2)$$

Momentum equations

$$\frac{\partial(\rho \vec{v})}{\partial t} + \nabla \cdot (\rho \vec{v} \vec{v}) = -\nabla p + \nabla \cdot (\bar{\tau}) + \rho \vec{g} + \vec{F} \quad (3)$$

$$\bar{\tau} = \mu \left[(\nabla \vec{v} + \nabla \vec{v}^T) - \frac{2}{3} \nabla \cdot \vec{v} I \right] \quad (4)$$

where P is pressure, $\bar{\tau}$ is the stress tensor, $\rho \vec{g}$ is the gravitational body force, \vec{F} is the sum of body forces including user defined sources, μ is the dynamic viscosity and I is the unit tensor.

Energy equation

$$\frac{\partial(\rho E)}{\partial t} + \nabla \cdot (\vec{v}(\rho E + p)) = \nabla \cdot \left(k_{eff} \nabla T - \sum_j h_j \vec{J}_j + (\bar{\tau}_{eff} \cdot \vec{v}) \right) + S_h \quad (5)$$

$$E = h - \frac{p}{\rho} + \frac{v^2}{2} \quad (6)$$

where E is the total energy, k_{eff} is the effective thermal conductivity, h_j is the sensible or latent enthalpy, \vec{J}_j is the diffusion flux of the species and S_h is the energy from a chemical reaction, if one exists.

Turbulence equations

The turbulence model used in this study is the realizable $k - \varepsilon$ model, which is more superior than the standard $k - \varepsilon$ model and reported to be excellent at capturing gravity slumping of dense gas flow, including the spatial and temporal concentration profiles of the vapour cloud in proximity of obstacles.^{118, 261} The realizable $k - \varepsilon$ model is presented below.

$$\mu_t = \rho C_\mu \frac{k^2}{\varepsilon} \quad (7)$$

$$\frac{\partial(\rho k)}{\partial t} + \frac{\partial(\rho k u_j)}{\partial x_j} = \frac{\partial}{\partial x_j} \left[(\mu + \frac{\mu_t}{\sigma_k}) \frac{\partial k}{\partial x_j} \right] + G_k + G_b - \rho \varepsilon - Y_M + S_k \quad (8)$$

$$\begin{aligned} \frac{\partial(\rho \varepsilon)}{\partial t} + \frac{\partial(\rho \varepsilon u_j)}{\partial x_j} \\ = \frac{\partial}{\partial x_j} \left[(\mu + \frac{\mu_t}{\sigma_\varepsilon}) \frac{\partial \varepsilon}{\partial x_j} \right] + \rho C_1 S_\varepsilon - \rho C_1 \frac{\varepsilon^2}{k + \sqrt{v\varepsilon}} + C_{1\varepsilon} \frac{\varepsilon}{k} C_{3\varepsilon} G_b \\ + S_\varepsilon \end{aligned} \quad (9)$$

where μ_t is the turbulence viscosity, k is the turbulence kinetic energy, ε is the turbulence eddy dissipation, G_k and G_b are turbulence kinetic energy generation due to velocity gradients and buoyancy respectively, while S_k and S_ε are the user defined source terms for k and ε .

Species transport equations

To account for species transport the following equations are used.

$$\frac{\partial}{\partial x} (\rho Y_i) + \nabla \cdot (\rho \vec{v} Y_i) = -\nabla \cdot \vec{J}_i + R_i + S_i \quad (10)$$

$$\vec{J}_i = - \left(\rho D_{i,m} + \frac{\mu_t}{Sc_t} \right) \nabla Y_i - D_{T,i} \frac{\nabla T}{T} \quad (11)$$

where Y_i is the mass fraction of each species, calculated, based on the compositions given in Table 25, \vec{J}_i is the diffusion flux, R_i is the net rate of species production, S_i is the source term, while $D_{i,m}$ and $D_{T,i}$ are the mass diffusion and thermal diffusion coefficients, respectively. Since there is no species production or source term but rather a mass transfer from liquid to gaseous mixture Eq. (10) can be modified to incorporate a mass transfer term as shown below in Eq. (12).

$$\frac{\partial}{\partial x} (\rho Y_i) + \nabla \cdot (\rho \vec{v} Y_i) = -\nabla \cdot \vec{J}_j + m_{lg} - m_{gl} \quad (12)$$

Mass transfer equations

To integrate phase change the above transport equations need to be closed. For mass transfer rate from a smooth phased interface, the Hertz-Knudsen-Schrage equation²⁶⁴ gives the following vaporization-condensation flux, based on gas kinetic theory. By tracking the volume fraction for LNG in each cell, it is possible to determine the interface between the LNG pool and the surround air and/or natural gas vapour; and subsequently the LNG pool size; from which the mass transfer will occur.

$$F = \beta \sqrt{\frac{M}{2\pi RT}} [P_{sat}(T) - P_v] \quad (13)$$

where F has units of kg/s/m^2 , β is the accommodating coefficient (molar fraction of condensation species in the gas mixture for condensation or molar fraction of evaporation species in the liquid mixture for evaporation), T , P and R are the temperature, pressure and universal gas constant, respectively. When Eq. (13) is coupled with the Clausius-Clapeyron equation,²⁶⁵ to account for saturation conditions, the following equation is derived.

$$F = \beta \sqrt{\frac{M}{2\pi RT}} L \left(\frac{\rho_g \rho_l}{\rho_l - \rho_g} \right) \frac{T - T_{sat}}{T_{sat}} \quad (14)$$

where L is the latent heat and T_{sat} represents the saturated temperature at vapour pressure. When modelling multiphase flows, the interfacial area density can be calculated as below.²⁶⁶

$$\frac{A_i}{V_{cell}} = \frac{6 a_{l,v}}{d} \quad (15)$$

where A_i is the area of contact between the phases of interest and V_{cell} is the cell volume, d is bubble diameter or pool length; when the interfacial area density is combined with Eq. (14) we arrive at the phase change source term (mass transfer equations).

$$\begin{aligned} \text{For vaporization, } T_L > T_{sat}, \quad m_{lg} &= F \frac{A_i}{V_{cell}} = C_{ev} \left[\rho_l \alpha_l \frac{T_l - T_{sat}}{T_{sat}} \right] \\ \text{For condensation, } T_L < T_{sat}, \quad m_{gl} &= F \frac{A_i}{V_{cell}} = C_{con} \left[\rho_g \alpha_v \frac{T_v - T_{sat}}{T_{sat}} \right] \end{aligned} \quad (16)$$

where $C_{ev} = \frac{6}{d} \beta \sqrt{\frac{M}{2\pi RT}} L \left(\frac{\rho_g \rho_l}{\rho_l - \rho_g} \right)$.

The coefficients C_{ev} and C_{con} are for vaporization and condensation, respectively.

4.2 Direct CFD Simulation Method Validation

4.2.1 Computation Geometry and Grid

As illustrated in Figure 12, the domain is a rectangular prism, oriented in such a way that the x -direction is the horizontal and parallel to the wind, the z -direction is horizontal and perpendicular to the wind and the y -direction is vertical. The origin of the domain is at the centre of the water pond and at ground level. The dimensions of the domain are $1000\text{ m} \times 50\text{ m} \times 500\text{ m}$ in the x , y and z directions, respectively. The domain was created in ANSYS design modeller by drawing a rectangular shape ($1000\text{ m} \times 50\text{ m}$) and then extruding to the desired width (500 m). A Boolean feature was then used to imprint the water pond at the desired location. The domain was discretised with hexahedral elements, which are known to be more computational efficient than tetrahedral elements. The mesh as shown in Figure 12 is non-uniform, this allows for a finer mesh to be used in areas of high flow gradients such as at the ground level and towards the centre of the water pond. This resulted in a total of approximately 430,200 hexahedra elements within the computational domain.

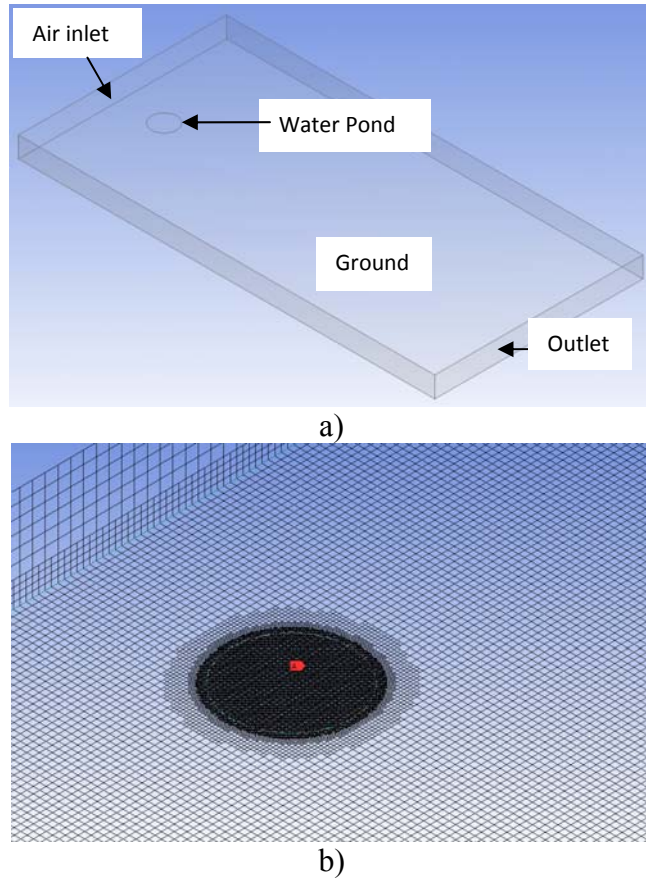


Figure 12: (a) Experimental layout and (b) hexahedral mesh with refinements towards the center of the water pond and approaching the ground surface.

4.2.2 Boundary Conditions and Initial Conditions

The computation domain consists of seven boundaries. The upwind boundary was set as a velocity inlet. The values for velocity, turbulence kinetic energy and dissipation and temperature were calculated as a function of height based on the Monin-Obukhov similarity theory,²⁶⁸ as shown below in Eq. (17) - (20).

For stable atmospheric conditions:

$$\phi_m = \phi_h = 1 + \frac{5Z}{L} \quad (17)$$

For unstable atmospheric conditions:

$$\phi_m = \left(1 - \frac{16Z}{L}\right)^{-0.25} \quad (18)$$

$$\phi_h = \left(1 - \frac{16Z}{L}\right)^{-0.5} \quad (19)$$

For neutral atmospheric conditions:

$$\phi_m = \phi_h = 1 \quad (20)$$

where ϕ_m and ϕ_h are the Monin-Obukhov similarity profile functions for momentum and heat transfer respectively, Z is the height and L is the Monin-Obukhov length (see Table 25).

For computational efficiency the side and top boundaries were set as symmetrical boundaries, since they are located far from the flow region of interest. This means that no flow crosses the top or side boundaries and there is no scalar flux across these boundaries. A wall boundary condition was applied to the ground with a surface roughness value of 0.0002 m, while temperature at this boundary was obtained by preventing heat flux out or in from this boundary. The outlet boundary was set as a pressure outlet boundary as flow conditions are not known at this boundary. This allows for the flow properties to be extrapolated based on the continuity equations. For the LNG inlet above the water pond, mass flow inlet was specified with a liquid mass flow rate, temperature and LNG properties set based on experimental data (see Table 25).

4.2.3 Solution Method

Boundary conditions throughout the domain such as the height-dependant velocity, temperature and turbulence were set according to the Monin-Obukhov theory.²⁶⁹ The following solution controls were selected, SIMPLE algorithm for pressure-velocity coupling scheme. The pressure, momentum and energy discretisations were changed to ‘Second Order upwind’ as it provides a higher level of accuracy. Parameters such as the under relaxation factors and the resolution were left as the default values as these parameters were suitable for the simulations been conducted. Prior to the injection of LNG, a steady state solution was obtained for the air velocity field. These values were then used as the initial conditions at time t= 0s, when LNG was injected into the computational domain. For the spill duration of 107 s, the LNG mass flow inlet boundary condition was maintained and then set to a mass flow rate of 0 kg/s for the remainder of the simulation (up to 560s).

4.2.4 Crosswind Dispersion

Figure 13 presents a time varying crosswind comparison of simulation to experimental results, vapour cloud concentration contours, at a 1m height, for 20, 60 and 100 s respectively after the LNG spill. The Burro 8 experiment had a stability class E, which means that the vapour cloud dispersion would be gravity-driven. This effect of gravity-driven flow, due to a heavier-than-air gas, leading to negative-buoyancy, can be clearly seen in the CFD simulation results. This coupled with a reduction in vertical turbulent mixing of the vapour cloud, has led to a more predominate growth in the lateral direction, earlier in the simulation and is in good agreement with dense gas behaviour.

The lateral spread of the vapour cloud was observed in both the experimental and simulated studies; however the lateral spread of the dense gas, for the simulated results, tends to be unpredicted throughout the simulation and becomes more accurate as the simulation progresses (Table 26). Earlier in the simulation, at 20 secs, the Direct CFD simulation method under predicts the vapour cloud lateral spread by up to 7.5% (Table 26) and this is due to the fact that the vapour cloud is in the early stages of forming so the effect of gravity flow is not as dominant. To add to this, the turbulent properties, such as the turbulent dissipation rate and kinetic energy were not provided in the Burro 8 experimental data (Table 25); as a result this was estimated based on other turbulent properties in the flow domain. As the vapour

cloud continued to spread, at 60 secs, the Direct CFD simulation method prediction for the vapour cloud lateral spread becomes more accurate, with an under prediction of 1.9%. At this point of the simulation the effect of gravity spreading and the atmospheric turbulent properties mixing the vapour cloud with the air is rightly captured. However as the simulation progress to 100 secs, it can be seen that the vapour cloud lateral spread under prediction is less accurate than that at 60 secs, but more accurate than that at 20 secs. This is a result of the vapour cloud approaching steady state and the estimated inlet wind conditions (due to fluctuating wind directions and speed in the Burro 8 experiments) which is now more dominant than the effect of gravity on the spreading process.

The comparison of vapour cloud lateral spread (Table 26) for the Direct CFD simulation method to the conventional estimated pool method shows that the Direct CFD simulation method is clearly in better agreement with experimental results; especially in the earlier stages of the simulation. This is because the conventional estimated pool method assumes that the LNG evaporates as fast as it is spilled, and that the evaporation process takes place over the entire water pond. However this is not the case, not only does the LNG not evaporate as soon as it is spilled but the turbulence generated during the spill and evaporating LNG pool has an overall effect on the LNG dispersion process. Therefore, capturing this phase change, which occurs earlier in the simulation including the properties of the different species involved, clearly has an impact on the lateral spread of the vapour cloud.

4.2.5 Downwind Dispersion

The downwind spread comparison of simulation to experimental results of vapour cloud concentration contours, at a 1m height, for 20, 60 and 100s respectively after the LNG spill, can also be analysed from Figure 13. As previously mentioned, due to a heavier-than-air gas, the effect of gravity leading to negative-buoyancy is well captured by the simulation; this including the effect of inlet wind flow has led to vapour cloud flow in the downwind direction and is in good agreement with dense gas behaviour.

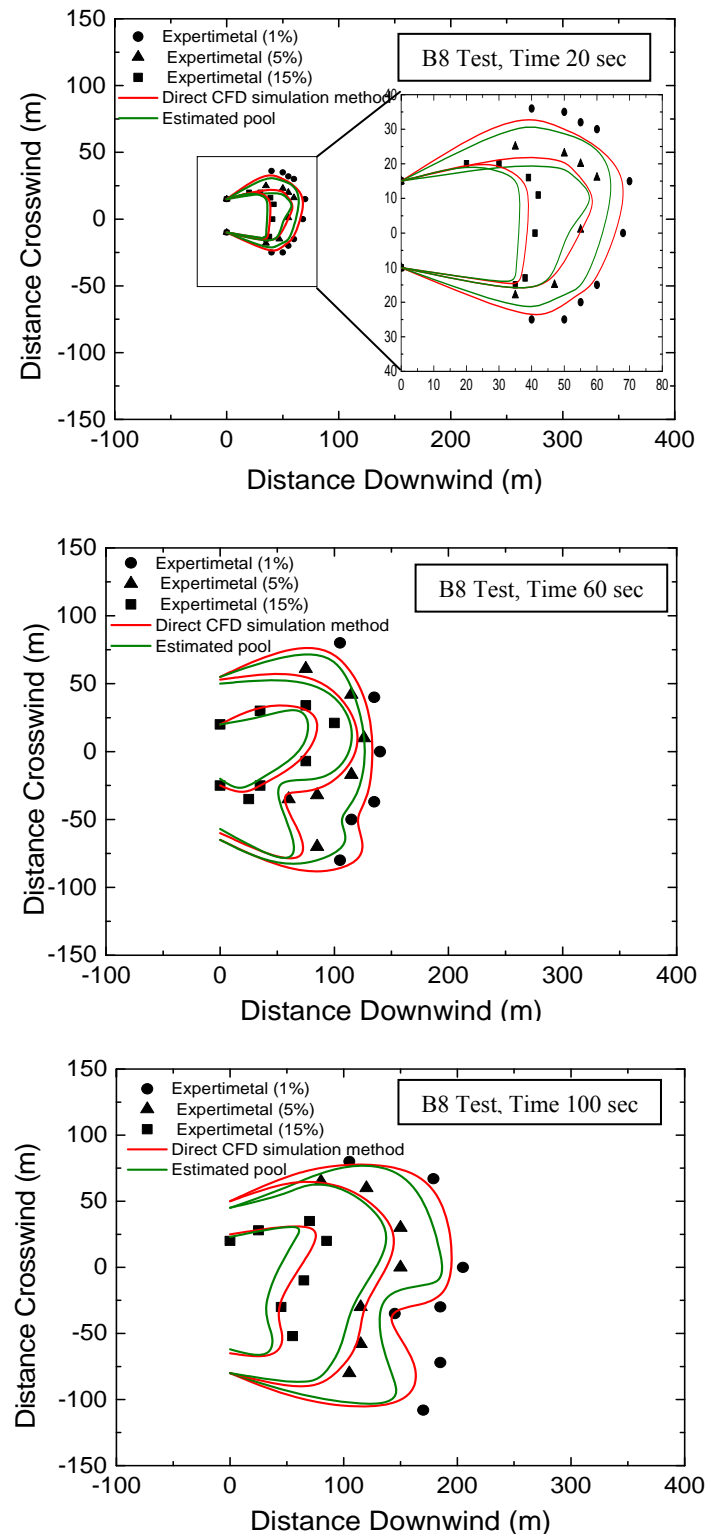


Figure 13: Comparison of CFD vapour cloud dispersion contours at a height of 1m to experimental results.

Table 26: Comparison of simulation crosswind and downwind dispersion to experimental data.

	20 sec		60 sec		100 sec	
	Direct CFD simulation method	Estimated pool	Direct CFD simulation method	Estimated pool	Direct CFD simulation method	Estimated pool
Width (m)	under predicted by 7.5%	under predicted by 17.5%	under predicted by 1.9%	under predicted by 9.5%	under predicted by 5.8%	under predicted by 5.8%
Length (m)	under predicted by 2.7%	under predicted by 8%	under predicted by 5.7%	under predicted by 10%	under predicted by 5.8%	under predicted by 8.7%

The downwind spread of the vapour cloud was observed for both experimental and simulated studies. It was noted that the downwind spread of the vapour cloud tends to be under predicted, and seems to be more accurate earlier in the simulation; as shown in Table 26. In the early stages of the simulation, at 20 secs, the vapour cloud downwind spread from the Direct CFD simulation method is under predicted by up to 2.7% and as previously mentioned, this is due to the fact that the vapour cloud is in the early stages of forming and therefore gravity flow is not as dominant. However, when the downwind spread and its lateral counterpart is compared to experimental data, at 20 secs, it is clear that the downwind spread is more accurate. The wind flow effect is more dominant in the downwind direction during this period of the simulation, this result in an increased vertical turbulent mixing and subsequently in a more accurate downwind vapour cloud spread. As the simulation progress, at 60 secs, the Direct CFD simulation method becomes less accurate, with an under prediction of 5.7%. The effect of gravity flow is becoming more dominated and therefore the vertical turbulence mixing of the vapour cloud with the surrounding air is reduced. This process decreases the effect the wind velocity and flow properties have on the vapour cloud and as a result the downwind spread is under predicted. By comparing the downwind and lateral spreads to experimental data, at 60 secs, it is clear that the lateral spread is more accurate. This can be attributed to the estimated inlet wind conditions provided (due to fluctuating wind directions and speed in the Burro 8 experiments) which are time averaged data and can result in under- or over

prediction of results. As the simulations approaches 100 secs, the Direct CFD simulation method has little to no change for downwind vapour cloud spread; as a result of the vapour cloud approaching steady state and the wind velocity/flow properties having a more dominate impact on the downwind spread of the vapour cloud due to increased vertical turbulence mixing.

Another important observed effect is the bifurcated vapour cloud effect, due to dominant gravity flow observed during the Burro experiments. At 100s into the simulation, the half lower flammability limit (1/2 LFL), for experimental results, was approximately at 196m downwind of the spill. This cloud bifurcation was well captured by the CFD simulation and overall has led to 1/2 LFL of 183m and 170m, for Direct CFD simulation method and the estimated pool respectively. The turbulence generated during LNG spill and phase change, captured by the Direct CFD simulation method induces earlier mixing with the atmosphere compared to the conventional estimated pool method; and complied with the energy utilisation/interaction with the environment and substrate can be seen to have an impact on the downwind vapour cloud spread and subsequently the LFL. This results in the Direct CFD simulation method providing results which are in better agreement with experimental data compared to the estimated pool method (Table 26).

4.2.6 Time Variant Vapour Gas Concentration Comparison

Time variant vapour gas concentration for both an estimated pool and Direct CFD simulation method formation are compared in Figure 14. Based on Figure 14 and Table 27, it can be seen that both Direct CFD simulation method and the estimated pool modelling under predict the maximum vapour cloud concentration; however the Direct CFD simulation method formation is in better agreement with experimental results.

The time required to reach peak concentration (arrival time) is similar for the simulation and experimental results (Figure 14) at sensors g02 and g07. On the other hand, the arrival time is shorter for the simulated methods when comparing to the experimental results for the sensor g10. It is can be seen that volume concentration of the methane at the g02 and g07sensors, for the experimental data is always higher than that of the simulated methods. The concentration vs time curve follows this

trend until approximately 300 secs and 350 secs for the g02 and g07sensors respectively. This under prediction by the simulated methods is due to not accurately capturing two main factors, the inlet conditions (namely the high momentum resulting from vertical turbulent mixing) and modelling of downwind dispersion. The high momentum from vertical turbulent mixing leads to a higher rate of vapour cloud production from the LNG pool and therefore a higher vapour cloud concentration in the atmosphere. On the other hand, the downwind dispersion influences the vapour cloud dispersion due to the turbulence properties of the flow field; higher turbulence will lead to more vertical mixing and subsequently a higher volume concentration vs time. As previously mentioned the atmospheric properties used in during the simulations were based on time averaged Burro 8 data and therefore does not accurately capture the peak concentration reached during the experiments. However, the ability of Direct CFD simulation method to utilise and capture phase change and mass transfer between the different phases allowed for a more accurate prediction of the peak methane concentration. This is because the vapour could dispersion and subsequently, methane peak concentration is link to the LNG entering the domain. Therefore accurately calculating the amount of LNG entering the domain will lead to a more accurate peak concentration.

As time passes, after the 300 secs and 350 secs mark, the methane concentration for the simulated methods are higher than that of the experimental results. This behaviour can be attributed to the downwind atmospheric turbulence and flow properties limiting the mixing of the vapour cloud with the surrounding air; because at this point of the simulation the vapour cloud is nearly completely dispersed, with the dispersion been primarily driven by atmospheric turbulence and flow properties. As previously mentioned, increased turbulence results in an increase in vertical mixing between the vapour cloud and the atmosphere. In the case of the simulated methods, the downwind turbulence properties were set equal to the upwind turbulence properties because they were not provided in the Burro 8 experimental data, this has contributed to an over prediction of the vapour cloud concentration after 300 secs as the vapour cloud approaches the downwind side of the domain. Other flow properties such as wind velocity, limit the speed at which the vapour cloud travels; temperature, control the rate of energy change between the LNG and vapour with the surrounds; and atmospheric turbulence can limit the mixing of the

vapour cloud with the atmosphere. However these atmospheric turbulence and flow properties were provided as time average data due to the fluctuating conditions experienced during the Burro 8 experiment and therefore not accurately represented during the CFD simulations. This behaviour is also the main reason for shorter arrival time presented by the simulated methods and subsequently the shape of the methane concentration curve for the g10 sensor. With the g10 sensor positioned far from the spill point, it is expected that the vapour cloud would be well mixed with the surrounding air and predominately driven by the atmospheric flow properties, resulting in a low volume concentration.

Statistical measures, as shown in equations (21) – (22), were also used for comparison of the experimental data to the two modelling methods, using fractional bias (FB), normalised mean square error (NMSE), geometric mean bias (MG) and geometric mean variance (VG).

$$FB = 2 \left(\frac{\bar{C}_P - \bar{C}_0}{\bar{C}_0 + \bar{C}_P} \right) \quad (23)$$

$$NMSE = \frac{(C_P - C_0)^2}{\bar{C}_P \times \bar{C}_0} \quad (24)$$

$$MG = \exp(\overline{\ln C_P - \ln C_0}) \quad (25)$$

$$\ln(VG) = \overline{(\ln C_P - \ln C_0)^2} \quad (26)$$

where C is the time average vapour cloud concentration, \bar{C} is the mean value of C based on all available sensors, subscripts (p) and (o), represent predicted and observed respectively.

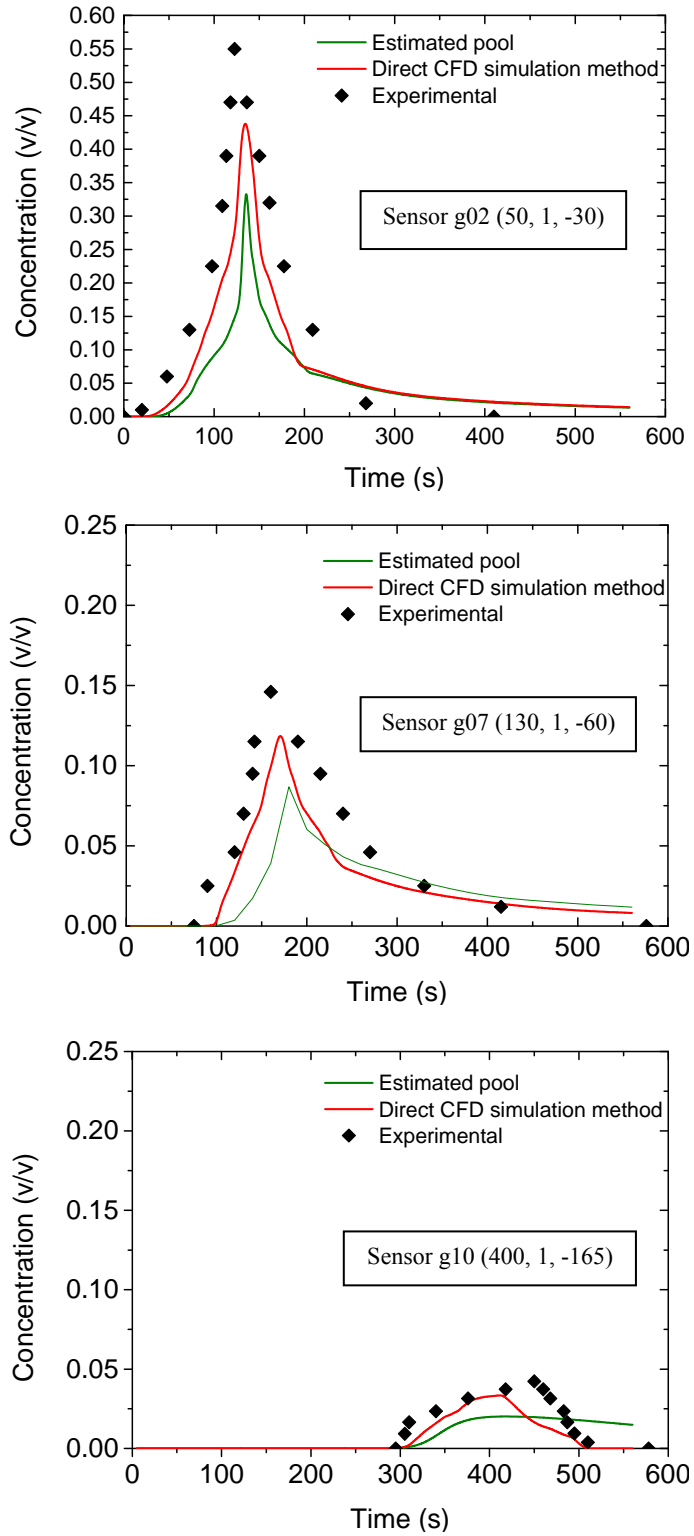


Figure 14: Comparison of time variant vapour gas volume concentration for predicted LNG pool formation vs direct CFD simulation method at different sensory locations with sensor's (x, y, z) coordinates given.

Table 27: Peak vapour gas concentrations at sensor locations.

Downwind distance (m)	Concentration (v/v)		
	Experimental	Estimated pool	Direct CFD simulation method
50	0.550	0.39	0.45
140	0.146	0.087	0.121
400	0.043	0.020	0.033

Table 28: Statistical performance comparison for the two source modelling methods.

Statistical number	Trial		
	Ideal value	Estimated pool	Direct CFD simulation method
FB	0	-0.340	-0.201
NMSE	0	0.119	0.041
MG	1	0.709	0.817
ln(VG)	0	0.118	0.041

Ideal values and the statistical performance measures are displayed in Table 28. Negative FB and MG lower than 1; means that vapour gas concentration is underestimated compared to experimental. Based on the statistical measure analysis, it is clear that the vapour gas concentration of both the modelling approaches under predicted the expected value, which was previously noted. Even though both inlet modelling methods under predict the expected vapour cloud concentration, it can be seen that the Direct CFD simulation method is closer to the ideal value and with less scatter than the estimated pool formation method.

4.3 Effect of Impoundments on LNG Dispersion

Impoundments are required for LNG spill control and depending on the type and size of the impoundment, LNG flow and vapour cloud dispersion can be controlled. In this study an impoundment of 80 m × 80 m × 3 m was used to enclose the water pond on which the LNG was spilt during the Burro 8 experiments. The geometry and mesh is shown in Figure 15. The boundary conditions and simulation setup are similar to that of the Burro 8 simulations with an LNG spill rate of 117 kg/s, wind

velocity of 2 m/s and direction of -9.3° and the simulation was run for 180 seconds (methodology detailed in Section 4.1). Two cases were considered; one without an impoundment and another with an impoundment.

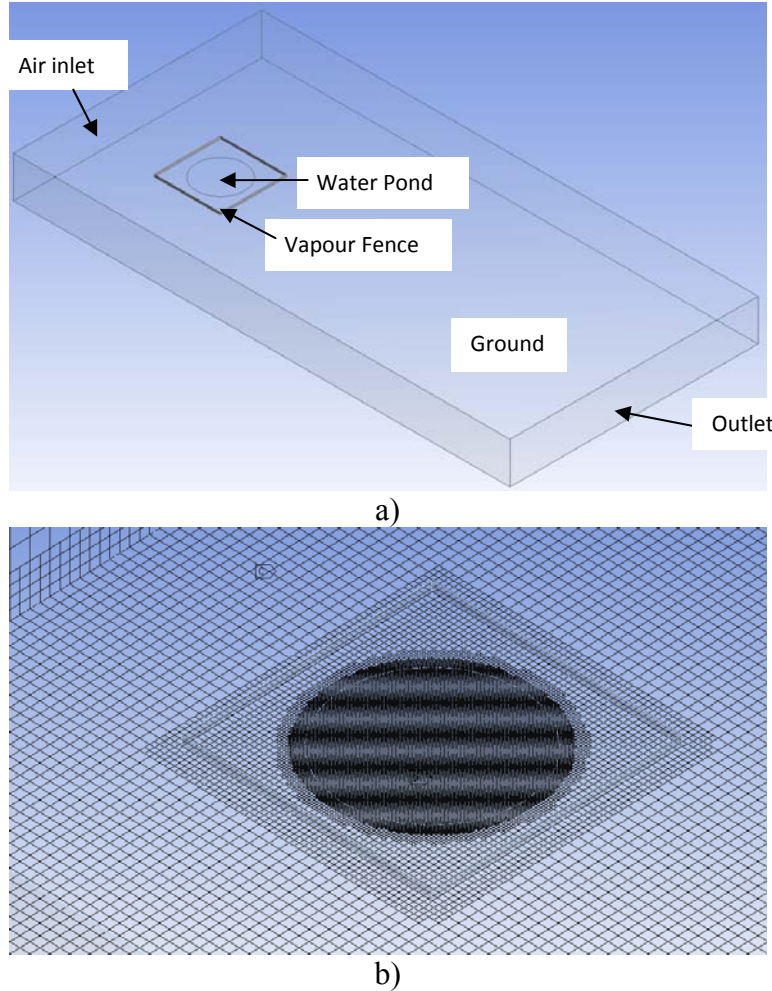


Figure 15: a) Experimental layout b) hexahedral mesh with refinements around water pond and vapour fence.

4.3.1 Vapour Cloud Dispersion

As mentioned in Section 4.2.4 the flow conditions of the Burro 8 experiment had a stability class of E, which led to a gravity driven flow and coupled with reduced vertical turbulence mixing led to a higher vapour cloud rate in the lateral direction, earlier in the simulation. This same effect can be seen in Figure 16. Table 29 contains the overall vapour cloud size, while Figure 16 shows the vapour cloud concentration contours for 15%, 5% and 1% respectively (left-right) and Figure 17 shows the iso-surface of $\frac{1}{2}$ LFL (2.5% v/v). At the 20 s mark, Figure 16, it can be seen that the case with an impoundment has a wider vapour cloud compared to that without an impoundment for concentration contours 15% and 5%. This is because at this point,

the vapour cloud within the impoundment has reached the upwind fence and therefore spreading in the lateral direction as the vapour cloud builds up at the vapour fence. Without an impoundment the vapour cloud has no obstacles restricting its flow and therefore continues to disperse downwind. The flow restrictions induced by the vapour fence then results in a thinner vapour cloud, 1% contour, past the vapour fence location compared to the case without a vapour fence. The length of the vapour cloud at this point in time is similar for all contours.

As the simulation progress, 100 s, the flow restrictions induced by the vapour fence is becoming more apparent; the vapour cloud without an impoundment already has a greater lateral and downwind spread. At this point the vapour cloud within the impoundment has fully encased the impoundment region and now with increased vertical turbulence and mixing with the atmosphere, is creeping over the impoundment (Figure 17).

At the 180 s mark, the different between the vapour cloud dispersion, with and without an impoundment, is quite drastic (Figure 16 and Figure 17). However it is interesting to note that there was little change in the overall vapour cloud spatial evolution from 100 s to 180 s (Figure 17). The main reason for this behaviour, in addition to its denser-than-air properties, is due to increased air flow turbulence and wind swirl/recirculation generated at the upwind side of the impoundment due to a reduced pressure gradient. This effect continues throughout the duration of the simulation, helping to contain most of the vapour cloud within the impoundment.

Table 29: Comparison of vapour cloud spatial evolution without impoundment vs with impoundment.

	20 s		100 s		180 s	
	Without	With impoundment	Without	With impoundment	Without	With impoundment
Width (m)	61	57	180	175	180	160
Length (m)	72	69	200	175	350	210

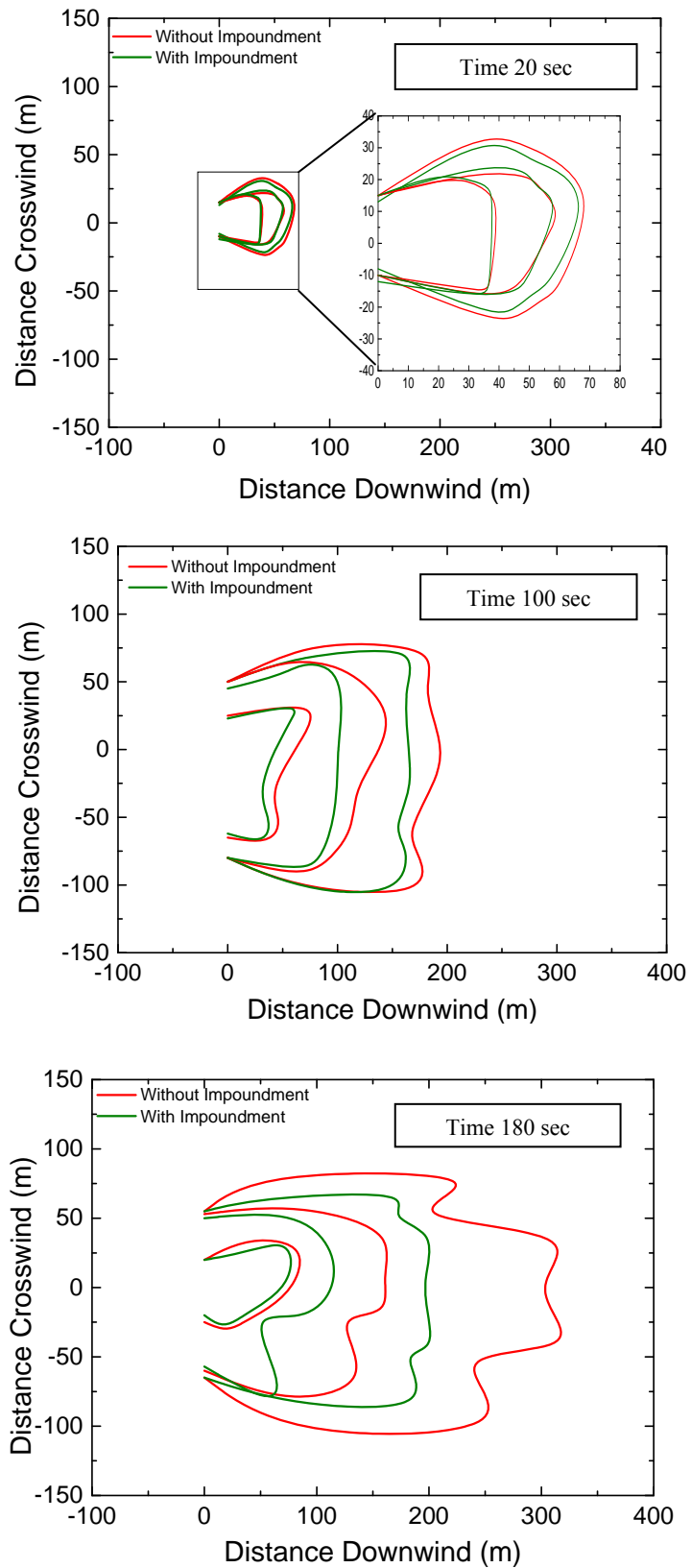


Figure 16: Comparison of CFD vapour cloud dispersion contours 15%, 5% and 1% respectively at a height of 1 m.

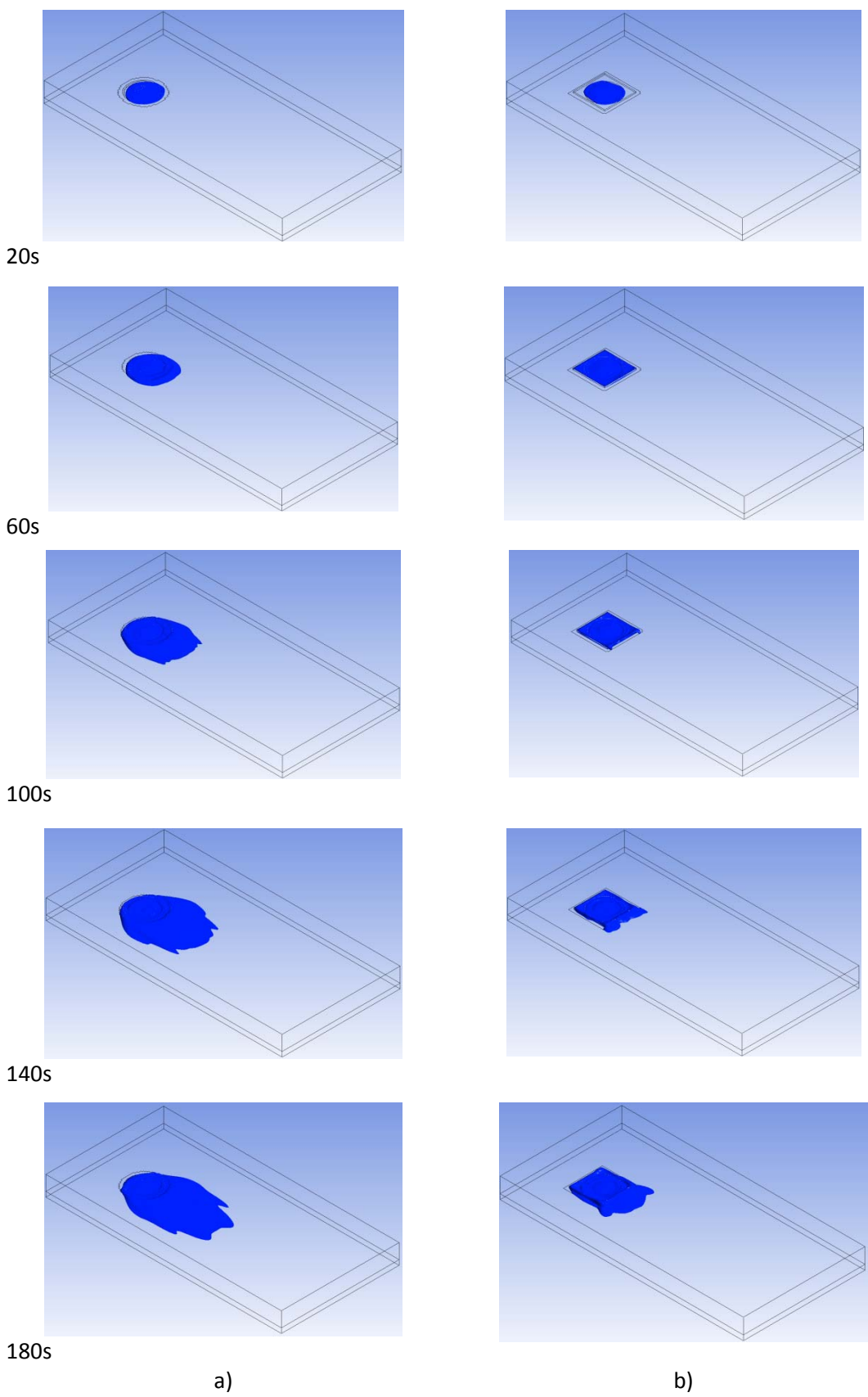


Figure 17: Comparison of 2.5% v/v at different times: (a) no impoundment (b) with impoundment.

4.3.2 Time Variant Vapour Gas Concentration Comparison

The time variant vapour gas concentrations are shown in Figure 18 with peak concentration values presented in Table 30 for the cases without and with an impoundment. Given that the dimensions of the impoundment are $80\text{ m} \times 80\text{ m} \times 3\text{ m}$, it is clear that vertex 1 is located within the impoundment. The temporal evolution of the vapour cloud concentration at this point shows that with an impoundment, the vapour cloud concentration is slightly higher (Table 30). This is because as previously mentioned in Section 4.3.1 with the vapour cloud contained within the vapour fence, it has a high amount of vertical turbulence mixing, however is unable to disperse downwind, unlike the case without an impound which is able to disperse downwind while mixing. The time required to reach peak concentration (arrival time) is similar for both cases (Figure 18), again the case with an impoundment has a higher arrival time, due to containment within the vapour fence.

Vertex 2 is located downwind of the vapour fence; therefore the peak concentration is now higher for the case without an impoundment (Table 30); as the vapour cloud for the case without an impoundment is now primarily driven by the flow field with increased vertical turbulence mixing. However, in the case with an impoundment, a majority of the vapour cloud is contained within the impoundment and the little amount that does manage to creep over the vapour fence is still primarily driven by the denser-than-air properties of the vapour cloud. This leads to the lower peak concentration at vertex 2; upon this the arrival time was still similar for both cases as was expected (Figure 18). This same trend continues as we move further away from the vapour fence; with vertex 3 located a significant distance from the vapour fence, the vapour cloud concentration, for the case with an impoundment, is almost non-existent Figure 18. However it is interesting to note that the difference between peak concentrations for the two cases at vertex 2 is also the same at vertex 3. This suggests that vapour fences have a fixed reduction on the peak concentration of vapour clouds that manage to creep over the vapour fence. In this case the reduction in peak concentration was 2.6% v/v.

Table 30: Comparison of peak vapour gas concentrations at different locations.

	Concentration (v/v)	
Downwind distance (m)	Without impoundment	With impoundment
Vertex 1	0.44	0.45
Vertex 2	0.121	0.095
Vertex 3	0.033	0.006

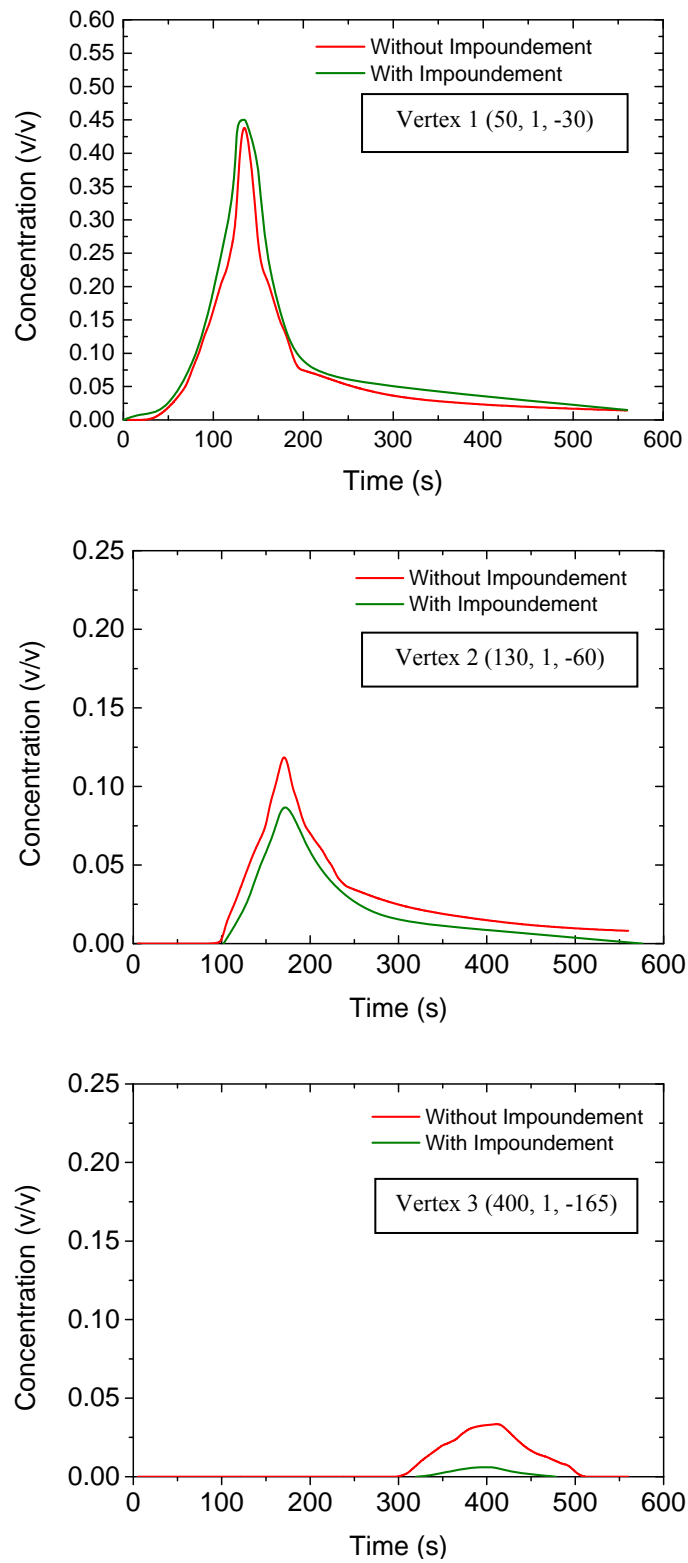


Figure 18: Comparison of time variant vapour gas volume concentration without impoundment vs with impoundment at different locations with sample points (x , y , z) coordinates given.

4.4 Conclusion

The Fluent CFD code was utilised to simulate the Burro 8 test, which involved LNG spill unto a water pond and dispersion downwind in an atmospherically stable environment. Two different input modelling methods were compared a) conventional estimated pool method and b) direct CFD simulation method. Both modelling methods were compared to experimental data and were noted to under predict both the general shape of the vapour cloud, the dispersion process, the volume concentration and arrival time of the vapour cloud. The underestimation of the vapour cloud behaviour is most likely due to many reasons with the two most significant been; the turbulence properties of the LNG inlet pipe been estimated and using a time averaged turbulent, atmospheric and boundary conditions. Upon this, when statistical measures were included in the analysis, it became clear that the LNG spill and phase change process, captured by the direct CFD simulation method, is significant and able to produce a more accurately representation of experimental data. These results show that, the direct CFD simulation method is more accurate and where possible, should be used when carrying out LNG dispersion simulations.

The DCSM was then utilised to investigate the effect of an impoundment on controlling LNG spill and dispersion in an atmospherically stable environment. An impoundment was found to contain an LNG spill and subsequent the vapour cloud to an extent. This was not only due to the barrier but also due to the increased air flow turbulence and swirl/recirculation at the upwind end of the impoundment. This analysis shows the power of an impoundment in controlling LNG spill and vapour dispersion, which will be valuable for LNG regasification terminals and LNG tankers. Overall, the effect of an impoundment on mitigating an LNG spill can be clearly seen. The impoundment contains the spill and limits its dispersion to an extent; in this case the impoundment was able to limit downwind dispersion by up to 55%, while limiting lateral spread by up to 25%, and led to a decrease in peak vapour cloud concentration of 2.6% v/v outside the vapour fence.

5 EFFECT OF SEA SURFACE AND AIR TEMPERATURE ON LNG DISPERSION

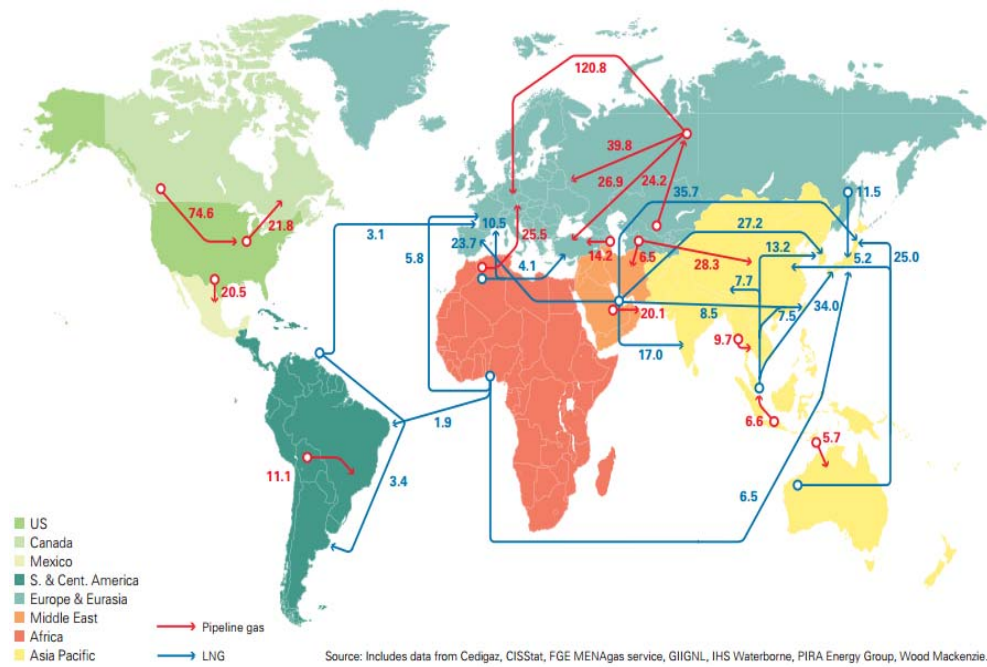
In this chapter, the direct CFD simulation code is used to investigate the thermal effects of substrates and surround atmosphere on LNG pool formation and dispersion process.

5.1 Modelling and Validation According to Sea Surface and Air Temperatures

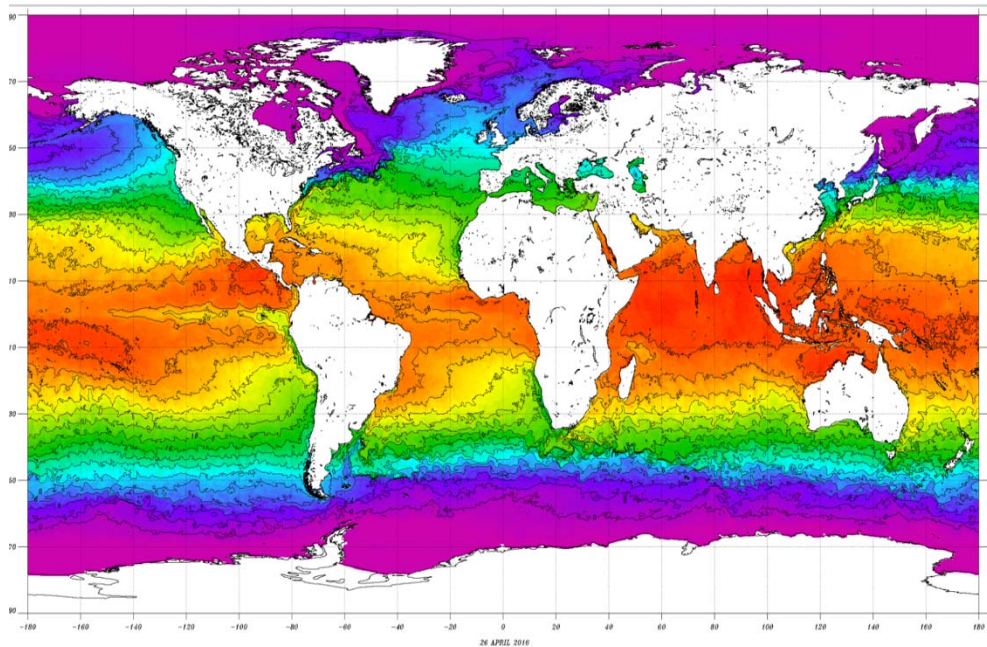
5.1.1 Introduction

Demands for natural gas as an energy source continue to grow as natural gas continues to be favoured as an environmentally friendly fuel.³ This growing demand of natural gas has led to the increased marine transportation of liquefied natural gas (LNG). The flammable characteristics of LNG and its growing demand and potential to impact economy make it a potential terrorist target.^{170, 270} Even though the safety records for marine transportation of LNG has been good since 1959,^{271, 272} it is crucial to understand the essential hazards involved in the transportation of LNG.¹

Various experiments were conducted to understand LNG spill and dispersion including Burro series,^{113, 114} Coyote series,^{254, 255} Falcon series,²⁵⁶ Maplin Sands tests,²⁵⁷ ESSO tests,²⁵⁸ Shell jettison tests,²⁵⁹ Avocet²⁶⁰ and Brayton Fire Training Field (BFTF).¹⁵¹ Of the previous LNG transportation spill studies conducted, certain factors that affect LNG spill and dispersion process have been considered such as but not limited to breach diameter and ullage pressure of containment tank,¹⁷⁰ unignited and ignited LNG pools¹²³, stationary and non-stationary tankers during spill process¹³³ and consideration of uncertainty during the modelling process.¹⁸³



a)



b)

Figure 19: (a) Major LNG trade movement in 2014 (billion cubic meters)²⁷³ and (b) correspond sea surface temperatures.

Figure 19 presents the major LNG trade movement in 2014²⁷³ and the corresponding sea surface temperatures.²⁷⁴ It is shown that the LNG transportation takes places in different oceans, which have a wide range of different environments and temperature conditions. Unfortunately, little has been done on the effects of such sea conditions on LNG spill and dispersion process. A recent study developed a LNG spill and dispersion modelling method based on computational fluid dynamics (CFD) that is able to model the complete LNG spill, pool formation and dispersion process.²⁶⁷ This direct CFD method eliminates the use of estimates such as the fixed vaporization rate or estimates mass flux source terms that are commonly used in the conventional methods^{118, 178} and lead to inaccurate predictions. Therefore the objective of this section is to utilise the direct CFD simulation method²⁶⁷ developed in Section 4.1 for assessing the effect of the ocean and surrounding temperatures on LNG spill, pool formation and dispersion. It is important to note that the case simulation includes an LNG tanker that will also act as an obstacle in the flow domain. Therefore, the Flacon series test experimental data that contain such obstacles were used for validation. Two tasks were completed in this section. One is the validation of the direct CFD simulation method using experimental data from the Falcon 1 series tests. The other is the use of the direct CFD simulation method to evaluate the thermal effect of the substrate and atmosphere on LNG spill and dispersion process.

5.1.2 Falcon Series Test

The Falcon series tests, sponsored by the U.S. Department of Energy, were performed by the Lawrence Livermore National Laboratory (LLNL) at the French Flat area, Nevada in 1987.²⁵⁶ The Falcon series tests were aimed at evaluating the effectiveness of impoundment walls and barriers for hazard mitigation from LNG spills and providing experimental data for model validations. Unlike other well-known large scale LNG spill tests, the Falcon series test contains obstacles such as the billboard and vapour fence. The Falcon series test consists of five LNG spills, during which the LNG was released through a 0.11 m diameter spill “spider” (Figure 20) straight downward at the center of a rectangular water pond with dimensions of 60 m × 40 m × 0.76 m.

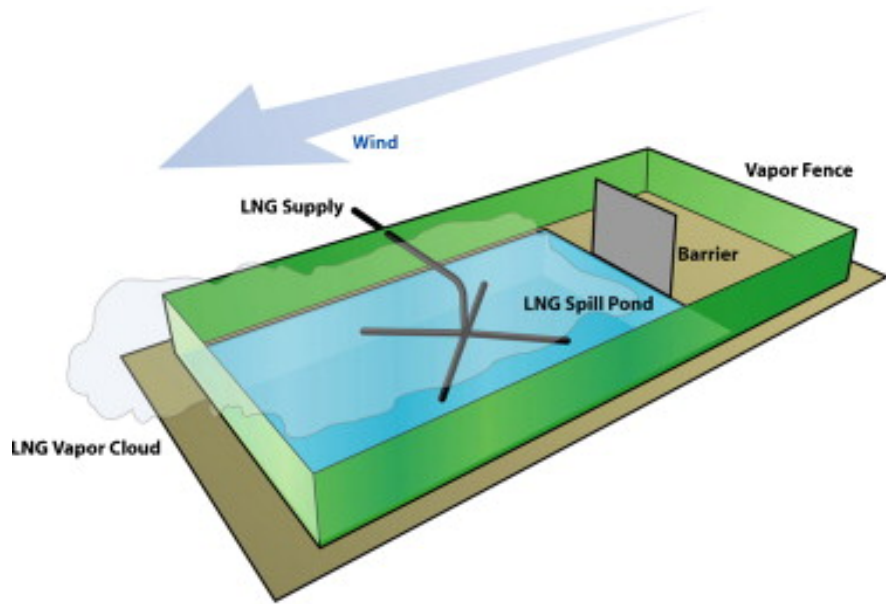


Figure 20: Falcon series experimental setup.¹¹⁸

The water pond was equipped with a recirculation system to maintain the surface temperature of the water pond, as would be expected of the water temperature at sea. The impoundment area $44\text{ m} \times 88\text{ m}$, was enclosed by a 8.7 m high vapour fence, with the addition of a 13.3 m tall, 17.1 m wide, billboard upwind of the water pond to act as a barrier as shown in Figure 2. The spill volumes ranged from 20.6 to 66.4 m^3 , the spill rate from 8.7 to $30.3\text{ m}^3/\text{min}$, the wind speed from 1.7 to 5.2 m/s , and atmospheric stability from neutral to stable. A total of 77 gas sensor stations, 18 turbulence stations, and 19 wind field stations were arranged all across the terrain to measure quantities such as pressure, humidity, temperature, heat flux, wind speed and direction, turbulence intensity and vapour gas concentration. In this study, Falcon 1 was selected to validate the model simulations because it was the most stable of the entire Falcon series tests with low wind speeds and large spill volume and flow rate. This is ideal for dispersion studies because it provides the worst case scenario in which the vapour cloud would not easily mix with the wind and would, therefore, linger with high concentrations compared to other cases. The experimental data of the Falcon 1 test is presented in Table 31.

Table 31: Falcon 1 Spill: Atmospheric and Boundary Layer Conditions.^a

LNG composition (%)	Methane – 87.4 Ethane – 10.3 Propane – 2.3
Spill rate (m^3/s)	28.7
Spill duration (s)	138.8
Spill volume (m^3)	66.4
Wind speed (m/s)	1.7
Relative humidity (%)	4.6
Ambient temperature (K)	306.25
Atmospheric stability	Slightly stable (Class E)
Friction velocity, u_* (m/s)	0.0605
Dynamical temperature, T_* (K)	0.0577
Surface temperature, T_0 (K)	304.5
Monin-Obukhov length (m)	4.963
Roughness height (m)	0.008

^aData extracted from Brown et al.²⁵⁶

5.1.3 Mathematical Formulation

The mathematical formulation is exactly the same as developed and explained in Section 4.1.3.

5.1.4 Computation Geometry and Grid

The computational domain is generated in a rectangular prism, as illustrated in Figure 21 oriented in such a way that the x -direction is the horizontal and parallel to the wind, the z -direction is horizontal and perpendicular to the wind and the y -direction is vertical. The origin of the domain is at the centre of the water pond, in-between the spill “spider” arms and at ground level. The dimensions of the domain are $500 \text{ m} \times 50 \text{ m} \times 500 \text{ m}$ in the x , y and z directions, respectively. The domain was created in ANSYS design modeller by first creating the individual faces of the vapour fence and billboard. A rectangular shape ($500 \text{ m} \times 50 \text{ m}$) was then drawn and extruded to the desired width (500 m). A Boolean feature was then used to subtract the vapour fence and billboard from the flow domain; while a Boolean-imprint feature was used to generate the water pond at the desired location. Hexahedral elements were used to discretise the domain and known to be more computational efficient than tetrahedral elements. The mesh as shown in Figure 21 is non-uniform, allowing for mesh refinement in areas of high flow gradients such as at the ground

level, including around the vapour fence and at spill points in the water pond. This resulted in a total of approximately 647683 hexahedra elements within the computational domain.

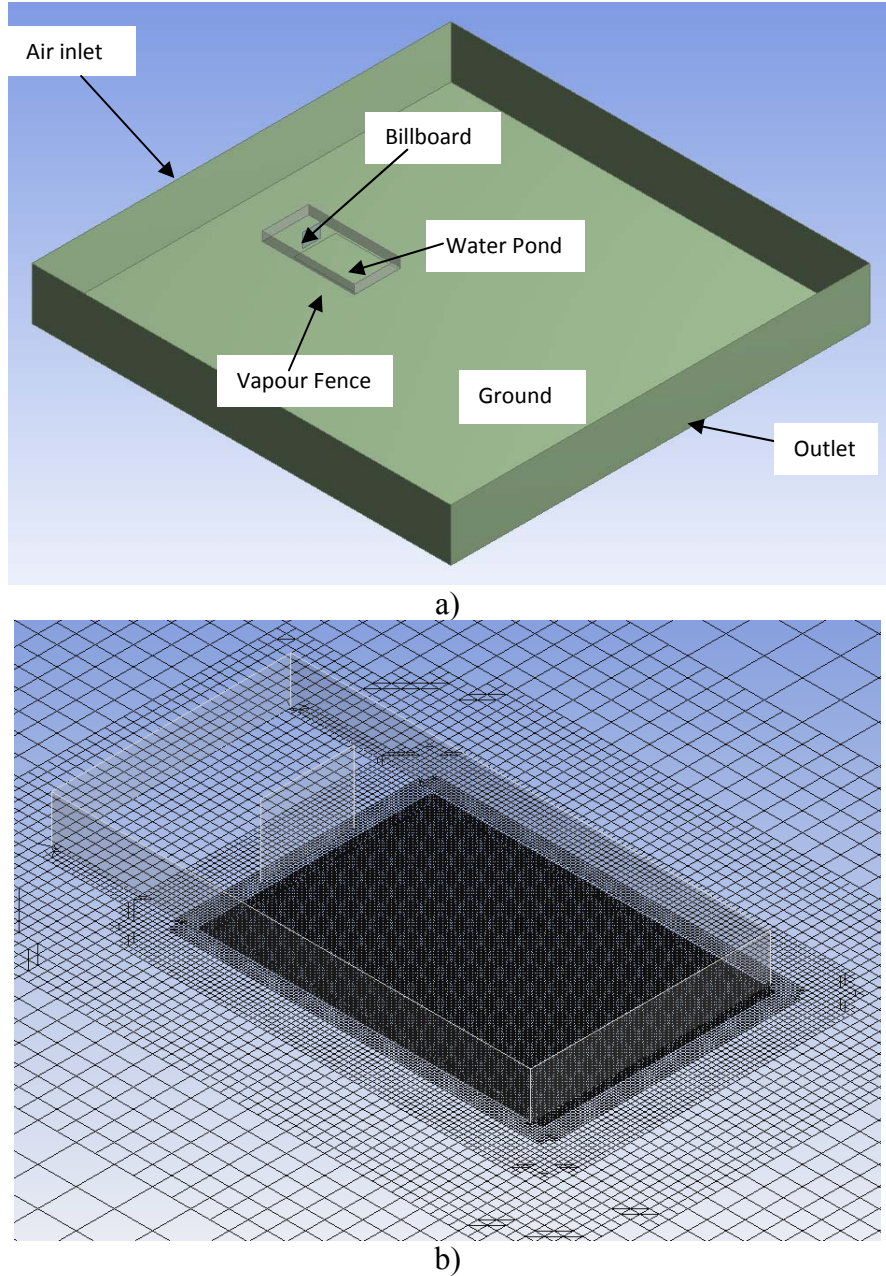


Figure 21: (a) Experimental layout and (b) hexahedral mesh with refinements around the water pond and approaching the ground surface.

5.1.5 Boundary Conditions and Initial Conditions

The boundary and initial condition setup is exactly the same as that demonstrated in Section 4.2.2, however with the use of experimental data from Table 31 for the Flacon test simulations. Once the validation simulations were completed the

following boundary and initial conditions were used to evaluate thermal effect of substrate and atmosphere on LNG dispersion process. A total of three scenarios were considered: the first scenario is a realistic scenario, in that both the air and sea temperatures are incremented from cool sea environments (toward the Arctic) to warmer sea environment (Pacific and Indian oceans) (Table 32), to accommodate for the travel routes of LNG tankers as depicted in Figure 19. In the second scenario the sea temperature is constant, while the surround air temperature is varied (Table 32). In the third and last scenario, the surround air temperature is held constant while the sea temperature is varied (Table 32). The simulation involved LNG spilling from a membrane LNG tanker, with a 1 m breach diameter, at a position 1 m above the sea surface (Figure 22). The LNG tanker was constructed to the dimensions reported previously:²⁷⁶ a double-hulled membrane tanker with full cargo capacity of 228000 m³, approximately 45600 m³ for each storage tank. The boundary conditions and simulation setup are similar to that of the Falcon 1 simulations, however with a wind velocity of 2 m/s.

Table 32: Air and Sea Surface Temperatures for the Different Scenarios and Corresponding Cases.

	Scenario 1 ^a		Scenario 2 ^b		Scenario 3 ^c	
	Temperature (K)		Temperature (K)		Temperature (K)	
	Air	Air	Air	Sea	Sea	Sea
Case 1	278.15	278.15	278.15	305.45	313.15	271.15
Case 2	286.90	286.90	286.90	305.45	313.15	279.73
Case 3	295.65	295.65	295.65	305.45	313.15	288.30
Case 4	304.40	304.40	304.40	305.45	313.15	296.88
Case 5	313.15	313.15	313.15	305.45	313.15	305.45

^aScenario 1: Realistic scenario with varying air and sea surface temperatures

^bScenario 2: Air temperature varied while sea surface temperature is constant

^cScenario 3: Constant air temperature while varying sea surface temperatures

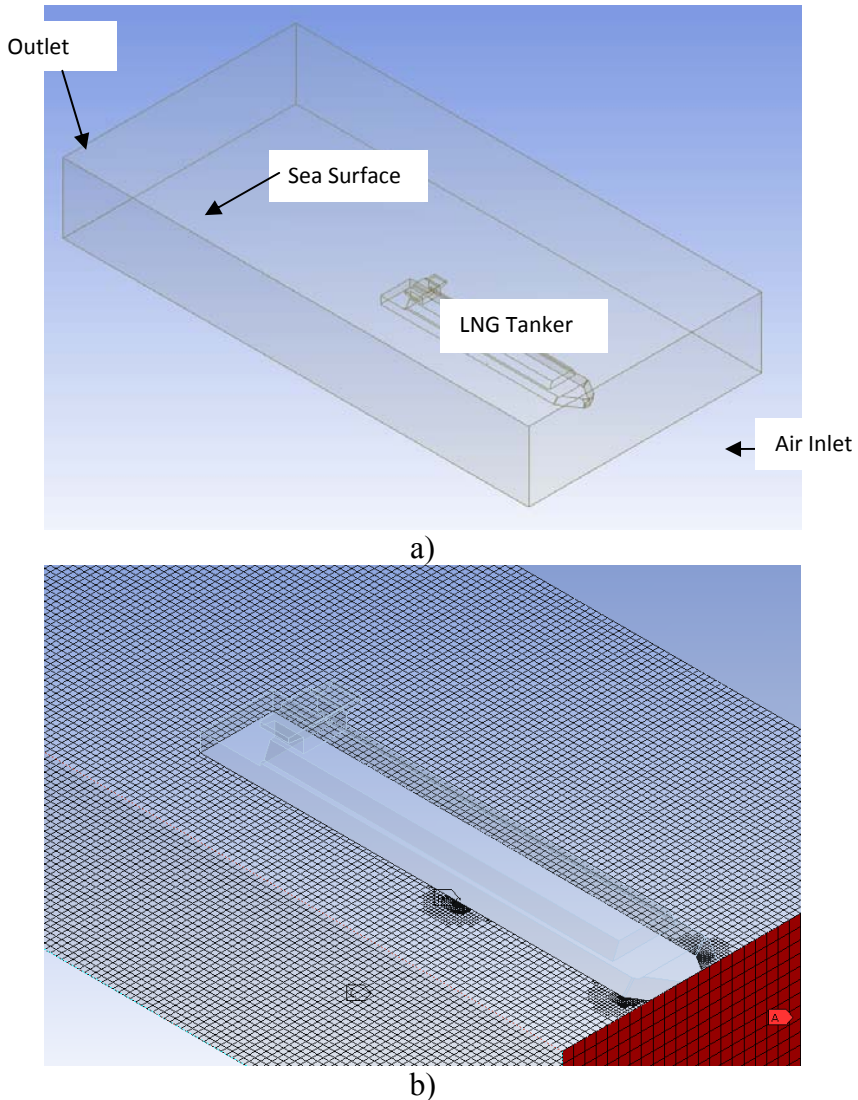


Figure 22: (a) Experimental layout and (b) hexahedral mesh with refinements in areas of high flow gradient.

5.1.6 Solution Method

The Monin-Obukhov theory and solution controls utilised in Section 4.2.3 were also used for the Falcon test and thermal effect simulation setups. For the Falcon test simulation, the following solution method was used; prior to the injection of LNG, a steady state solution was obtained for the air velocity field. These values were then used as the initial conditions at time $t=0$ s, when LNG was injected into the computational domain. For the spill duration of 138.8s, the LNG mass flow inlet boundary condition was maintained and then set to a mass flow rate of 0 kg/s for the remainder of the simulation (up to 800s). Prior to the injection of LNG, a steady state solution was also obtained for the air velocity field. These values were used as the initial conditions at time $t=0$ s, when LNG was injected into the computational

domain. The location of the 1 m breach led to a 27 m, LNG level above the breach, with a working pressure of 22 KPa driving the spill from the tanker and resulted in a spill time of 1297.89 seconds.

5.1.7 Vapour Cloud Dispersion Analysis

Figure 23 shows comparisons at different time frames between experimental and modelling results. The vapour cloud concentration contours were measured at a 1m height, for 100, 140, and 180 s at a plane 150 m downwind of the spill point. The low-wind and stable atmospheric conditions of the Falcon 1 test, including the vapour fence and billboard acting as obstacles, meant that the vapour was not easily mixed with the wind and, as a result, was primarily gravity-driven. This led to negative-buoyancy effects and when coupled with the reduced vertical turbulent mixing of the vapour cloud, has led to a more predominate growth in the lateral direction, earlier in the simulation, and is in good agreement with dense gas behaviour.

The general shape of the vapour cloud, both lateral spread and height, including the maximum methane concentrations were well-captured by the simulated studies. However as recorded in Table 33, the general shape of the vapour cloud tends to be slightly underpredicted earlier in the simulation. According to Table 2, at 100 s, the vapour cloud shape is slightly underpredicted by 1% and 3.3%, for width and height, respectively. This is primarily due to the turbulence properties, such as turbulence kinetic energy and dissipation rate, not been provided for the LNG inlet (Table 31). The turbulence properties were therefore estimated on the basis of the turbulence properties of the flow domain, primarily the turbulence generated as a result of the billboard and vapour fence. This coupled with the fact that the LNG pool (radius) is still growing, has led to the underprediction of the vapour cloud plume. As the vapour cloud dispersion continued, 140 s, the LNG spill has already ceased, which led to the LNG pool completely vaporizing with the vapour cloud rising higher within the impoundment. This eliminated the need of estimating the turbulence properties of the LNG inlet; therefore, with the turbulence properties now solely calculated on the basis of interactions with the billboard and vapour fence, has resulted in a more accurate simulated vapour cloud shape prediction, albeit with slight underpredictions of 0.7% and 2.1% for width and height, respectively. As the

simulation progresses to 180 s, the LNG pool is now non-existent, the vapour cloud is now approaching steady state, and the wind conditions now have a high impact in the dispersion process with increased mixing as the vapour cloud continues to rise. This is due to vertical turbulence and the billboard, resulting in increased wake effects. Overall, this lead to the direct CFD simulation method accurately capturing the vapour cloud shape at 180 s (Table 33). The effect of bifurcation and lofted plume dispersion was also observed and occurred as a result of the billboard acting as an obstacle (Figure 20), and the interaction of the vapour cloud with the wind. This effect, in addition to the lofted plume dispersion behaviour, led to a $\frac{1}{2}$ lower flammability limit (LFL) of approximately 450 m downwind of the spill point.

5.1.8 Time Variant Vapour Gas Concentration Comparison

Time variant vapour gas concentration at three different sensory locations, 50, 150, and 250 m, and at a height of 1 m were analysed and present in Figure 24, with peak concentrations recorded in Table 34. The arrival time and temporal concentration behaviour of sensors g04 and g11 are well-captured by the direct CFD simulation method. However, for sensor g18, 250 m downwind, the direct CFD simulation does not accurately capture the temporal concentration; this was expected because the arrival time at this sensor was slightly earlier than the experimental results. In addition, the peak concentration of the vapour cloud at all sensors was underpredicted. This underprediction of peak concentration, including the earlier arrival time at sensor g18 can be attributed to not accurately capturing the high momentum of the LNG inlet and mixing imparted by the billboard and vapour fence, which is a result of the turbulence properties at the LNG inlet not been provided and estimated from the flow domain.

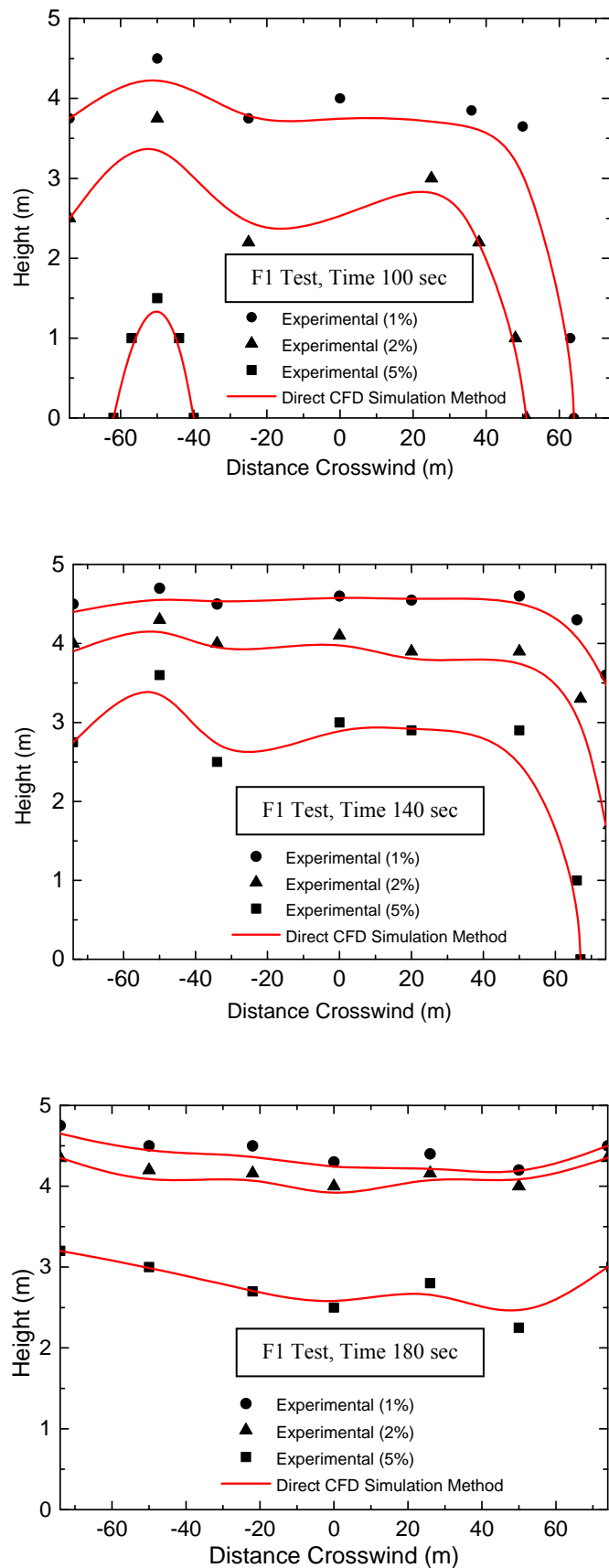


Figure 23: Comparison of CFD vapour cloud dispersion to experimental results at the 150 m sensory row.

Table 33: Comparison of simulation crosswind and downwind dispersion to experimental data.

	50 s	150 s	250 s
Width (m)	underpredicted by 1%	underpredicted by 0.7%	accurately predicted
Height (m)	underpredicted by 3.3%	underpredicted by 2.1%	accurately predicted

Table 34: Peak vapour gas concentrations at sensor locations.

Downwind distance (m)	Concentration (v/v)	
	Experimental	Direct CFD Method
50	0.230	0.210
150	0.110	0.100
250	0.073	0.060

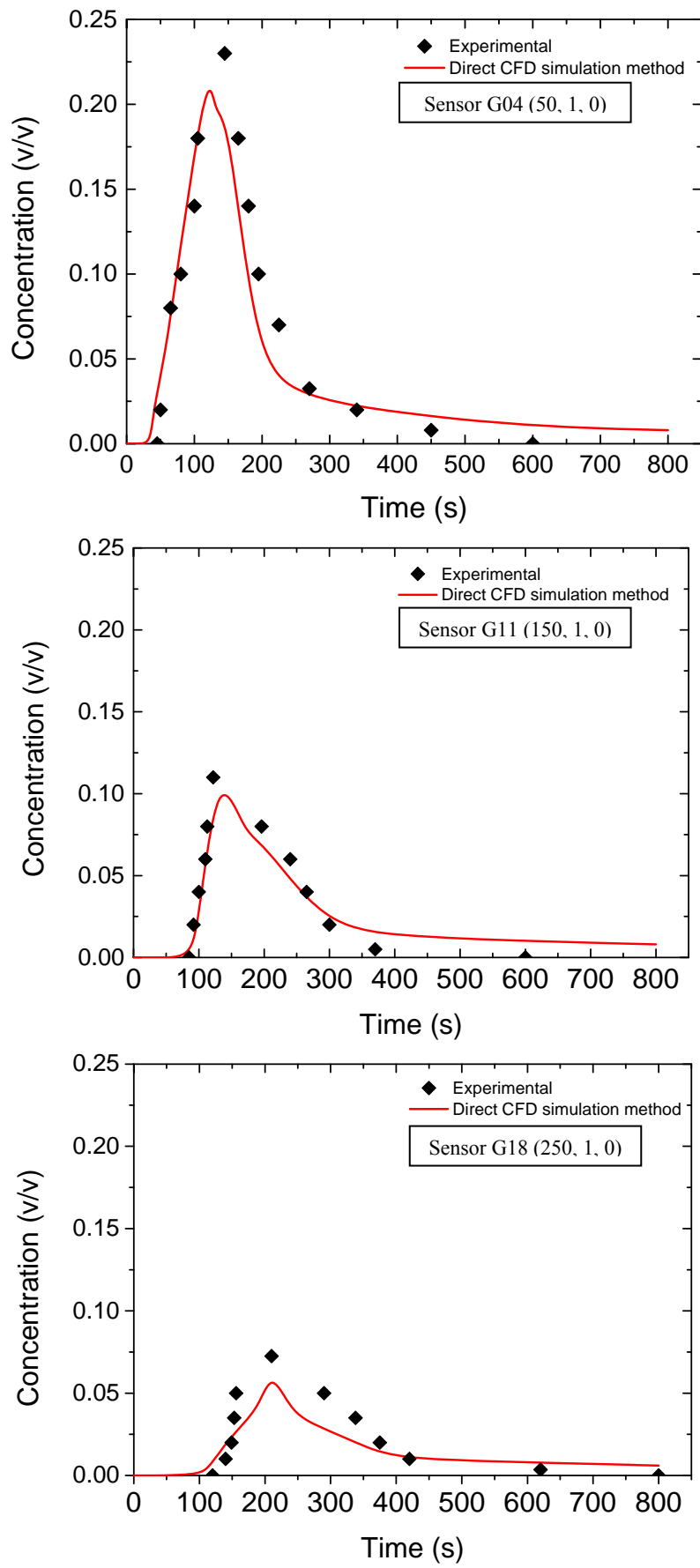


Figure 24: Comparison of time variant vapour gas volume concentration at different sensory locations with sensor's (x, y and z) coordinates given.

Statistical performance measures previously introduced in Section 4.2.6 were also used for quantitative comparison of the direct CFD simulation method with the experimental data. Statistical performance values for the direct CFD simulation method including ideal values are shown in Table 35. Negative fractional bias (FB) and geometric mean bias (MG) lower than 1 mean that vapour gas concentration is underestimated. The statistical measure analysis shows that, even though the vapour gas concentration is underpredicted, which was previously noted, it is still in good agreement with experimental data.

Table 35: Statistical performance of the direct CFD simulation method.

Statistical number	Trial	
	Ideal value	Direct CFD Method
FB	0	-0.091
NMSE	0	0.008
MG	1	0.913
ln(VG)	0	0.008

5.2 Effect of Sea Surface and Air Temperature Analysis

At the initial stage of the spill (0 – 50 s), the LNG pool radius increases rapidly; however, the growth rate starts to decrease as the discharge rate from the LNG tanker decreases (~50 – 400 s). Once the evaporation rate of LNG is equal to the discharge rate from the tanker, the pool reaches a steady state (~400 – 1297 s). After the discharge of LNG from the tanker has ceased (1297s and onward), the pool radius starts to decrease rapidly as a result of the evaporative losses exceeding that of the discharge. This trend was observed in all five cases. As the temperature increases in cases 1 - 5 (Figure 25), it is clear that there is little change in the initial growth rate of the LNG pool (0 – 50 s). The difference in pool radius growth starts becoming apparent as the reduction in discharge rate becomes significant (~50 – 400 s) and this trend remains for the duration of the spill. The largest pool radius, 110 m, occurred in case 1, which was expected given the cooler conditions, 278.15 K (air) and 271.15 K (sea), that would allow the pool to spread and linger with a lower vaporization rate.

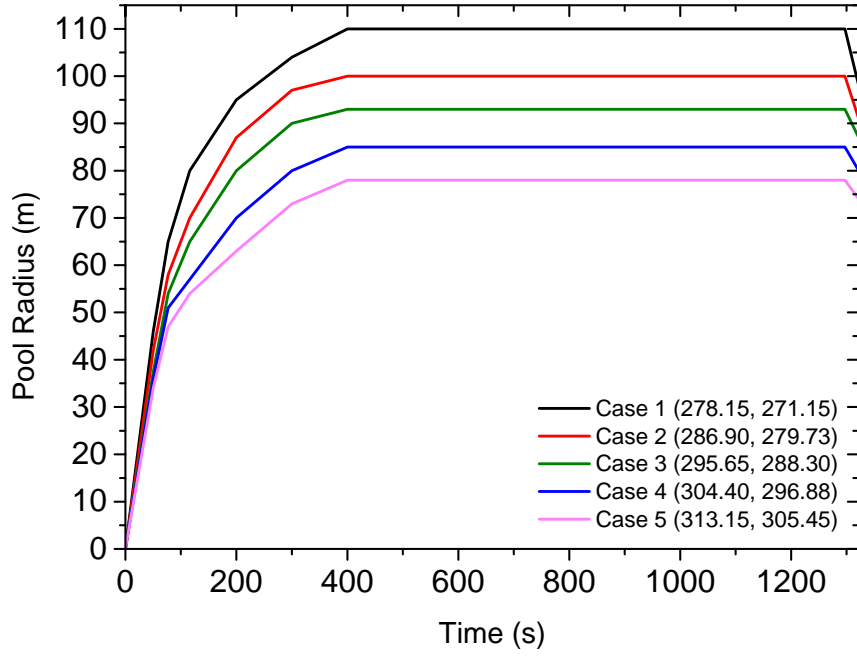


Figure 25: Pool radius (m) versus time (s) comparison for a realistic scenario with (air and sea) temperatures given for each case.

The $\frac{1}{2}$ LFL of the vapour cloud for the different cases are presented in Figure 26 - Figure 28. On analysis it can be seen that as temperature increases, from cases 1 – 5, the length and height of the vapour cloud increase, while the width of the vapour cloud decreases. This is due to the fact that the energy available for the vapour cloud is increasing; therefore allowing the vapour cloud to rise higher and disperse further downwind. The width of the vapour cloud decreases because in such stable atmospheric conditions, the vapour cloud would linger as a result of reduced vertical turbulence mixing; however with the increasing energy added to the system, the vapour cloud is able to travel further and, therefore, not spread laterally.

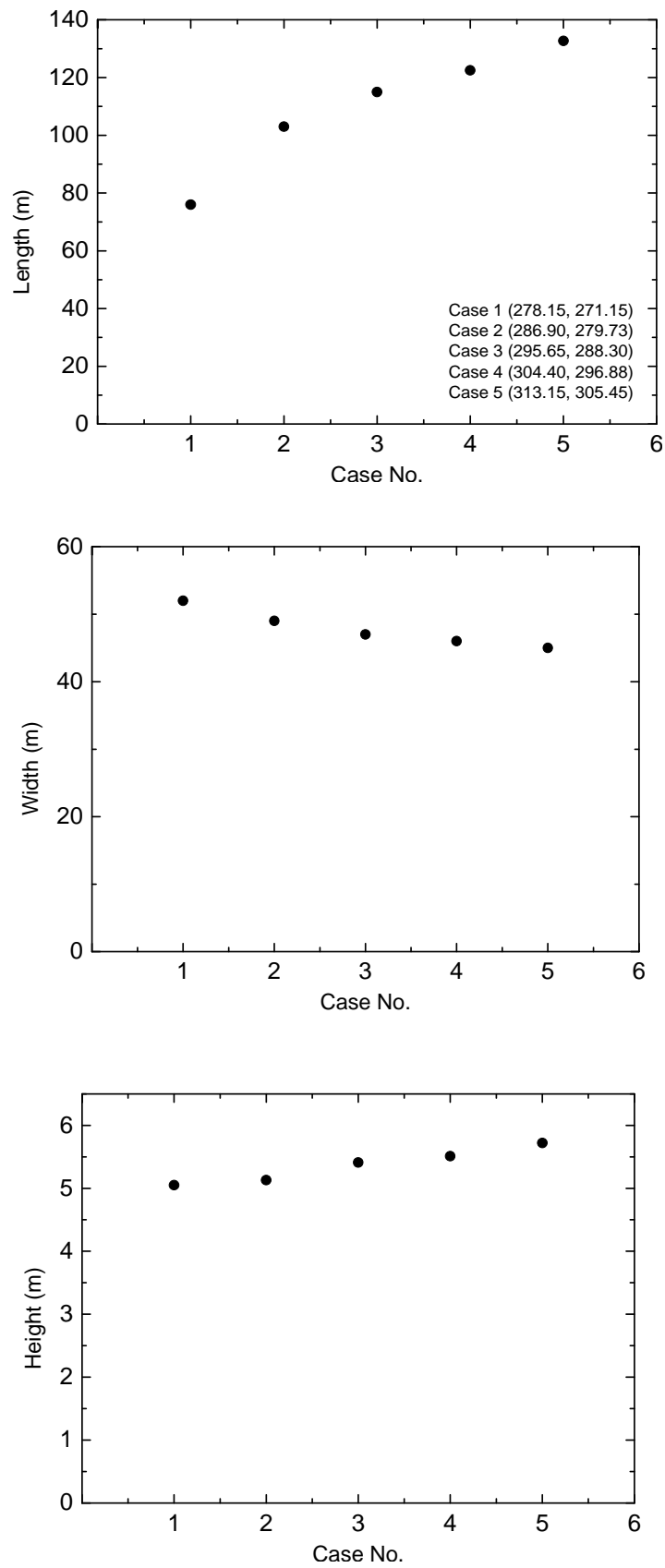


Figure 26: Effect of the temperature on vapour cloud dispersion of (air and sea) temperatures for each case, with varying air and sea surface temperatures (results obtained at $\frac{1}{2}$ LFL).

Figure 26 presents the data for varying both air and sea temperatures. As the environmental temperature increases from case 1 to 2, the growth rate of the vapour cloud downwind dispersion is at a maximum. This is because at such low atmospheric stability, the vapour cloud is obtaining its energy from the turbulence generated during the spill as well as the temperature of the sea surface. Therefore as the sea temperature changes from below to above 273.15 K (0 °C) between case 1 and case 2 (scenario 1 of Table 32), the enthalpy of the whole system increase significantly. Between cases 2 and 5, the growth rate of the vapour cloud downwind dispersion follows a steadier trend. A similar trend was also observed for the lateral growth rate of the vapour cloud, with a significant decrease in lateral spread, followed by a more steady decrease in vapour cloud lateral spread. With this observation, it is easy to deduce that a correlation with an inverse relation might be possible for such dispersion scenarios. The growth rate of the vapour cloud in the vertical direction (height) is quite steady and has little change as the environmental temperatures are increased in the system compared to the downwind and lateral spread of the vapour cloud.

As the air temperatures are increased while maintaining the sea surface temperatures (Figure 27 and scenario 2 of Table 32) the growth of the vapour cloud still follows a similar trend to that mentioned above. By comparison of the results from Figure 27 (varying atmospheric temperature) to that in Figure 26 (varying atmospheric and sea temperatures), it was observed that with a high sea surface temperature and the same air temperature, the vapour cloud disperses further downwind, is narrower and rises higher. This is expected because the enthalpy of the system is still increasing.

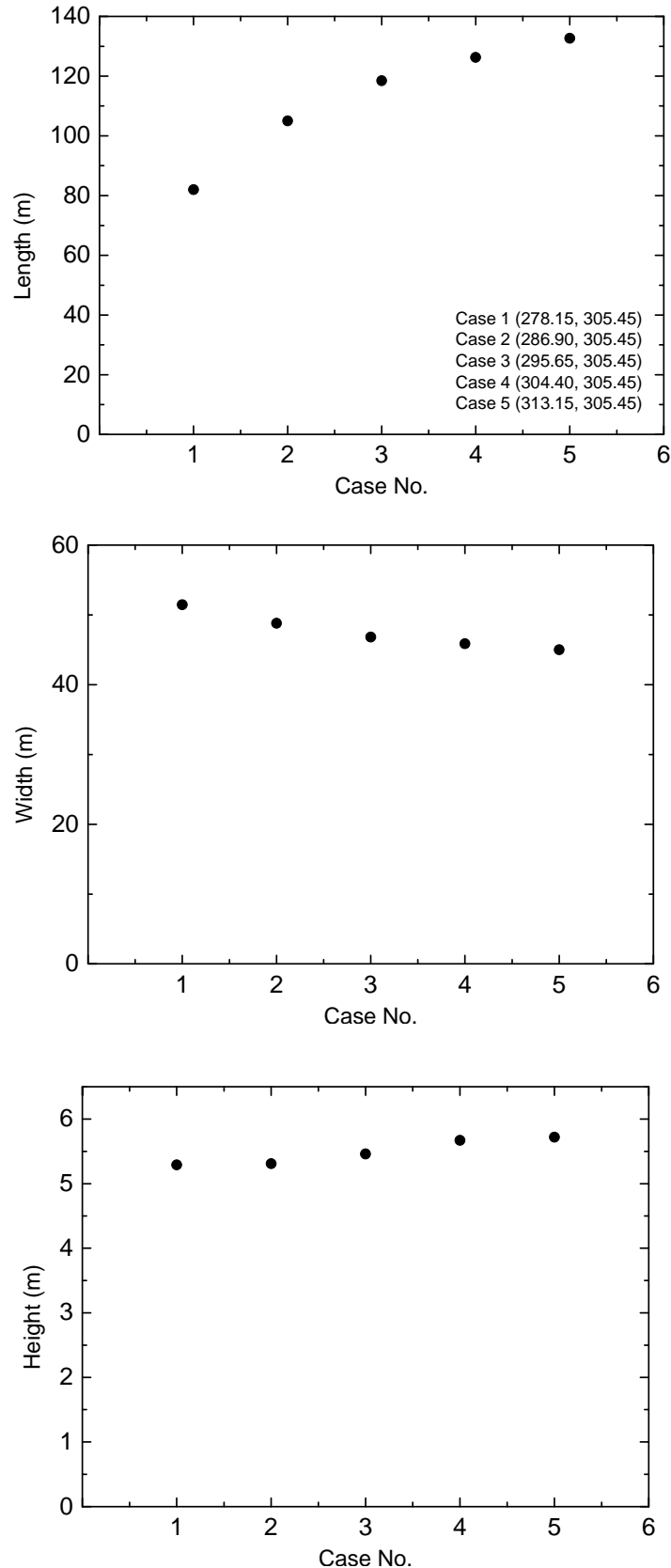


Figure 27: Effect of the temperature on vapour cloud dispersion of (air and sea) temperature for each case, with varying air temperatures and constant sea surface temperatures (results obtained at $\frac{1}{2}$ LFL).

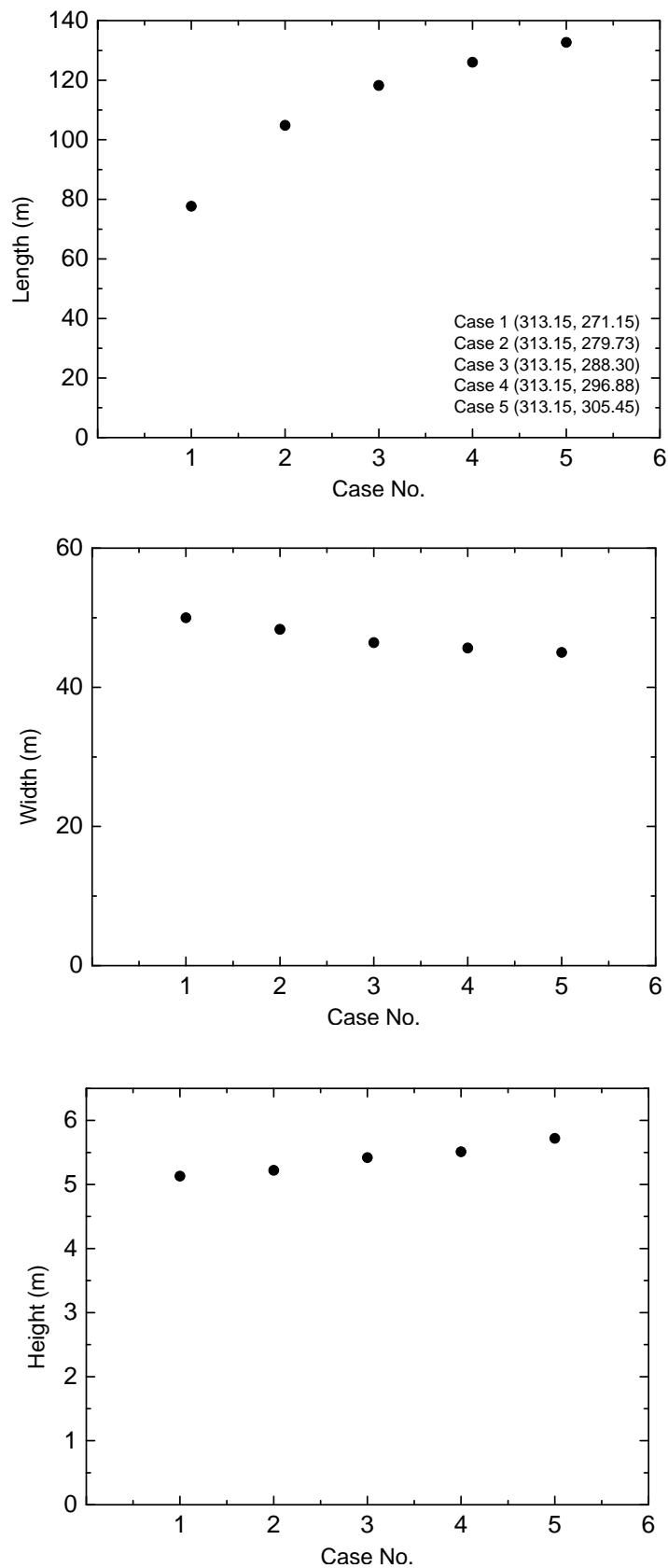


Figure 28: Effect of the temperature on vapour cloud dispersion of (air and sea) temperatures for each case, with constant air temperatures and varying sea surface temperatures (results obtained at $\frac{1}{2}$ LFL).

Figure 28 show the results for maintaining the air temperature while changing the sea surface temperature. By comparison of the results from Figure 28 (varying sea temperature) to that of Figure 26 (varying both sea and air temperatures), it is clear that, with a higher air temperature and the same sea temperature, the vapour cloud still disperses further downwind, is narrower, and rises higher. This is expected because the enthalpy of the system is still increasing. However, the cases in Figure 27 represents a larger vapour cloud, when compared to Figure 26, unlike the cases in Figure 28; albeit with a similar increment rate on the varying conditions (whether sea or air temperatures). This suggests that a majority of the energy needed to disperse the vapour cloud is initially obtained from the interaction with the sea surface or substrate below, especially in stable atmospheric conditions such as the conditions used during this study.

5.3 Conclusion

A Fluent CFD code for predicting LNG spill and dispersion was used to simulate the Falcon 1 test; it involved spilling LNG onto a water pond with obstacles. A newly developed CFD code, direct CFD simulation method, was shown to accurately capture vapour cloud dispersion behaviour and was in very good agreement with experimental data. The code was then used to investigate the effect of the air temperature and sea surface on LNG spill and dispersion. It was shown that, as the temperature of the environment increases, the length of the vapour cloud increases, by up to 26%, the width decreases, by up to 6%, and the height increases, by up to 5%, as a result of increasing enthalpy in the system. When isolated, the sea temperatures were shown to have a greater impact on the overall dispersion process compared to that of the air. It was also interesting to note that, in cooler conditions (sea temperature below 273.15 K), the growth of the vapour cloud follows a different trend compared to that at warmer conditions (sea temperature above 273.15 K). With further studies and analysis, a correlation might be possible that will assist hazard response personnel to make quick estimates based on spill and environmental conditions in order to contain and control LNG spills and vapour cloud dispersion.

6 EFFECT OF ATMOSPHERIC AND SEA STABILITY ON LNG DISPERSION AND IMPLICATIONS TO AUSTRALIAN LNG MARINE TRANSPORT

In this chapter, wave modelling techniques are incorporated into the direct CFD simulation code with the aim of investigating the stability effects of sea waves and the surround wind dynamics on LNG pool formation and dispersion process.

6.1 Wave Modelling and Stability Effect Simulation Methodology

6.1.1 Introduction

Liquefied natural gas (LNG) has been playing an increasingly role in the world's energy market since last decade because of its environmental-friendly properties and increasingly demand (at an average annual growing rate of 2.3%³). This has led to increasing marine transport of LNG for reducing overall costs²⁷⁷. Marine transport of LNG (especially the LNG vessels) has been having a good safety record^{271, 272}. However, LNG's flammable nature, its impact to economy and likelihood being a potential terrorist target^{170, 270} have led to substantial R&D on LNG technology and the essential hazards associated with LNG transport^{1, 4, 39, 40, 224, 237, 278-280}. Previous experimental studies^{113, 114, 151, 254-260} were focused on large-scale LNG spill and subsequent pool fires to understand LNG spill and dispersion. However, none of these large scale studies has incorporated the scenarios of LNG tankers during transport. Recent studies^{123, 170, 267} are focused on LNG spills during marine transport, considering a range of various parameters and factors. Unfortunately, little has been done on the effect of atmospheric stability and sea waves on LNG spill and dispersion process.

Australia's LNG is mainly exported the Asian market, with Japan and China among the main consumers; importing 80% and 16% respectively²⁸¹. Figure 29 illustrates the key global LNG marine transport in 2014²⁷³ and the corresponding sea wave conditions.²⁸² The figure clearly shows that the marine transport for Australia's LNG export travels across various oceans with varying atmospheric and wave conditions. The objective of this chapter is therefore to utilise the direct CFD simulation

method²⁶⁷ developed in Section 4.1 for assessing the stability effect of the atmosphere and sea waves on LNG spill, pool formation and dispersion. The findings are then used to investigate LNG spill and dispersion behaviour during transport from Australia to the Asian markets.

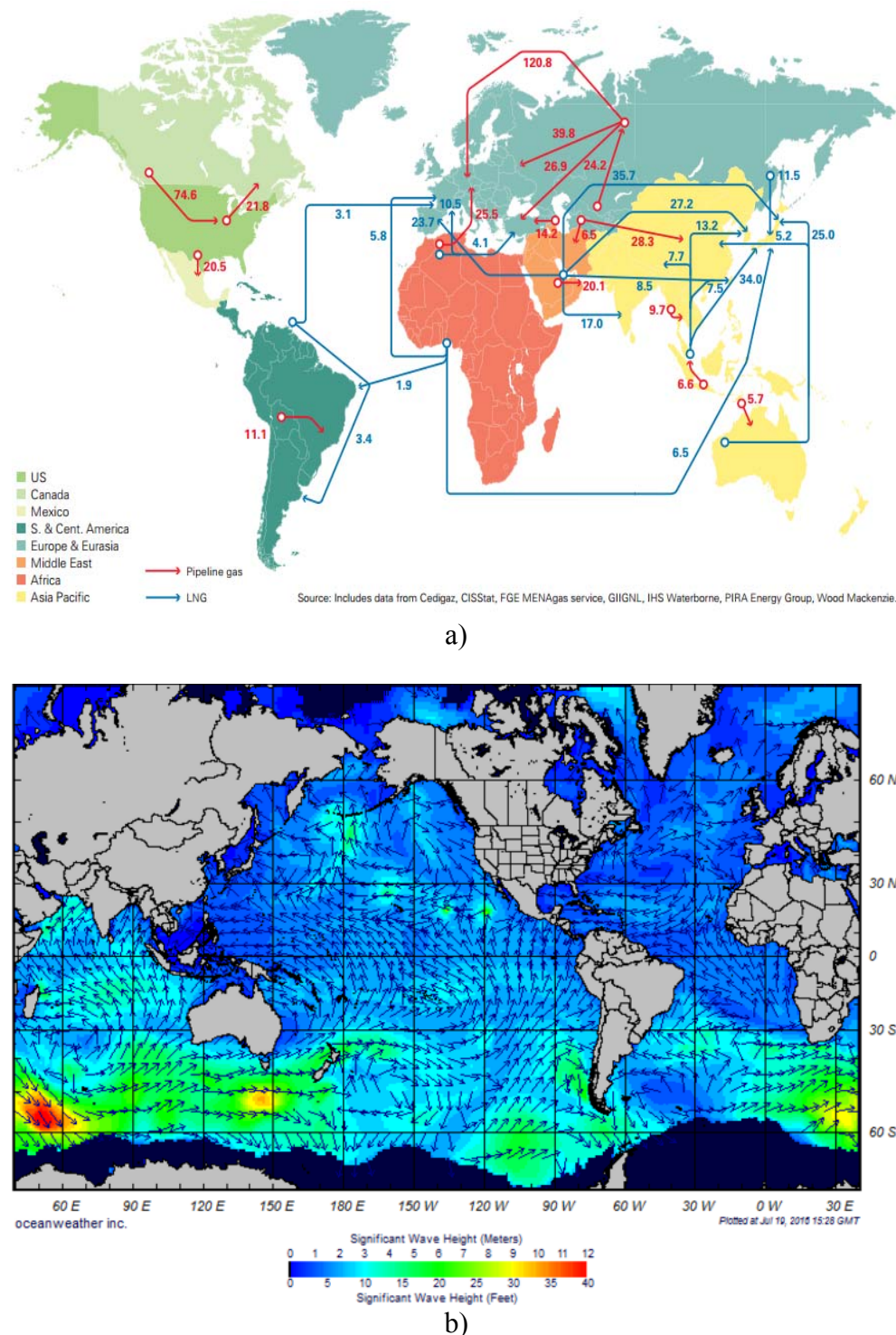


Figure 29: (a) Major LNG trade movement in 2014 (billion cubic meters)²⁷³ and (b) Corresponding wave conditions.

6.1.2 Pasquill Stability

Turbulence increases the dispersion of air borne pollutants by increasing the entrainment and mixing of air into the plume; and therefore reduces the concentration of pollutants in the plume. The oldest and most common method for categorizing atmospheric turbulence is the Pasquill atmospheric stability classes. The Pasquill stability classes was developed in 1961 and involves the categorization of atmospheric turbulence into six stability classes A, B, C, D, E and F as shown in Table 36²⁸³ with class A been the most unstable (most turbulent) to class F been the most stable (least turbulent). These stability levels are due to correlations between wind speeds and incoming solar radiation. For this study we have selected different stability classes (Table 37) as the base case, to match the different travel routes of LNG tankers as shown in Figure 29. The wind speeds will be used as presented, while the effect of incoming solar radiation will be modelled as sea surface temperatures and atmospheric (wind) temperatures. The given wind speed/turbulence will then give rise to different sea wave conditions which are the main focus of this study.

Table 36: Meteorological Conditions Defining Pasquill Turbulence.^a

A: Extremely unstable conditions	D: Neutral condition^b				
B: Moderately unstable conditions	E: Slightly stable conditions				
C: Slightly unstable conditions	F: Moderately stable conditions				
Daytime insolation (W/m²)					
Surface wind speed (m/s)	Strong (> 600)	Moderate (300 – 600)	Slight<br (<="" 300)<="" b=""/>	Thin overcast or ≤ 4/8 cloudiness^c	≤ 3/8 cloudiness
< 2	A	A - B	B	-	-
2	A - B	B	C	E	F
4	B	B - C	C	D	E
6	C	C - D	D	D	D
> 6	C	D	D	D	D

^aData extracted from the study by Ermak et al.²⁸⁴

^bApplicable to heavy overcast day or night

^cThe degree of cloudiness is defined as that fraction of the sky above the local apparent horizon that is covered by clouds

Table 37: Base Stability Conditions and Resultant Sea and Atmospheric temperatures
(Conditions used in Scenario I).

Surface wind speed (m/s)	Insolation (W/m ²)	Stability class	Sea surface temperature (K)	Atmospheric temperature (K)
1	650	A	305.45	313.15
3	450	B	294.02	301.48
4	280	C	282.60	289.82
7	250	D	271.15	278.15

6.1.3 Mathematical Formulation

The mathematical formulation is the same as developed and explained in Section 4.1; however with the addition of wave modelling techniques which shall be described below.

Wave modelling for this study shall utilise the wave modelling equations in WAVEWATCH III code and ANSYS 15.^{263, 286} The governing equations for wave motion, in particular, the stokes wave theory for gravity waves are presented below.

Wave height

$$H = 2A = A_t + A_c \quad (27)$$

where A is the wave amplitude, A_t is the amplitude at the trough and A_c is the amplitude at the crest.

Wave number

$$\begin{aligned} k &= 2\pi/\lambda \\ k_x &= k \cos \theta \\ k_z &= k \sin \theta \end{aligned} \quad (28)$$

where λ is the wave length, k_x is the wave number in the direction of flow and k_z , the wave number in the cross flow direction.

Wave frequency

$$\omega = [gk(1 + A^2k^2c_3 + A^4k^4c_5) \tanh kh]^{1/2} \quad (29)$$

where g is gravity magnitude, k is the wave number, A is the wave amplitude, c_3 and c_5 are functions of wave length and liquid height,²⁸⁷ and h is the liquid height.

Effective wave frequency

$$\omega_e = \omega + k_x U \quad (30)$$

where ω is the wave frequency, k_x is the wave number in the direction of flow and U is the uniform flow velocity magnitude.

Wave speed

$$c = \frac{\omega}{k} \quad (31)$$

where c is the wave speed, ω is the wave frequency and k is the wave number.

Velocity potential

$$\begin{aligned} \phi(X, t) &= c A e^{ky} \sin \alpha \\ \alpha &= k_x x + k_z z - \omega_e t + \varepsilon \end{aligned} \quad (32)$$

where ϕ is the velocity potential, c is the wave speed, A is the wave amplitude, k is the wave number, x , y and z are the space coordinates, ω_e is the effective wave frequency, t is time and ε is the wave phase difference.

Velocity vector

$$\vec{V} = (U + u)\hat{x} + v\hat{y} + w\hat{z}$$

$$\begin{aligned} u &= \frac{\partial \phi}{\partial x} \cos \theta \\ v &= \frac{\partial \phi}{\partial y} \\ w &= \frac{\partial \phi}{\partial z} \sin \theta \end{aligned} \quad (33)$$

where \vec{V} is the velocity vector for incoming waves, U is the uniform flow velocity magnitude, u , v , w are the velocity components of the gravity wave in the respective \hat{x} , \hat{y} and \hat{z} directions.

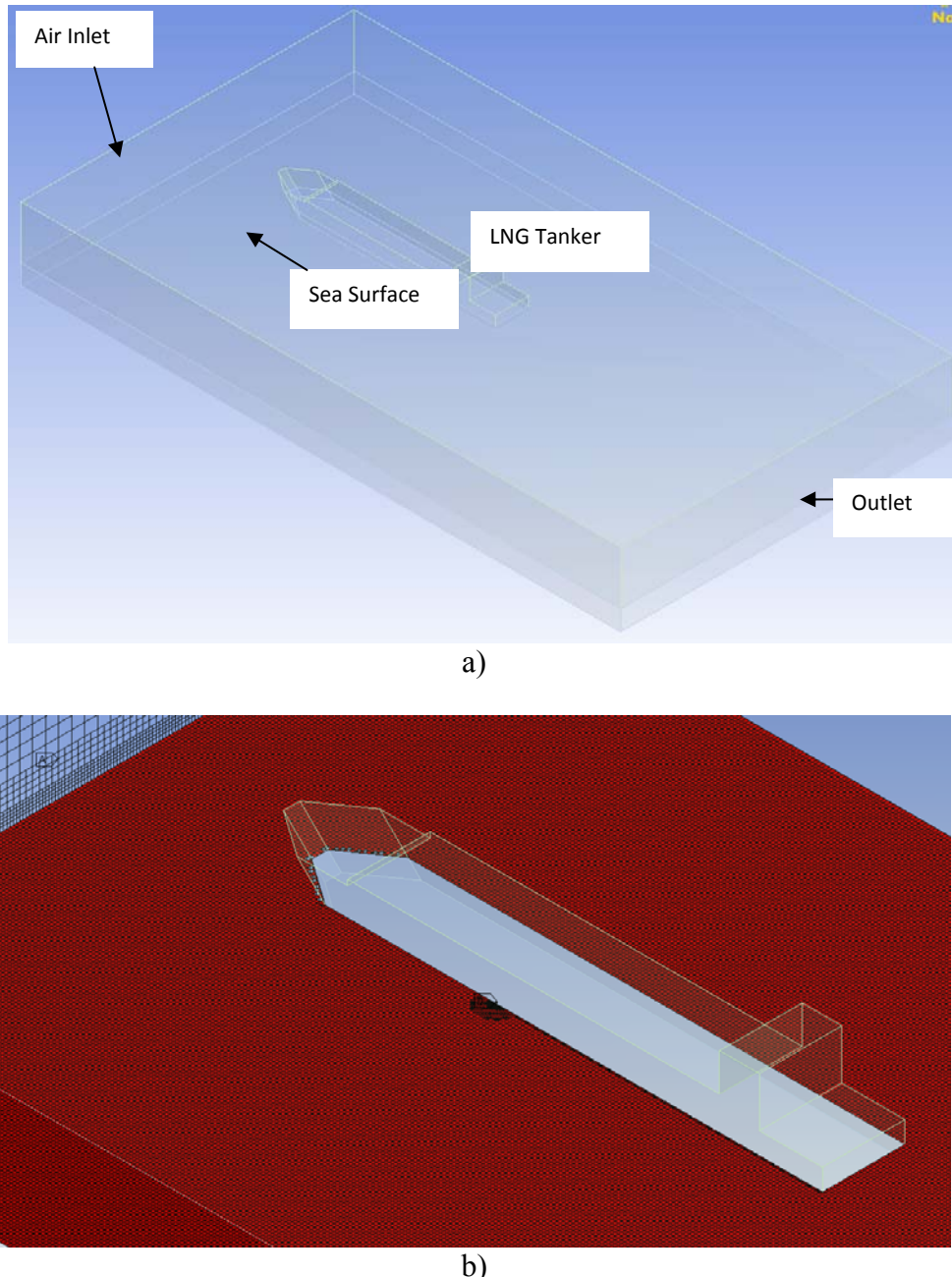


Figure 30: (a) Experimental layout and (b) hexahedral mesh with refinements in areas of high flow gradient.

6.1.4 Computation Geometry and Grid

The dimensions of the domain are $500 \text{ m} \times 110 \text{ m} \times 500 \text{ m}$ in the x, y and z direction respectively (Figure 30). The domain is oriented so that the x-direction is the horizontal and parallel to the wind, the z-direction is horizontal and perpendicular to the wind and the y-direction is vertical. The origin of the domain is at the centre of the breach and 1 m above the sea surface. The domain was created in ANSYS design modeller by first creating a double-hulled membrane LNG tanker with a full cargo capacity of 228000 m^3 , approximately 45600 m^3 for each storage tank.²⁷⁶ The flow

domain was the created by first generating a rectangular shape (500 m × 110 m), which was then extruded to the desired width (500 m). A Boolean-imprint feature was then used to create the 1 m breach (LNG inlet) on the side of the LNG tanker. Hexahedral elements are known to be more computational efficient than tetrahedral elements, and therefore were used to discretise the domain; resulting in a total of 1069321 hexahedra elements. The mesh as shown in Figure 30 is non-uniform, allowing for mesh refinement in areas of high flow gradients such as at sea surface, contact points between the tanker and the sea and around the breach location.

6.1.5 Boundary Conditions and Initial Conditions

The boundary and initial condition setup are exactly the same as that demonstrated in Section 4.2.2, however to evaluate the stability effect of the atmosphere and sea on LNG spill and dispersion, a total of three scenarios were investigated:

- Scenario I that is a realistic scenario consists of four cases, where both the wind and sea conditions are incremented in each case to match the Pasquill stability classes (Table 38);
- Scenario II, also consists of four cases, however the wind conditions and surrounding temperatures are held constant in order to evaluate the effect of sea waves on the dispersion process with each subsequent case (Table 39); and
- Scenario III consists of four cases, in which the sea wave conditions and surrounding temperatures are held constant in order to evaluate the effect of wind dynamics on LNG spill and dispersion process with each subsequent case (Table 40).

Table 38: Scenario I as realistic scenario under varying wind and sea conditions.

Temperatures			Wave Conditions			
Surface wind speed (m/s)	Sea surface (K)	Atmospheric (K)	Height (m)	Wavelength (m)	Period (s)	Wave speed (m/s)
1	305.45	313.15	0.25	8.50	3.00	2.80
3	294.02	301.48	0.90	21.66	4.00	4.45
4	282.60	289.82	1.20	27.73	5.05	5.20
7	271.15	278.15	1.50	33.80	5.70	5.94

Table 39: Scenario II under varying wave conditions while wind speed and surrounding temperatures are constant.

Temperatures			Wave Conditions			
Surface wind speed (m/s)	Sea surface (K)	Atmospheric (K)	Height (m)	Wavelength (m)	Period (s)	Wave speed (m/s)
7	271.15	278.15	0.25	8.50	3.00	2.80
7	271.15	278.15	0.90	21.66	4.00	4.45
7	271.15	278.15	1.20	27.73	5.05	5.20
7	271.15	278.15	1.50	33.80	5.70	5.94

Table 40: Scenario III at varying wind speed while wave conditions and surround temperatures are held constant.

Temperatures			Wave Conditions			
Surface wind speed (m/s)	Sea surface (K)	Atmospheric (K)	Height (m)	Wavelength (m)	Period (s)	Wave speed (m/s)
1	271.15	278.15	0.25	8.50	3.00	2.80
3	271.15	278.15	0.25	8.50	3.00	2.80
4	271.15	278.15	0.25	8.50	3.00	2.80
7	271.15	278.15	0.25	8.50	3.00	2.80

6.1.6 Solution Method

The Monin-Obukhov theory and solution controls utilised in Section 0 was also used for the stability effect simulation setup.

6.2 Analysis of Stability Effect on LNG Spill and Vapour Cloud Dispersion

6.2.1 Effect of Sloshing on LNG Dispersion

Sloshing has been studied over a long period of time because of its significance across numerous disciplines.²⁸⁸⁻²⁹² In most cases, the study of sloshing is focused on the damage that could result due to sloshing.²⁵⁰⁻²⁵³ However, this study is focused on how sloshing can affect LNG spill process. Table 38 shows the conditions for Scenario I, the realistic scenario, with four cases under which both wind and sea conditions are incremented to match the Pasquill stability classes; a simplified way to model this would be to allow the LNG to spill from a stationary LNG carrier onto the sea. However this is not ideal, as any sloshing that would occur due to roll and pitch of the LNG carrier, induced by sea waves, would not be captured. To evaluate the effect of sloshing on LNG spill, the pressure on the tank walls and the spill time of the LNG (see Figure 31) can be observed. When roll and pitch are introduced to the LNG carrier, the LNG inside the storage tanks moves and has a higher dynamic pressure than if the roll and pitch were not introduced. This higher dynamic pressure coupled with the hydrostatic pressure distribution of the LNG increases the overall pressure impacted on the tank walls, as can be seen in Figure 31. As the wind speed, wave height and wave length increase, from case 1 to case 4, the maximum pressure exerted on the LNG storage tank walls also increases. This is expected as a large wave height and/or wave length would result in more LNG motion inside the storage tanks. The differences in pressures exerted on the LNG storage tank walls range from 17% in case 1 to 31% in case 4, further reinforcing the need to include wave induced motion into LNG tanker simulations. Furthermore, as the LNG level approaches the breach location, the sloshing can lead to air entering the storage tank, as the LNG backpressure is lower than atmospheric pressure. This condition would increase the spill time as the LNG spill would not be as continuous, as in a case without sloshing (see Figure 31). The difference in spill times were not drastic; however by including sloshing in this study, the LNG spill time was noted to take up to 100 seconds longer than if sloshing was not considered.

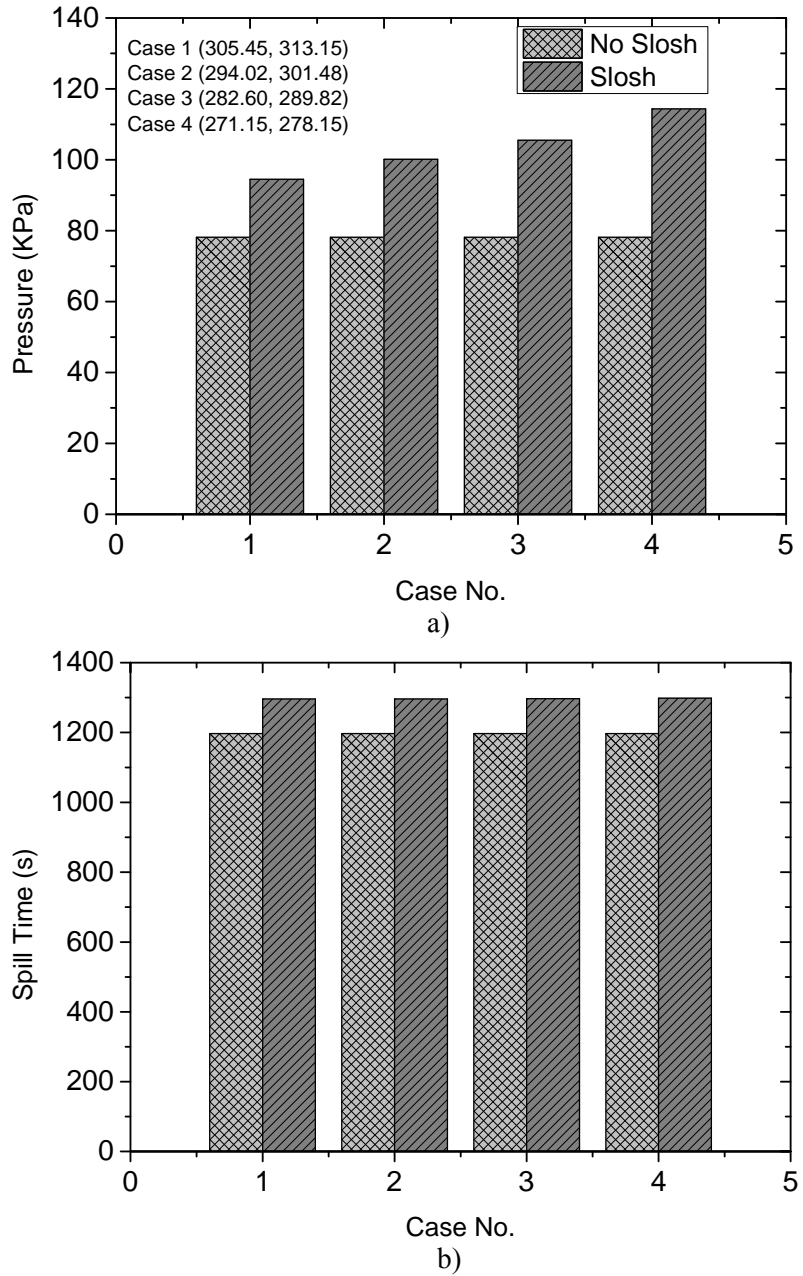


Figure 31: The effect of sloshing (in Scenario I) on (a) Maximum pressure on tank wall and (b) total LNG spill time with each case's (sea, air) temperatures given.

6.2.2 Stability Effect and Vapour Cloud Dispersion Analysis

Figure 32 presents the LNG pool evaporation rate and pool radius evolution for Scenario I, the realistic scenario, with four cases under which both wind and sea conditions are incremented to match the Pasquill stability classes (see Table 38 for wind and sea conditions). In the early stage (0 – 50 s), the LNG pool radius is growing at a high rate; however, as the process progresses (~50 – 400 s), this growth rate is noted to decrease as the discharge rate from the LNG tanker is also

decreasing. Once the evaporation rate of LNG is equal to the discharge rate from the tanker, the pool reaches a steady state (~400 – 1297 s); until the LNG spill has ceased (1297s and onward) during which evaporative losses exceed that of the discharge, resulting in the pool radius decreasing at a rapid rate.

This trend was noted in all four cases; however the evaporation rate *vs* time follows a different curve (see Figure 32). The evaporation rate grows at a steady rate in the early stage (0 – 400 s), until the evaporation rate of LNG is equal to the discharge rate from the tanker (~400 – 1297 s), followed by the evaporation rate dropping rapidly as the evaporative loses are greater than the release rate of LNG from the tanker (1297s and onward). As stability conditions increase, from case 1 to case 4 (Figure 32), the initial growth rate (0 – 50s) of the LNG pool follows a similar trend across all cases. As the spill continues (~50 – 400 s), the difference in LNG pool growth rate can now be differentiated; and this difference is clear for the remainder of the LNG spill. It is important to note that as stability increases the pool radius also increases subsequently (see Figure 32). However, the opposite effect is evident for the evaporation rate (see Figure 32) that decreases with increasing stability. This is because an increase in stability means the environmental conditions are calmer and therefore less turbulence to increase mixing, evaporation, and dispersion of the LNG. The largest pool radius was observed in case 4, at 121 m while the highest evaporation rate was occurred in case 1 at 3630 kg/s.

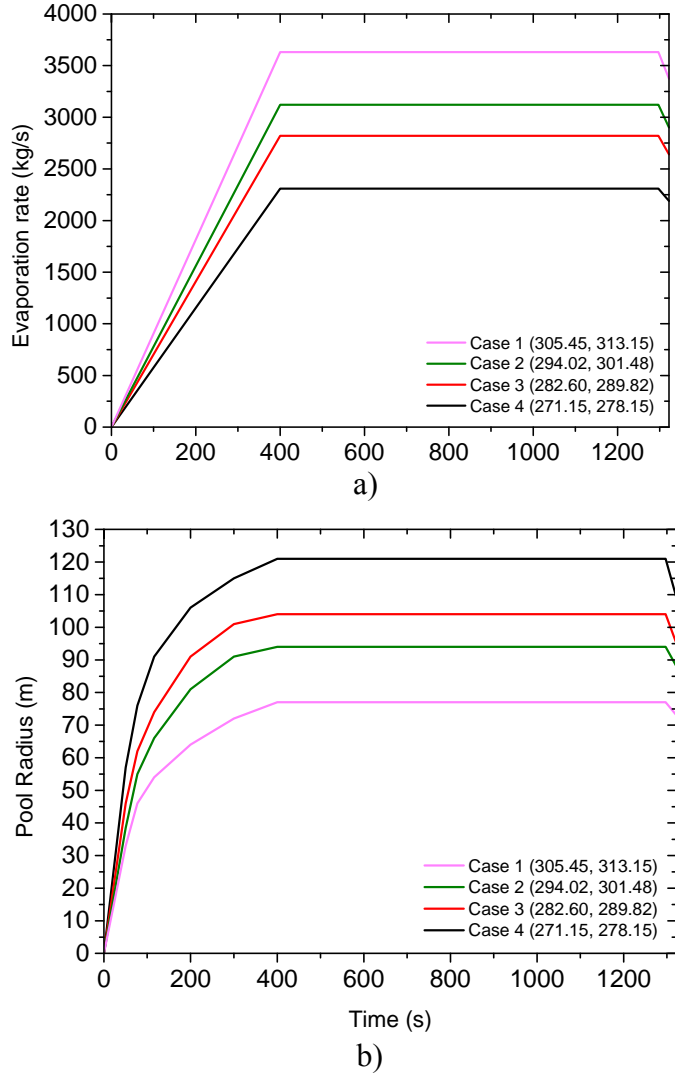


Figure 32: Scenario I case comparison: a) Pool evaporation rate (kg/s) vs time (s); b) Pool radius (m) vs time (s) with each case's (sea, air) temperatures given.

The half lower flammability limit ($\frac{1}{2}$ LFL) represents the distance at which methane in the vapour cloud is 2.5% v/v; at this distance the vapour cloud cannot sustain a flame if ignited.³⁸ Figure 33 presents the results on the $\frac{1}{2}$ LFL data for Scenario I, which is a realistic scenario, with four cases under which both the wind and sea conditions increment matching the Pasquill stability classes (see Table 38). As the stability conditions of the environment increases, from case 1 to case 4, the downwind dispersion (length) of the vapour cloud is noted to follow a steady growth. This is due to the turbulence and overall energy in the system decreasing as stability decreases; and therefore reducing the rate at which the vapour cloud mixes and disperses. This trend is also illustrated in the lateral (width) growth of the vapour, with a steady growth in lateral spread as the stability of the environment increases.

However, the vertical (height) growth of the vapour cloud follows an opposite trend; the height of the vapour cloud decreases as the stability in the environment increases. This is simply due to the fact that as the stability conditions increase; the thermal conditions are decreasing, wind speed increasing and wave conditions increasing (see Table 38). Overall, this stable condition and high wind speed results in a majority of the energy in the system focused in dispersing the vapour cloud downwind and in the lateral direction, with reduced vertical turbulent mixing.

For Scenario II, in which the wind speed, sea and atmospheric temperatures are held constant while varying the wave conditions, the results are showed in Figure 34. It can be seen that the growth of the vapour cloud follows an opposite trend to that of Scenario I; the downwind and crosswind dispersion of the vapour decreases (with increasing wave conditions), while vertical growth of the vapour cloud increases. The reason was that with these fixed wind speeds and thermal conditions, increasing wave conditions results in less stability and therefore more turbulence and mixing on the sea surface. Overall this lead to an increase in the evaporation rate of LNG from the LNG pool due to increased vertical turbulence. This increased vertical turbulence mixing appears to lead to an increase in the vertical growth of the vapour cloud; and with majority of the energy spent on dispersing the vapour cloud vertically, lead to a reduction in downwind and crosswind dispersion.

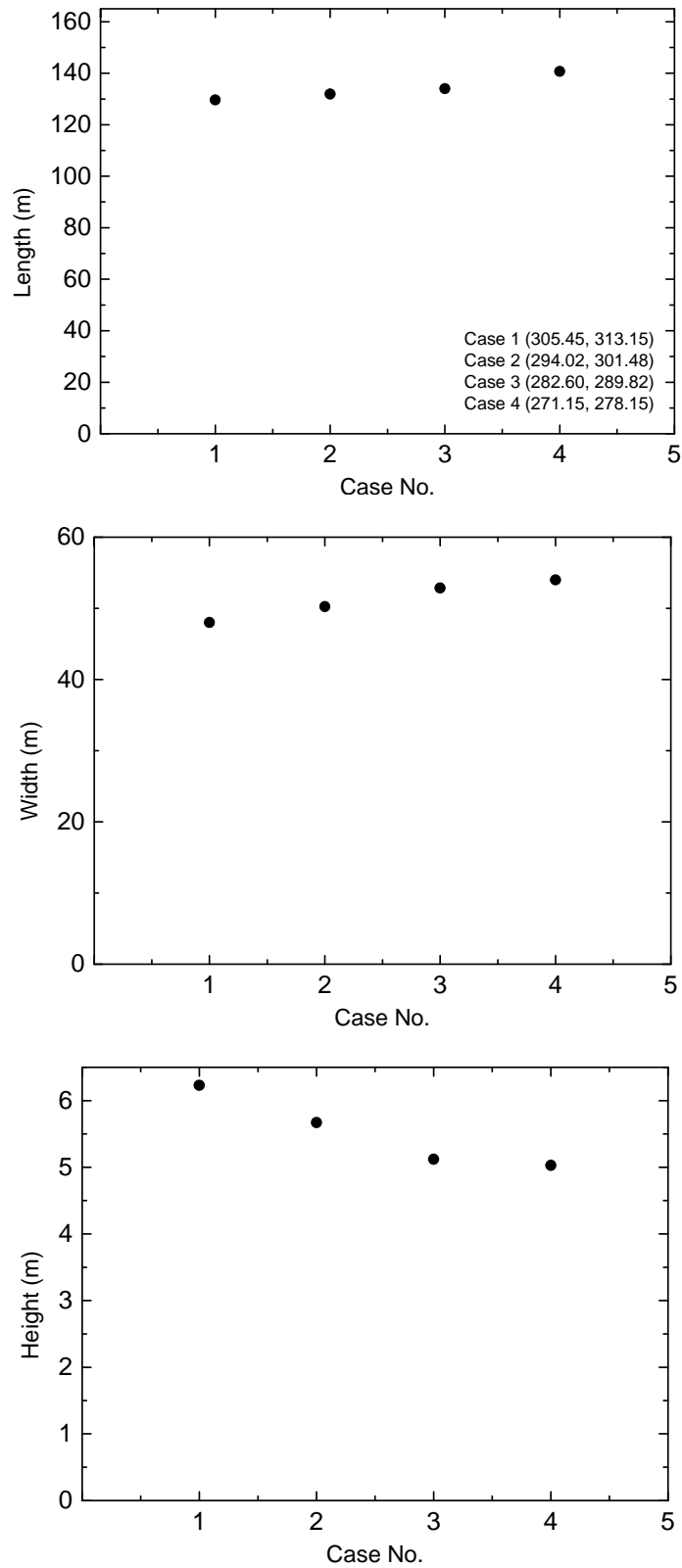


Figure 33: Stability effect on vapour could dispersion for Scenario I under varying ocean and atmospheric conditions, with each case's (sea, air) temperatures given (results obtained at $\frac{1}{2}$ LFL).

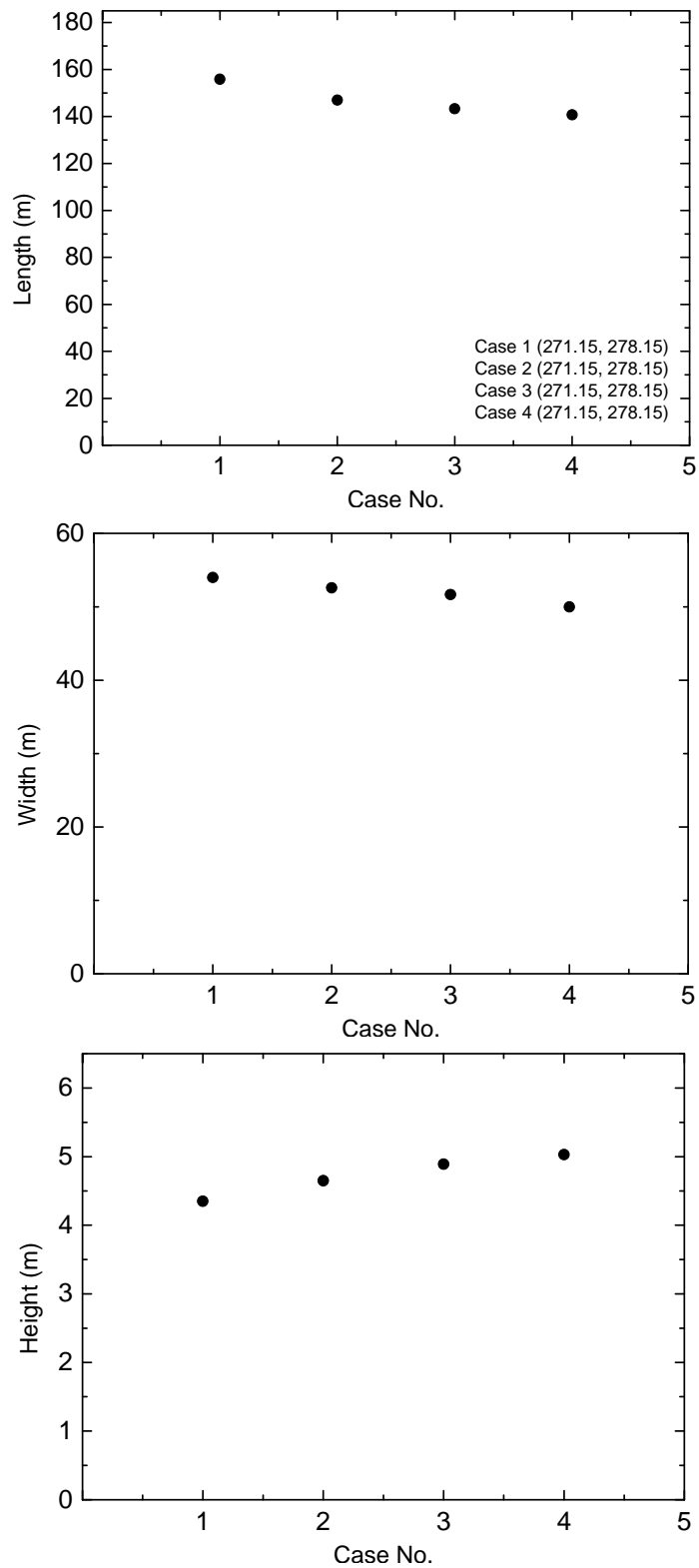


Figure 34: Stability effect on vapour could dispersion for Scenario II under varying wave conditions, constant wind speed and constant temperatures, with each case's (sea, air) temperatures given (results obtained at $\frac{1}{2}$ LFL).

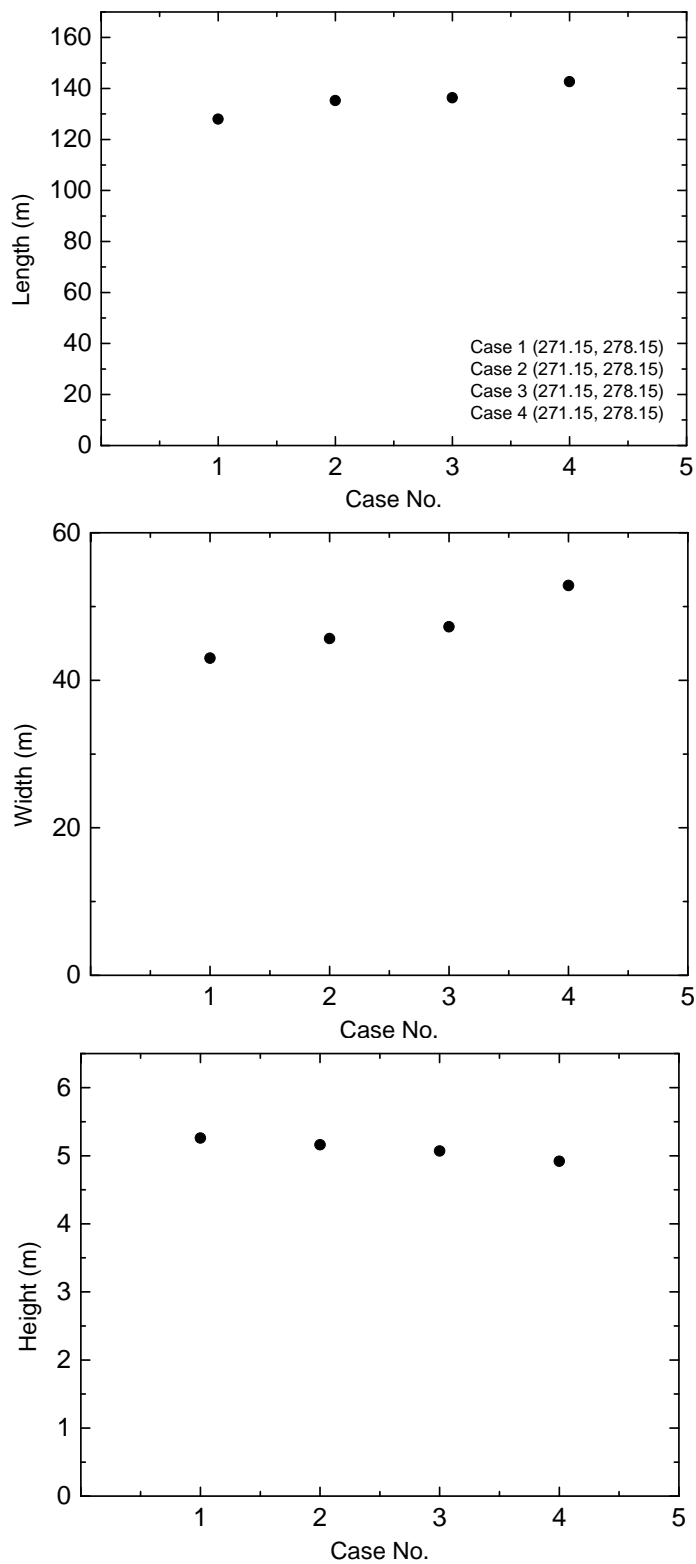


Figure 35: Stability effect on vapour could dispersion for Scenario III at varying wind speeds, constant wave conditions and constant temperatures, with each case's (sea, air) temperatures given (results obtained at $\frac{1}{2}$ LFL).

For Scenario III, in which wind speed was increased while maintaining thermal and wave conditions, the results are presented in Figure 35. The growth of the vapour cloud in Scenario III mirrors that of Scenario I with an increase in downwind and crosswind dispersion. However, the vertical growth of the vapour cloud decreases, albeit with different growth rates. As the wind speed is increased, the turbulence in the system is increased and therefore the vapour cloud is able to mix and disperse further in the downwind and crosswind directions. It is important to note that as the wind speed increases, the ability of the vapour cloud to linger, while mixing, decreases as the dispersion of the vapour cloud becomes primarily driven by the wind speed. By comparing case 4 in Figure 35 (Scenario III) to case 4 in Figure 33 (Scenario I), it can be seen that the larger wave conditions, case 4 in Table 38 (Scenario I), results in a lingering effect with the vapour cloud not dispersing as far downwind as case 4 in Table 40 (Scenario III) but disperses locally with larger crosswind and vertical dispersion.

6.3 Implications to Australian LNG Marine Transport

Australia is currently the world's second largest LNG exporter and export most of LNG exported to Asian market with major customers being Japan and China who import 80% and 16%, respectively.²⁸¹ Figure 36 show the LNG carrier travel routes from Australia to China or Japan. The LNG carrier starts off from Australia and travels through the Java sea, past Indonesia then goes through the Celebes and Sulu seas, between Indonesia and Philippines to enter the South China sea, from which the LNG carrier travels on to China (total of approximately 5078 km) or changes direction and heads northeast, through the North Pacific ocean to arrive in Japan (total of approximately 7542 km). The analysis in this section is focused on LNG spilling from a double-hulled membrane tanker with a full cargo capacity of 228000 m³ (the same tanker described in Section 0). As shown in Figure 36, the LNG carrier travel routes are segmented based on the corresponding sea conditions, with sea and wave conditions listed in Table 41 and Table 42. The analysis then considers the implications of an LNG spill during summer (December 2015 – February 2016) vs. an LNG spill during winter (June 2016 – August 2016), with the season in question based on the corresponding Australian season. It is noted that the discussion in this section is addressed mainly on the travel route from Australia to Japan, as it

encompasses that to China. In addition the following naming convention shall be used for the travel route segments: Section ab, implies that the LNG carrier travels from point a to point b; Section ad, implies that the LNG carrier travels from point a to point d; Section df implies that the LNG carrier travels from point d to point f bypassing point e.

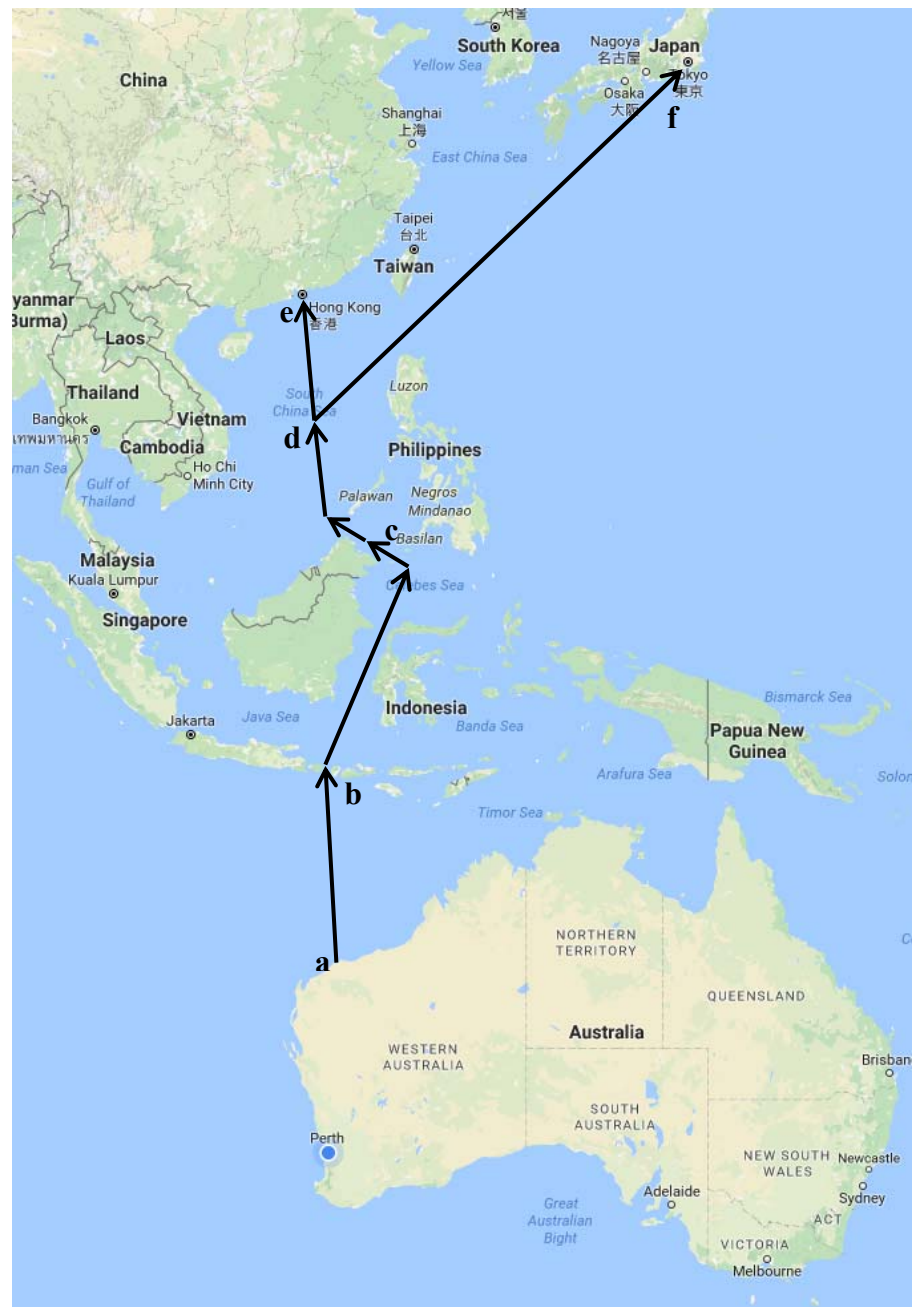


Figure 36: LNG carrier travel routes with segmented sections for analysis; China: a-e and Japan: a-d-f.

Table 41: Sea surface temperature and wave conditions during LNG transport in summer.

Australia to Japan					
	Temperatures		Wave Conditions		
Section	Sea surface (K)	Height (m)	Wavelength (m)	Period (s)	Wave speed (m/s)
ab	307.15	2.50	50.22	9.5	9.9
bc	307.15	2.50	50.22	9.5	9.9
cd	294.70	0.30	10.20	3.60	3.36
df	291.65	1.30	30.04	5.47	5.63

Australia to China					
	Temperatures		Wave Conditions		
Section	Sea surface (K)	Height (m)	Wavelength (m)	Period (s)	Wave speed (m/s)
ab	307.15	2.50	50.22	9.5	9.9
bc	307.15	2.50	50.22	9.5	9.9
cd	294.70	0.30	10.20	3.60	3.36
de	294.70	0.30	10.20	3.60	3.36

Table 42: Sea surface temperature and wave conditions during LNG transport in winter.

Australia to Japan					
	Temperatures		Wave Conditions		
Section	Sea surface (K)	Height (m)	Wavelength (m)	Period (s)	Wave speed (m/s)
ab	294.70	2.50	50.22	9.5	9.9
bc	301.15	0.30	10.20	3.60	3.36
cd	301.15	0.30	10.20	3.60	3.36
df	307.15	1.30	30.04	5.47	5.63

Australia to China					
Section	Temperatures		Wave Conditions		
	Sea surface (K)	Height (m)	Wavelength (m)	Period (s)	Wave speed (m/s)
ab	294.70	2.50	50.22	9.5	9.9
bc	301.15	0.30	10.20	3.60	3.36
cd	301.15	0.30	10.20	3.60	3.36
de	301.15	0.30	10.20	3.60	3.36

For the summer journey, the LNG carrier begins in warmer sea and high wave conditions (see Table 41), from Australia to the Sulu Sea, Section a-c (see Figure 36); an LNG spill would result in a vapour cloud of length 102.33 m, width of 55 m and height of 7.45 m. These warm conditions would typically result in the vapour cloud dispersing further downwind; however with the high wave conditions, the LNG pool and subsequent vapour cloud is contained to a localized area (see Table 41). This leads to an increased vertical turbulence mixing and therefore the vapour cloud dispersing more in the vertical direction, resulting in such a high vapour cloud height. As the LNG carrier continues its journey through from the Sulu Sea into the South China Sea, the conditions become cooler and wave conditions are at the lowest, Section cd (see Table 41). During this period of the journey, an LNG spill would lead to a higher vapour cloud downwind dispersion, lower crosswind and vertical dispersion, than that in Section ab (see Table 43). This is because under the lower thermal conditions, less energy is transferred to the LNG pool and subsequent vapour cloud. In addition to this, the overall more stable sea and environmental conditions, allows the vapour cloud to travel and stay closer to ground level due to a reduction in air entrainment and mixing. By this point the LNG carrier should have reached China, however if the LNG carrier was headed for Japan it would now be in Section df (see Table 41). At this point the thermal conditions are at the lowest, while the wave conditions are higher than that of Section cd but lower than that of Section a-c. This lower thermal condition again further reduces the energy that can be transferred to the LNG pool and subsequent vapour cloud. However, with a more unstable condition compared to Section cd, the reduction in downwind dispersion is transferred to an increase in lateral and vertical dispersion.

Table 43: $\frac{1}{2}$ LFL of vapour cloud in summer.

Section	Sea Surface Temperature (K)	Length (m)	Width (m)	Height (m)
ab	307.15	102.33	55	7.45
bc	307.15	102.33	55	7.45
cd	294.70	140.10	48.68	5.39
df	291.65	128.48	51.98	5.80

It's interesting to note that for the winter journey, the wave conditions are relatively similar to summer, with the main differences being observed in the thermal conditions (see Table 41 and Table 42). As the LNG carrier begins its journey, Section ab, the thermal conditions are at the lowest while the wave conditions are at the highest (see Table 42). This low thermal condition reduces the amount of energy that could otherwise be transferred into the LNG pool and vapour cloud, which should result in a small LNG vapour cloud formation. However, with the high wave conditions, the vapour cloud was able to spread lateral and in the vertical direction due to increase air entrainment as a result of the unstable conditions (see Table 44). As the LNG carrier moves on, Section bd, the thermal conditions increase while the wave conditions are at the lowest (see Table 42). This increase in thermal conditions leads to an increase in the energy transferred into the LNG pool and vapour cloud, allowing the vapour cloud to travel further downwind than in Section ab (see Table 44). However, with a more stable and low wave conditions, it leads to a reduction in lateral and vertical dispersion of the vapour cloud. The LNG carrier would have reached China at Point e, however if the LNG carrier was headed for Japan, it would now move on into Section df (see Figure 36). In this Section the thermal conditions are at the highest and the wave conditions are higher than Section bd but lower than Section ab (see Table 42). The high thermal conditions of Section df allowed for the vapour cloud to travel further than in Section ab. However, with more unstable conditions compared to Section bd, the vapour cloud was able to disperse further in the lateral and vertical directions.

Table 44: $\frac{1}{2}$ LFL of vapour cloud in winter.

Section	Sea Surface Temperature (K)	Length (m)	Width (m)	Height (m)
ab	294.70	113.47	55.55	6.59
bc	301.15	132.54	48.45	5.95
cd	301.15	132.54	48.45	5.95
df	307.15	116.2	51.06	6.82

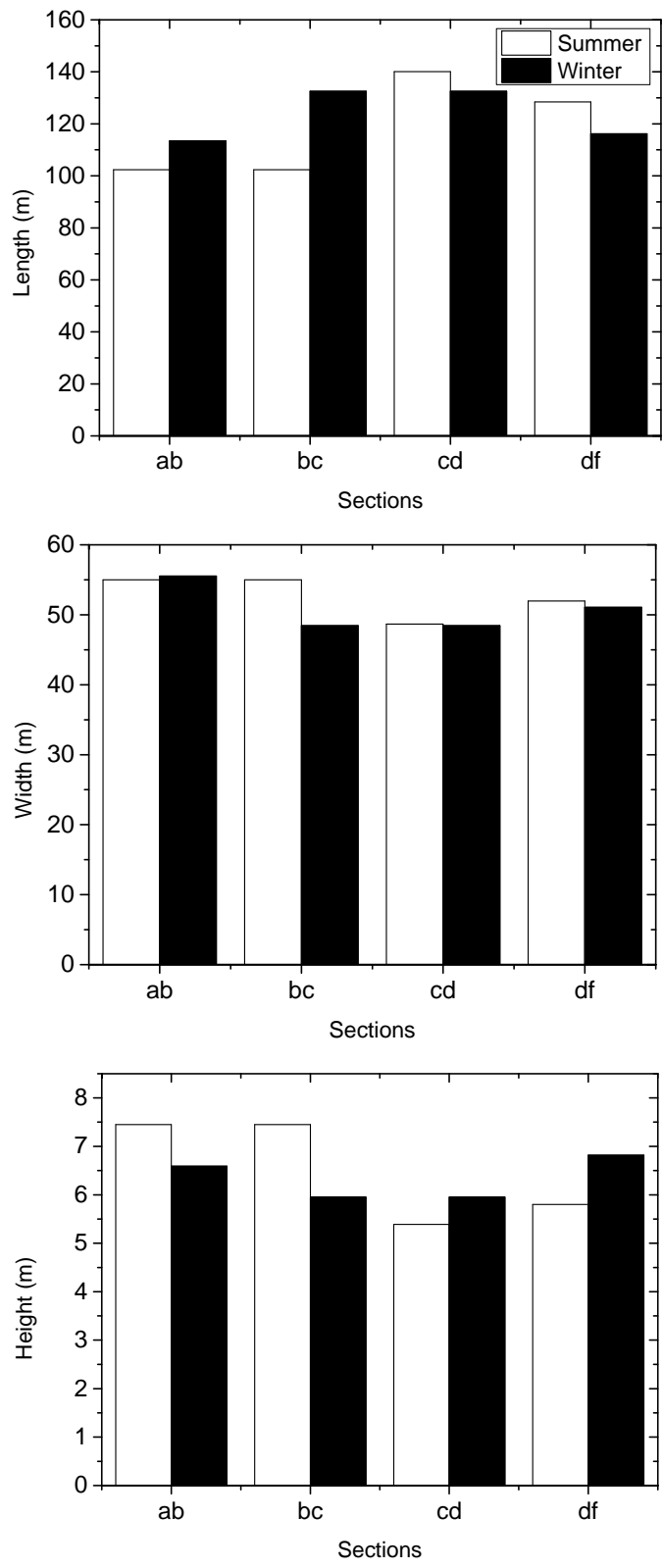


Figure 37: Summer vs. winter comparison of vapour cloud dimensions in each section (results obtained at $\frac{1}{2}$ LFL).

Figure 37 summarises a comparison of the vapour cloud dimensions at $\frac{1}{2}$ LFL between summer and winter transport. It can be seen that the height length of the vapour cloud has the highest difference between the two seasons, while the difference in width of the vapour cloud was minuscule. This analysis and results in Figure 37 are useful for deducing which routes need to be watched carefully in order to reduce potential hazards that would occur from an LNG spill during LNG transport. In the earlier parts of Section ab, the LNG carrier is in open seas and in order to minimise affected zones during an LNG spill, the length of the vapour cloud should be an area of focus across both seasons. As the LNG carrier travels on, it soon approaches Bail and is passing between islands; therefore the width and height of the vapour cloud are the main areas of interest in this Section. Based on the results presented in Figure 37, the winter season leads to the lowest vapour cloud height while there is little difference in the width of the vapour cloud. As the LNG carrier passes Indonesia and the Philippines, it is now in Section bc, again amongst islands; in this Section the length, width and height of the vapour cloud are all important. Figure 37 shows us that LNG spill during either summer or winter transport can lead to the most affected zone and depends on the orientation of the LNG carrier when the spill occurs. This conclusion can also be applied to the earlier parts of Section cd before the LNG carriers arrives at the South China Sea. Once in the South China Sea, the LNG carrier is now in open waters and in order to reduce any potential hazardous, the area of focus should be on how to control the length of the vapour cloud. As the LNG carrier now enters the North Pacific Ocean towards Japan, Section df of the LNG carrier is now in open waters therefore the vapour cloud size is not a major concern in such environments. However, with safety in mind, it is always idea to minimise the affect zone, and in this case an LNG spill during summer can lead to the most affect zone.

Overall this analysis suggests that an LNG spill during winter can lead to the least affect zone for Australian LNG transport compared to a spill during summer. By analysing the seasons individually, in order to minimise potential hazards from an LNG spill during summer, the main focus should be on Section bc as the LNG carrier would be surrounded by islands. On the other hand, during winter, Section bd should be the area of focus; due to the LNG carrier being surrounded by islands. In each season, these potential hazardous sections, Section bc (summer) and Section bd

(winter) are dependent on the orientation of the LNG carrier. Assuming that the length of the vapour cloud is not as significant due to the relatively clear/straight, kilometres long, path that the LNG carrier can follow, then devising a method to control or limit the vertical dispersion of the vapour cloud can mitigate any potential hazards.

It's also important to note that in this analysis it was assumed that the LNG carrier stops after the LNG spill occurs. This is ideal if the aim is to reduce the LNG vapour cloud dispersion, therefore containing the vapour cloud within a certain area; however if the aim is not to contain the vapour cloud, then continued motion of the LNG carrier will allow the vapour cloud to disperse and not linger. Many environmental, spill and LNG carrier conditions would lead to different results and this analysis provides a basis for further simulations of the like, to be carried out where/and when needed. For example, at the time of writing of this paper, typhoon Meranti was causing havoc in the South China Sea with winds of up to 370 km/hr and waves up to 11m;²⁹³ needless to say, an LNG carrier should not be operating under such conditions, however the variability of environmental conditions makes it necessary that simulations should be conducted for every scenario that is of interest.

6.4 Conclusion

A wave modelling code was developed based on CFD and used to investigate the stability effects of the sea waves and the atmosphere on LNG spill and dispersion. The importance of including ship motion that would induce sloshing was discussed. It was shown that by including sloshing the overall pressure on the tank walls were increased by up to 31% while the spill time was increased by up to 100s due to air back flowing into the storage tanks. The effect of stability were then considered and was observed that as stability effects increase, LNG pool size increases and evaporation rate decreases subsequently as a result of the decreased turbulence and mixing in the process. The stability/turbulence induced by the sea waves was noted to have a higher impact on the overall pool formation and dispersion process than that of the wind speed. An increase in stability effects were shown to quantitatively affect vapour cloud dispersion across possible LNG trade routes: up to 8% increase in vapour cloud length, 11% increase in vapour loud width and a 19% decrease in

vapour cloud height. There are numerous wind speed, thermal conditions and wave conditions that can lead to different stability conditions, and with further studies a correlation could be developed to assist both researchers and hazard response personnel in making quick estimates on vapour cloud behaviour, given a set of conditions. The implications of an LNG spill from Australian LNG transport to China and Japan were investigated. It was concluded that across both seasons, areas that can lead to the greatest hazards are the travel routes surrounded by islands; such as between Bali, Indonesia and the Philippines. On another hand, when compared to summer, an LNG spill during winter was shown to result in the least hazard or affect area. In order to mitigate the potential hazard in either season, a method to control or limit the vertical dispersion of the vapour cloud is needed; in addition to stopping the LNG carrier once a spill has occurred.

7 CONCLUSION AND FUTURE WORK

7.1 Introduction

Significant research advances have been made in LNG value chain and the understanding and management of the associated risks/safety issues during the handling, storage and transport of LNG. Recent developments in LNG production chain were focused on optimising the process for efficiency improvement, particularly those in the liquefaction and regasification processes, of which several have been implemented. Extensive research has improved our understanding of the fundamental mechanisms that control the dynamics of an LNG spill and the pool formation, vapour dispersion and potential combustion/fire following such a spill. Such knowledge and discovery has allowed for establishing and validating mathematical models for hazard prediction and for developing methods for improving the safety of personnel, facilities and ships. This chapter summarizes the key findings of this study, in addition with recommendations for future work, to better improve and expand on our understanding of the present research.

7.2 Conclusion

7.2.1 Simulation and Analysis of LNG Dispersion

- There are still various important technical gaps, which led to the development of a Fluent CFD code, the direct CFD simulation method;
- This new modelling method was compared to conventional estimated pool methods and experimental data from the Burro 8 tests. Both modelling methods under predicted the general shape of the vapour cloud, the dispersion process, volume concentration and arrival time of the vapour cloud;
- However, with the inclusion of statistical measures in the analysis, the direct CFD simulation method was shown to be superior to the conventional pool estimation method; by being able to accurately capture the LNG spill and phase change process.
- The power of an impoundment on controlling LNG spill and vapour cloud dispersion was observed; with the vapour fence both acting as a barrier and also increasing air flow, turbulence and swirl/recirculation at the upwind fence;

- Lead to a reduction in downwind dispersion by up to 55%, while limiting lateral spread by up to 25%;
- Also led to a decrease in peak vapour cloud concentration of 2.6% v/v outside the vapour fence;
- These finds will be valuable for LNG regasification terminals and LNG tankers.

7.2.2 Effect of Sea Surface and Air Temperatures Simulation

- Falcon 1 test was simulated with the direct CFD simulation method and shown to have good agreement with experimental data;
- The effect of air and sea surface temperatures on LNG spill and dispersion was investigated with the effect of the sea surface temperature shown to have a greater impact on the dispersion process;
- Overall, an increase in the temperature of the environment led to the following vapour cloud spatial evolution, the length of the vapour cloud increased, by up to 26%, the width decreased, by up to 6%, and the height increased, by up to 5%, as a result of increasing enthalpy in the system;
- It was also noted that in cooler conditions (sea temperature below 0 °C), the growth of the vapour cloud flows a different trend compared to that at warmer conditions (sea temperature above 0 °C).

7.2.3 Stability Effect Simulation and Analysis of LNG Dispersion

- A wave modelling method was incorporated into the direct CFD simulation method and used to investigate stability effect on LNG spill and dispersion;
- The importance of modelling sloshing, induced by ship motion was shown, with sloshing leading to an increase of tank wall pressure by up to 31% and an increase in spill times by up to 100 s;
- Analysis on the effect of stability showed that as stability increases, LNG pool size also increases, while evaporation rate decreases as a result of the decreased turbulence and mixing in the process;
- The stability/turbulence induced by the sea waves, were noted to have a greater impact on the dispersion process;
- Overall, it was shown that increasing the stability of the system, leads to an 8% increase in vapour cloud length, 11% increase in vapour cloud width and a 19% decrease in vapour cloud height;

- Finally the overall implications of this study to Australian LNG transport to China and Japan was conducted, from which it was concluded that across both seasons, travel routes surrounded by islands can lead to the greatest hazards in the event of a LNG spill. On another hand, a LNG spill during winter, compared to summer, has shown to result in a reduced hazardous area;
- To mitigate potential hazards, a method to control or limit the vertical dispersion of the vapour cloud is needed, in addition to stopping the LNG carrier once a spill has occurred.

7.3 Future Work

Basis on the conclusions drawn from this PhD study, the following future research is suggested.

- (1) The ability of impoundments to control LNG spills and subsequent vapour cloud dispersion was investigated. As good as impoundments being for containing and controlling spill, the use of impoundments can also cause another hazard due to the build-up of vapour cloud within the impoundment. Further research is needed in order to determine best practices of increasing the dispersion within the vapour cloud and how different vapour fence sizes can affect this dispersion process.
- (2) The thermal effect of spill substrate and atmosphere on LNG pool formation and dispersion was investigated; formation of ice can lead to decreased evaporation rate and other uncertainties. Ice formation was not observed in this study; however ice formation can occur in confined LNG spills under certain conditions.¹⁸² Therefore further research is needed by focusing on confined LNG spills to understand how ice formation affects LNG pool formation and vapour cloud dispersion.
- (3) Effect of stability (sea and atmospheric dynamics) was investigated; as was address in Section 6.1 Pasquill stability is determined primarily based on a combination of atmospheric and incoming solar radiation and this study focused primarily on LNG tanker routes. For LNG transports in other oceans and regions, there are possibly other combinations that may lead to different stability class. Therefore, future research is needed to investigate those possible combinations specific to those conditions in order to understand how

atmospheric and sea dynamics effect the LNG spill, pool formation and dispersion process under the prevailing conditions.

- (4) This PhD study only concerns the simulation of LNG spill, pool formation and dispersion. It is important to extend the model to include LNG pool firing and cloud combustion.

Future research is warranted in these important areas for addressing the challenges arising from the rapid increases in production and use of LNG, potential terrorist threats and public confidence in LNG safety. While there have been no major incidents in the LNG industry with the use of current systems, with further studies and continuous improvements, this safety record can be maintained while developing correlations which could assist both researchers and hazard response personnel in making quick estimates, based on spill and environmental conditions in order to contain and control LNG spills and vapour cloud dispersion.

REFERENCES

1. Ikealumba, W. C.; Wu, H., Some Recent Advances in Liquefied Natural Gas (LNG) Production, Spill, Dispersion, and Safety. *Energy & Fuels* **2014**, 28, (6), 3556-3586.
2. BP *BP Statistical review of world energy 2013*; British Petroleum (BP): London, 2013.
3. IEA *World Energy Outlook 2012*; International energy agency: Paris, 2012.
4. Lim, W.; Choi, K.; Moon, I., Current status and perspectives of liquefied natural gas (LNG) plant design. *Industrial & engineering chemistry research* **2012**, 52, (9), 3065-3088.
5. EIA Carbon dioxide emissions coefficients. http://www.eia.gov/environment/emissions/co2_vol_mass.cfm (Last accessed, November 2013)
6. US-EIA *Annual Energy Outlook 2013-With Projections to 2040*; DOE/EIA-0383(2013); U.S. Energy information administration: 2013.
7. Foss, M. M. *Introduction to LNG*; Center for Energy Economics, Bureau of Economic Geology, The University of Texas at Austin: 2003.
8. Starling, K. E.; Savidge, J. L. In *Compressibility factors of natural gas and other related hydrocarbon gases*, American Gas Association, Washington, DC, 1992; American Gas Association, Operating Section: Washington, DC, 1992.
9. Shaw, B.; Shaw, G. LPG, LNG and CNG. http://www.envocare.co.uk/lpg_lng_cng.htm (Last accessed, November 2013)
10. Katz, D. L., *Handbook of natural gas engineering*. McGraw Hill Book Company, Inc.: New York, Toronto, London, 1959.
11. NIST NIST chemistry webbook. <http://webbook.nist.gov/chemistry/> (Last accessed, November 2013)
12. Consulting, A., *Consequence assessment methods for incidents involving releases from liquified natural gas carriers*. ABS Consulting: Unknown, 2004; p 128.
13. Murdock, J. W., *Fundamental fluid mechanics for the practicing engineer* 1st ed.; CRC Press: 1993.
14. Wegrzyn, J.; Powars, C. *Best practices to avoid liquefied natural gas fueling station venting losses*; Brookhaven National Laboratory: Washington D.C., 2012.
15. Howell, J.; Harger, J. *CNC and LNG: what's best for your fleet*; Westport: New York, 2013.
16. Australia, W. *LNG industry profile - Strategic policy*; Australia, 2012; p 5.
17. Boskalis *The Brass LNG project (Nigeria)*; Dredging & Marine Experts: The Netherlands, 2013.
18. Castillo, L.; Nadales, R.; Gonzalez, C.; Dorao, C. A.; Viloria, A., Technology selection for liquefied natural gas (LNG) on baseload plants. In *XIX Internation gas conventionAVPG*, Caracas, Venezuela, 2010.
19. Humphrey, G. Current State and Outlook for the LNG Industry. http://www.forum.rice.edu/wp-content/uploads/2011/06/RT_110909_Humphries.pdf (accessed Nov 2013)
20. EIA *Algeria overview*; U.S. Energy Information Administration: New York, 2013.

21. Prasetyo, N. H. *maintaining excellence in a declining production*; Process & SHE Engineering: 2013.
22. Ukpohor, E. T. O., Nigerian gas masster plan: strenthening the nigeria gas infreastucture blueprint as a base for expanding regional gas market. In *24th Wolrd Gas Conference*, Nigeria Liquefied Natural Gas Company, Bonny Island: Agenthina, 2009.
23. Qatargas *Inovation in global energy*; Qatargas operating company limited: Qatar, 2012.
24. Total Yamal LNG: harnessing the arctic's gas resources. <http://total.com/en/energies-expertise/oil-gas/exploration-production/projects-achievements/lng/yamal-lng> (Last accessed, November 2013)
25. Wood, D. A., A review and outlook for the global LNG trade. *Journal of natural gas science and engineering* **2012**, 9, (0), 16-27.
26. EIA *International energy outlook 2013*; U.S. Energy information administration: Washington, DC, 2013.
27. Okamura, T.; Furukawa, M.; Ishitani, H., Future forecast for life-cycle greenhouse gas emissions of LNG and city gas 13A. *Applied energy* **2007**, 84, (11), 1136-1149.
28. Foss, M. M. *An overview on liquefied natural gas (LNG), its properties, the LNG industry, and safety considerations*; The University of Texas at Austin: 2012.
29. Tusiani, M.; Shearer, G., *LNG : A Nontechnical Guide*. PennWell Corp: Tulsa, Okla, 2007; p 436.
30. EIA *The global liquefied natural gas market: status and outlook*; Energy Information Administration, U.S. Department of Energy: Washington, DC, 2003.
31. Barnett, P. J. Life cycle assessment (LCA) of liquefied natural gas (LNG) and its environmental impact as a low carbon energy source. University of Southern Queensland, 2010.
32. Burnham, A.; Han, J.; Clark, C. E.; Wang, M.; Dunn, J. B.; Palou-Rivera, I., Life-Cycle Greenhouse Gas Emissions of Shale Gas, Natural Gas, Coal, and Petroleum. *Environmental science & technology* **2011**, 46, (2), 619-627.
33. Lavray, H. *Life cycle assessment of electricity generation* Eurelectric: Europe, 2011.
34. Cherubini, F.; Bird, N. D.; Cowie, A.; Jungmeier, G.; Schlamadinger, B.; Woess-Gallasch, S., Energy- and greenhouse gas-based LCA of biofuel and bioenergy systems: Key issues, ranges and recommendations. *Resources, conservation and recycling* **2009**, 53, (8), 434-447.
35. Ou, X.; Zhang, X.; Chang, S.; Guo, Q., Energy consumption and GHG emissions of six biofuel pathways by LCA in (the) People's Republic of China. *Applied energy* **2009**, 86, Supplement 1, (0), S197-S208.
36. Jaramillo, P.; Griffin, W. M.; Matthews, H. S., Comparative Life-Cycle Air Emissions of Coal, Domestic Natural Gas, LNG, and SNG for Electricity Generation. *Environmental science & technology* **2007**, 41, (17), 6290-6296.
37. Bridgwood, P. *Improved LNG process*; Liquefied Natural Gas Ltd: Perth, 2013.
38. Luketa-Hanlin, A., A review of large-scale LNG spills: Experiments and modeling. *Journal of hazardous materials* **2006**, 132, (2–3), 119-140.
39. Cleaver, P.; Johnson, M.; Ho, B., A summary of some experimental data on LNG safety. *Journal of hazardous materials* **2007**, 140, (3), 429-38.
40. Koopman, R. P.; Ermak, D. L., Lessons learned from LNG safety research. *Journal of hazardous materials* **2007**, 140, (3), 412-28.

41. Raj, P. K., LNG fires: A review of experimental results, models and hazard prediction challenges. *Journal of hazardous materials* **2007**, 140, (3), 444-464.
42. Havens, J.; Spicer, T., United states regulations for siting LNG terminals: Problems and potential. *Journal of hazardous materials* **2007**, 140, (3), 439-43.
43. NGSA Natural gas - Background. <http://naturalgas.org/overview/background/> (Last viewed, November 2013)
44. Cook, P. P.; Beck, D. V.; Brereton, P. D.; Clark, P. R.; Fisher, D. B.; Kentish, P. S.; Toomey, M. J.; Williams, D. J. *Engineering energy: Unconventional gas production*; ACOLA: Melbourne, Victoria, 2012, 2013.
45. Al-shobi, S. A. Simulation and integration of liquefied natural gas (LNG) processes. Texas A&M university, 2007.
46. Associates, P. P. a. M., *LNG Cost & Competition*. Poten & Partners and Merlin Associates: New York, 2004.
47. LNG, A. *Environmental impact statement*; Arrow Energy: Australia, 2012.
48. Mokhatab, S.; Economides, M. J. In *Onshore LNG Production Process Selection*, SPE Annual Technical Conference and Exhibition, San Antonio, Texas, USA, 24-27 September 2006, 2006; Society of Petroleum Engineers: San Antonio, Texas, USA, 2006.
49. Marin, Special Issue on LNG. *Report - a newsletter of MARIN* **2003**, 81, 1-19.
50. Næss, J.; Giske, S. I.; Bjerkeli, L., Concrete gravity-based structures used for offshore LNG storage and regasification in the Adriatic Sea. *Structural Concrete* **2010**, 11, (2), 73-81.
51. Andress, D. L. *The Phillips Optimized Cascade LNG Process: A Quarter Century of Improvements*; Phillips Petroleum Company: Bartlesville, OK, 1996.
52. Martin, P. Y.; Fischer, B. In *Natural Gas Liquefaction Processes Comparison*, 14th International Conference and Exhibition on Liquefied Natural Gas (LNG-14), Doha, Qatar, March 21 - 24, 2004; Doha, Qatar, 2004.
53. Shukri, T., LNG Technology Selection. *Hydrocarbon Engineering* **2004**.
54. ConocoPhillips ConocoPhillips Optimized Cascade Process. http://lnglicensing.conocophillips.com/EN/Documents/ConocoPhillipsLNG_Brochure.pdf (Last accessed, November 2013)
55. Michelsen, F. A.; Lund, B. F.; Halvorsen, I. J., Selection of optimal, controlled variables for the TEALARC LNG process. *Industrial & engineering chemistry research* **2010**, 49, (18), 8624-8632.
56. Stebbing, R.; O'brien, J. In *An updated report on the PRICO (TM) process for LNG plants*, GASTECH 75: LNG & LPG Technology congress, Paris, France, 1975; Paris, France, 1975.
57. Singh, A.; Hovd, M. In *Dynamic modeling and control of the PRICO LNG process*, AIChE annual meeting, San Francisco, CA, 2006; San Francisco, CA, 2006.
58. Swenson, L. K. Single mixed refrigerant, closed loop process for liquefying natural gas. 1977.
59. Schmidt, W.; Kennington, B., Air Products meets requirements of full range of Floating LNG concepts. *LNG J* **2011**.
60. McKeever, J.; Pillarella, M.; Bower, R., An ever evolving technology. *LNG industry* **2008**, (Spring).
61. Pillarella, M.; Liu, Y.-N.; Petrowski, J.; Bower, R. In *The C3MR liquefaction cycle: versatility for a fast growing, ever changing LNG industry*, Proceedings of the 15 th International Conference and Exhibition on Liquefied Natural Gas, Barcelona, Spain, April 24 - 27, 2007; Barcelona, Spain, 2007.

62. Longsworth, R. C. Cryostat with serviceable refrigerator. 1981.
63. Liu, Y.-N.; Newton, C. L. Feed gas drier precooling in mixed refrigerant natural gas liquefaction processes. 1988.
64. Martin, P.-Y.; Pigourier, J.; Fischer, B., LNG process selection, no easy task. *Hydrocarbon engineering* **2004**, 9, (5), 75-79.
65. Dam, W.; Ho, S.-M., Unusual design considerations drive selection of Sakhalin LNG plant facilities. *Oil & Gas Journal* **2001**, 99, (40), 58-58.
66. Newton, C. L. Dual mixed refrigerant natural gas liquefaction with staged compression. 1985.
67. van de Graaf, J. M.; Pek, B., Large-capacity LNG trains: The shell parallel mixed refrigerant process. *Business Briefing: LNG Review* **2005**.
68. Flesch, E.; Raillard, J.-C.; de France, G. In *CII Liquefaction Process: 2 cascades into 1*, 12th International Conference and Exhibition on Liquefied Natural Gas (LNG-12), Perth, Australia, 1998; Perth, Australia, 1998; pp 4-7.
69. Roberts, M. J.; Agrawal, R. Hybrid cycle for the production of liquefied natural gas. 2001.
70. Roberts, M.; Liu, Y.; Bronfenbrenner, J.; Petrowski, J. In *Reducing LNG Capital Cost in Today's Competitive Environment*, 14th International Conference & Exhibition on Liquefied Natural Gas (LNG14), Doha, Qatar, 2004; Doha, Qatar, 2004.
71. Bauer, H. In *A Novel Concept for Large LNG Baseload Plants*, 2001 AIChE Spring National Meeting, Houston, TX, April 22 - 26, 2001; Houston, TX, 2001.
72. Berger, E.; Forg, W.; Heiersted, R.; Paurola, P. *The MFC®(Mixed Fluid Cascade) Process for the first European Baseload LNG Production Plant*; Linde Technology: 2003; pp 12-23.
73. Barron, R. F., *Cryogenic systems*. Oxford University Press ; Clarendon Press: New York; Oxford [Oxfordshire], 1985.
74. Walker, G., *Cryocoolers*. Plenum Press: New York, London, 1983; p 392.
75. Timmerhaus, K. D. F. T. M., *Cryogenic process engineering*. Plenum Press: New York, 1989.
76. Alabdulkarem, A.; Mortazavi, A.; Hwang, Y.; Radermacher, R.; Rogers, P., Optimization of propane pre-cooled mixed refrigerant LNG plant. *Applied thermal engineering* **2011**, 31, (6-7), 1091-1098.
77. Paradowski, H.; Bamba, M.; Bladanet, C., Propane precooling cycles for increased LNG train capacity. In *14th International conference and exhibition on liquefied natural gas*, 2004; pp 107 - 124.
78. Venkatarathnam, G. *Cryogenic mixed refrigerant processes*; Springer: New York, 2008.
79. Khan, M. S.; Lee, S.; Rangaiah, G. P.; Lee, M., Knowledge based decision making method for the selection of mixed refrigerant systems for energy efficient LNG processes. *Applied Energy* **2013**, 111, (0), 1018-1031.
80. Castillo, L.; Majzoub Dahouk, M.; Di Scipio, S.; Dorao, C. A., Conceptual analysis of the precooling stage for LNG processes. *Energy conversion and management* **2013**, 66, (0), 41-47.
81. Baek, S.; Hwang, G.; Lee, C.; Jeong, S.; Choi, D., Novel design of LNG (liquefied natural gas) reliquefaction process. *Energy conversion and management* **2011**, 52, (8-9), 2807-2814.
82. Lim, W.; Lee, I.; Tak, K.; Cho, J. H.; Ko, D.; Moon, I., Efficient Configuration of a Natural Gas Liquefaction Process for Energy Recovery. *Industrial & Engineering Chemistry Research* **2014**, 53, (5), 1973-1985.

83. Chaker, M.; Meher-Homji, C. B.; Pillai, P.; Bhattacharya, D.; Messersmith, D. In *Application of Boil Off Gas Compressors in LNG Plants*, ASME Turbo Expo 2014: Turbine Technical Conference and Exposition, 2014; American Society of Mechanical Engineers: 2014.
84. Yan, J.; Shamim, T.; Chou, S. K.; Li, H.; Liu, S.; Li, X.; Huo, Y.; Li, H., An Analysis of the Primary Energy Consumed by the Re-Liquefaction of Boil-off Gas of LNG Storage Tank. *Energy Procedia: The 7th International Conference on Applied Energy (ICAE2015)* **2015**, 75, 3315-3321.
85. Rodgers, P.; Mortazavi, A.; Eveloy, V.; Al-Hashimi, S.; Hwang, Y.; Radermacher, R., Enhancement of LNG plant propane cycle through waste heat powered absorption cooling. *Applied thermal engineering* **2012**, 48, (0), 41-53.
86. Fazlollahi, F.; Bown, A.; Ebrahimzadeh, E.; Baxter, L. L., Design and analysis of the natural gas liquefaction optimization process- CCC-ES (energy storage of cryogenic carbon capture). *Energy* **2015**, 90, Part 1, 244-257.
87. Fazlollahi, F.; Bown, A.; Ebrahimzadeh, E.; Baxter, L. L., Transient natural gas liquefaction and its application to CCC-ES (energy storage with cryogenic carbon captureTM). *Energy* **2016**, 103, 369-384.
88. Wahl, P. E.; Løvseth, S. W.; Mølnvik, M. J., Optimization of a simple LNG process using sequential quadratic programming. *Computers & chemical engineering* **2013**, 56, (0), 27-36.
89. Chang, H.-M.; Lim, H. S.; Choe, K. H., Effect of multi-stream heat exchanger on performance of natural gas liquefaction with mixed refrigerant. *Cryogenics* **2012**, 52, (12), 642-647.
90. Rian, A. B.; Ertesvåg, I. S., Exergy Evaluation of the Arctic Snøhvit Liquefied Natural Gas Processing Plant in Northern Norway—Significance of Ambient Temperature. *Energy & Fuels* **2012**, 26, (2), 1259-1267.
91. Li, Y.; Wang, X.; Ding, Y., An optimal design methodology for large-scale gas liquefaction. *Applied Energy* **2012**, 99, (0), 484-490.
92. Li, Q. Y.; Ju, Y. L., Design and analysis of liquefaction process for offshore associated gas resources. *Applied Thermal Engineering* **2010**, 30, (16), 2518-2525.
93. Yuan, Z.; Cui, M.; Xie, Y.; Li, C., Design and analysis of a small-scale natural gas liquefaction process adopting single nitrogen expansion with carbon dioxide pre-cooling. *Applied Thermal Engineering* **2014**, 64, (1-2), 139-146.
94. Lukaszewski, M. W.; Zimmerman, W. B. J.; Tennant, M. T.; Webster, M. B., Application of inverse methods based algorithms to Liquefied Natural Gas (LNG) storage management. *Chemical engineering research and design* **2013**, 91, (3), 457-463.
95. Turbo, M. D. *Propulsion trends in LNG carriers*; MAN Diesel & Turbo: Denmark, 2009.
96. Woehrling, J.-M.; Cotterell, C. D. *International safety guide for inland navigation tank-barges and terminals* Central Commission for the Navigation of the Rhine Strasbourg, 2010.
97. Peebles, M. W. H., *Natural gas fundamentals*. Shell International Gas Limited: 1992.
98. Rudan, S.; Ascic, B.; Visic, I., Crashworthiness study of LPG ship with type C tanks. *Collision and Grounding of Ships and Offshore Structures* **2013**, 331-337.
99. Querol, E.; Gonzalez-Regueral, B.; García-Torrent, J.; Ramos, A., Available power generation cycles to be coupled with the liquid natural gas (LNG) vaporization process in a Spanish LNG terminal. *Applied Energy* **2011**, 88, (7), 2382-2390.

100. Liu, C.; Zhang, J.; Xu, Q.; Gossage, J. L., Thermodynamic-Analysis-Based Design and Operation for Boil-Off Gas Flare Minimization at LNG Receiving Terminals. *Industrial & Engineering Chemistry Research* **2010**, 49, (16), 7412-7420.
101. Tsatsaronis, G.; Morosuk, T., Advanced exergetic analysis of a novel system for generating electricity and vaporizing liquefied natural gas. *Energy* **2010**, 35, (2), 820-829.
102. Morosuk, T.; Tsatsaronis, G., Comparative evaluation of LNG – based cogeneration systems using advanced exergetic analysis. *Energy* **2011**, 36, (6), 3771-3778.
103. Morosuk, T.; Tsatsaronis, G.; Boyano, A.; Gantiva, C., Advanced exergy-based analyses applied to a system including LNG regasification and electricity generation. *International Journal of Energy and Environmental Engineering* **2012**, 3, (1), 1-9.
104. Dispenza, C.; Dispenza, G.; La Rocca, V.; Panno, G., Exergy recovery during LNG regasification: Electric energy production – Part one. *Applied Thermal Engineering* **2009**, 29, (2–3), 380-387.
105. Dispenza, C.; Dispenza, G.; Rocca, V. L.; Panno, G., Exergy recovery during LNG regasification: Electric energy production – Part two. *Applied Thermal Engineering* **2009**, 29, (2–3), 388-399.
106. Shi, X.; Che, D., A combined power cycle utilizing low-temperature waste heat and LNG cold energy. *Energy Conversion and Management* **2009**, 50, (3), 567-575.
107. Liu, Y.; Guo, K., A novel cryogenic power cycle for LNG cold energy recovery. *Energy* **2011**, 36, (5), 2828-2833.
108. Zhang, N.; Lior, N., A novel near-zero CO₂ emission thermal cycle with LNG cryogenic exergy utilization. *Energy* **2006**, 31, (10–11), 1666-1679.
109. Dispenza, C.; Dispenza, G.; Rocca, V. L.; Panno, G., Exergy recovery in regasification facilities – Cold utilization: A modular unit. *Applied Thermal Engineering* **2009**, 29, (17–18), 3595-3608.
110. La Rocca, V., Cold recovery during regasification of LNG part one: Cold utilization far from the regasification facility. *Energy* **2010**, 35, (5), 2049-2058.
111. La Rocca, V., Cold recovery during regasification of LNG part two: Applications in an Agro Food Industry and a Hypermarket. *Energy* **2011**, 36, (8), 4897-4908.
112. Messineo, A.; Panno, G., LNG cold energy use in agro-food industry: A case study in Sicily. *Journal of Natural Gas Science and Engineering* **2011**, 3, (1), 356-363.
113. Koopman, R. P.; Baker, J.; Cederwall, R. T.; Goldwire, H. C. J.; Hogan, W. J.; Kamppinen, L. M.; Kiefer, R. D.; McClure, J. W.; McRae, T. G.; Morgan, D. L. *Burro series data report - LLNL/NWC 1980 LNG spill tests.* ; Lawrence Livermore National Laboratory: Berkeley, CA, 1982a.
114. Koopman, R. P.; Baker, J.; Cederwall, R. T.; Goldwire, H. C. J.; Hogan, W. J.; Kamppinen, L. M.; Kiefer, R. D.; McClure, J. W.; McRae, T. G.; Morgan, D. L. *Burro series data report - LLNL/NWC 1980 LNG spill tests.* ; Lawrence Livermore National Laboratory: Berkeley, CA, 1982b.
115. Conrado, C.; Vesovic, V., The influence of chemical composition on vaporisation of LNG and LPG on unconfined water surfaces. *Chemical engineering science* **2000**, 55, (20), 4549-4562.
116. D. Little; P.P. Raj; Guard, U. S. C., *Assessment models in support of the hazard assessment handbook*. Cambridge, Mass., 1974.

117. Opschoor, G., Investigations into the spreading and evaporation of LNG spilled on water. *Cryogenics* **1977**, 17, (11), 629-634.
118. Gavelli, F.; Bullister, E.; Kytomaa, H., Application of CFD (Fluent) to LNG spills into geometrically complex environments. *Journal of hazardous materials* **2008**, 159, (1), 158-168.
119. Atallah, S.; Sirdesai, M.; Jennings, D. M. *Source1: A model for creating a DEGADIS input file*; Gas Research Institute: 1993.
120. Raj, P. K.; O'Farrel, P. M. *Development of additional hazard assessment models*; Arthur D. Little, Inc: 1977.
121. Webber, D. M.; Jones, S. J. In *A model of spreading vaporising pools*, International conference on Vapour Cloud Modelling, Boston Massachusetts, USA, 1987; Woodward, J., Ed. AIChE: Boston Massachusetts, USA, 1987.
122. TNO, *Methods for the calculation of physical effects (TNO Yellow Book)*. The Hague, Netherlands, 1997.
123. Woodward, J. L., Coupling dynamic blow down and pool evaporation model for LNG. *Journal of hazardous materials* **2007**, 140, (3), 478-487.
124. Woodward, J. L.; Pierorazio, A. J., SS3G - An Integrated Risk Analysis Program Using Engineering Principles for Building Damage. In *Mary K O'Connor 2001 Annual Symposium*, Center, M. K. O. C. P. S., Ed. College Station, Texas, 2001; pp 365-382.
125. Witlox, H. W. M.; Oke, A. *Verification and validation of consequence and risk models for accidental releases of hazardous chemicals to the atmosphere*; DNV Software: London, UK, 2007.
126. McQuaid, J., *Some Experiments on the Structure of Stable-stratified Shear Flows*. Health and Safety Executive, Safety in Mines Research Establishment: 1976.
127. Petersen, R. L., Effect of homogeneous and heterogeneous surface roughness on heavier-than-air gas dispersion. *Journal of Wind Engineering and Industrial Aerodynamics* **1990**, 36, Part 1, (0), 643-652.
128. Pitblado, R.; Baik, J.; Hughes, G.; Ferro, C.; Shaw, S., Consequences of LNG marine incidents. *Process safety progress* **2004**, 24, (2), 108 - 114.
129. Pitblado, R.; Baik, J.; Raghunathan, V., LNG decision making approaches compared. *Journal of Hazardous Materials* **2006**, (130), 148 - 154.
130. D.C. Thoman; K.R. O'Kula; J.C. Laul; M.W. Davis; Knecht, K. D., Comparison of ALOHA and EPIcode for Safety Analysis Applications. *Journal of Chemical Health and Safety* **2006**, 13, (6), 20 - 33.
131. Bernatik, A.; Libisova, M., Loss prevention in heavy industry: risk assessment of large gasholders. *Journal of loss prevention in the process industries* **2004**, 17, (4), 271-278.
132. Mazzoldi, A.; Hill, T.; Colls, J. J., CFD and Gaussian atmospheric dispersion models: A comparison for leak from carbon dioxide transportation and storage facilities. *Atmospheric environment* **2008**, 42, (34), 8046-8054.
133. Spaulding, M. L.; Swanson, J. C.; Jayko, K.; Whittier, N., An LNG release, transport, and fate model system for marine spills. *Journal of hazardous materials* **2007**, 140, (3), 488-503.
134. Mike Hightower; Louis Gritzo; Anay Luketa-Hanlin; John Covian; Sheldon Tieszen; Gerry Wellman; Mike Irwin; Mike Kaneshige; Brian Melof; Charles Morrow; Ragland, D., *Guidance on risk analysis and safety implications of a large liquefied natural gas (LNG) spill over water*. Sandia National Laboratories: United States, 2004; p 168.

135. Dharmavaram, S., Consequence analysis - Using a CFD model for industrial sites. *Process safety progress* **2005**, 24, (4), 316-272.
136. Hanna, S. R.; Hansen, O. R.; Dharmavaram, S., FLACS CFD air quality model performance evaluation with Kit Fox, MUST, Prairie Grass, and EMU observations. *Atmospheric environment* **2004**, 38, (28), 4675-4687.
137. Fay, J. A., Spread of large LNG pools on the sea. *Journal of hazardous materials* **2007**, 140, (3), 541-51.
138. Dandrieux, A.; Dusserre, G.; Thomas, O., The DVS model: a new concept for heavy gas dispersion by water curtain. *Environmental Modelling & Software* **2003**, 18, (3), 253-259.
139. Hald, K.; Buchlin, J.-M.; Dandrieux, A.; Dusserre, G., Heavy gas dispersion by water spray curtains: A research methodology. *Journal of Loss Prevention in the Process Industries* **2005**, 18, (4-6), 506-511.
140. McQuaid, J.; Fitzpatrick, R. D., Air entrainment by water sprays: Strategies for application to the dispersion of gas plumes. *Journal of Occupational Accidents* **1983**, 5, (2), 121-133.
141. McQuaid, J.; Fitzpatrick, R. D. *The uses and limitations of water-spray barriers*; IChemE: 1981.
142. Moodie, K., The use of water spray barriers to disperse spill in the event of heavy gases – the performance characteristics of full-scale water spray barriers when dispersing spills of heavy gases. *Plant Operation Progress* **1985**, 4, 234 - 241.
143. Moore, P. A. C.; Rees, W. D. *Forced dispersion of gases by water and steam*; IChemE: 1981.
144. Rana, M. A.; Cormier, B. R.; Suardin, J. A.; Zhang, Y.; Mannan, M. S., Experimental study of effective water spray curtain application in dispersing liquefied natural gas vapor clouds. *Process safety progress* **2008**, 27, (4), 345-353.
145. Rana, M. A.; Guo, Y.; Mannan, M. S., Use of water spray curtain to disperse LNG vapor clouds. *Journal of loss prevention in the process industries* **2010**, 23, (1), 77-88.
146. Rana, M. A.; Mannan, M. S., Forced dispersion of LNG vapor with water curtain. *Journal of loss prevention in the process industries* **2010**, 23, (6), 768-772.
147. Olewski, T.; Nayak, S.; Basha, O.; Waldram, S.; Véchot, L., Medium scale LNG-related experiments and CFD simulation of water curtain. *Journal of loss prevention in the process industries* **2011**, 24, (6), 798-804.
148. Kim, B. K.; Ng, D.; Mentzer, R. A.; Mannan, M. S., Modeling of water-spray application in the forced dispersion of LNG vapor cloud using a combined eulerian-lagrangian approach. *Industrial & engineering chemistry research* **2012**, 51, (42), 13803-13814.
149. Kim, B. K.; Ng, D.; Mentzer, R. A.; Mannan, M. S., Key parametric analysis on designing an effective forced mitigation system for LNG spill emergency. *Journal of Loss Prevention in the Process Industries* **2013**, 26, (6), 1670-1678.
150. Qi, R.; Raj, P. K.; Mannan, M. S., Underwater LNG release test findings: Experimental data and model results. *Journal of loss prevention in the process industries* **2011**, 24, (4), 440-448.
151. Cormier, B. R.; Qi, R.; Yun, G.; Zhang, Y.; Sam Mannan, M., Application of computational fluid dynamics for LNG vapor dispersion modeling: A study of key parameters. *Journal of loss prevention in the process industries* **2009**, 22, (3), 332-352.

152. Morse, T. L.; Kytömaa, H. K., The effect of turbulence on the rate of evaporation of LNG on water. *Journal of loss prevention in the process industries* **2011**, 24, (6), 791-797.
153. Ermak, D. L.; Rodean, H. C.; Lange, R.; Chan, S. T. *A survey of denser-than-air atmospheric dispersion models*; Lawrence Livermore National Laboratory: United States, 1988.
154. Sykes, R. I.; Cerasoli, C. P.; Henn, D. S., The representation of dynamic flow effects in a Lagrangian puff dispersion model. *Journal of Hazardous Materials* **1999**, 64, (3), 223-247.
155. Hankin, R. K.; Britter, R. E., TWODEE: the Health and Safety Laboratory's shallow layer model for heavy gas dispersion. Part 1. Mathematical basis and physical assumptions. *J Hazard Mater* **1999**, 66, (3), 211-26.
156. Hankin, R. K. S., Heavy gas dispersion: integral models and shallow layer models. *Journal of Hazardous Materials* **2003**, 103, (1–2), 1-10.
157. Ermak, D. L., *User's manual for SLAB: An atmospheric dispersion model for denser-than-air releases*. Lawrence Livermore National Laboratory: California, 1990.
158. Witlox, H. W. M., The HEGADAS model for ground-level heavy-gas dispersion—I. Steady-state model. *Atmospheric environment* **1994**, 28, (18), 2917-2932.
159. Witlox, H. W. M., The HEGADAS model for ground-level heavy-gas dispersion II. Time-dependent model. *Atmospheric environment* **1994**, 28, (18), 2933-2946.
160. Blackmore, D. R.; Herman, M. N.; Woodward, J. L., Heavy gas dispersion models. *Journal of hazardous materials* **1982**, 6, (1–2), 107-128.
161. Spicer, T. O.; Havens, J. A., Field test validation of the degadis model. *Journal of hazardous materials* **1987**, 16, (0), 231-245.
162. Hanna, S. R.; Chang, J. C.; Strimaitis, D. G., Hazardous gas model evaluation with field observations. *Atmospheric Environment. Part A. General Topics* **1993**, 27, (15), 2265-2285.
163. Qi, R.; Ng, D.; Cormier, B. R.; Mannan, M. S., Numerical simulations of LNG vapor dispersion in Brayton Fire Training Field tests with ANSYS CFX. *Journal of hazardous materials* **2010**, 183, (1–3), 51-61.
164. Chan, S. T.; Ermak, D. L.; Morris, L. K., FEM3 model simulations of selected thorney island phase I trials. *Journal of hazardous materials* **1987**, 16, (0), 267-292.
165. Sun, B.; Utikar, R. P.; Pareek, V. K.; Guo, K., Computational fluid dynamics analysis of liquefied natural gas dispersion for risk assessment strategies. *Journal of loss prevention in the process industries* **2013**, 26, (1), 117-128.
166. Riddle, A.; Carruthers, D.; Sharpe, A.; McHugh, C.; Stocker, J., Comparisons between FLUENT and ADMS for atmospheric dispersion modelling. *Atmospheric environment* **2004**, 38, (7), 1029-1038.
167. Rigas, F.; Sklavounos, S., Simulation of Coyote series trials—Part II: A computational approach to ignition and combustion of flammable vapor clouds. *Chemical engineering science* **2006**, 61, (5), 1444-1452.
168. Hanna, S. R.; Chang, J. C., Use of the Kit Fox field data to analyze dense gas dispersion modeling issues. *Atmospheric environment* **2001**, 35, (13), 2231-2242.
169. Luketa-Hanlin, A.; Koopman, R. P.; Ermak, D. L., On the application of computational fluid dynamics codes for liquefied natural gas dispersion. *Journal of hazardous materials* **2007**, 140, (3), 504-17.

170. Qiao, Y.; West, H. H.; Mannan, M. S.; Johnson, D. W.; Cornwell, J. B., Assessment of the effects of release variables on the consequences of LNG spillage onto water using FERC models. *Journal of hazardous materials* **2006**, 130, (1-2), 155-162.
171. Johnson, D. W.; Cornwell, J. B., Modeling the release, spreading, and burning of LNG, LPG, and gasoline on water. *Journal of hazardous materials* **2007**, 140, (3), 535-540.
172. Fay, J. A., Model of spills and fires from LNG and oil tankers. *Journal of hazardous materials* **2003**, 96, 2-3.
173. Lehr W; D., S.-B., Comparison of hypothetical LNG and fuel oil fires on water. *Journal of hazardous materials* **2004**, 107, (1-2), 1-2.
174. Vílchez, J. A.; Villafaña, D.; Casal, J., A dispersion safety factor for LNG vapor clouds. *Journal of hazardous materials* **2013**, 246–247, (0), 181-188.
175. Ponchaut, N. F.; Kytömaa, H. K.; Morrison, D. R.; Chernovsky, M. K., Modeling the vapor source term associated with the spill of LNG into a sump or impoundment area. *Journal of loss prevention in the process industries* **2011**, 24, (6), 870-878.
176. Melton, T. A.; Cornwell, J. B., LNG trench dispersion modeling using computational fluid dynamics. *Journal of loss prevention in the process industries* **2010**, 23, (6), 762-767.
177. Gavelli, F.; Chernovsky, M. K.; Bullister, E.; Kytomaa, H. K., Modeling of LNG spills into trenches. *Journal of hazardous materials* **2010**, 180, (1-3), 332-339.
178. Giannissi, S. G.; Venetsanos, A. G.; Markatos, N.; Bartzis, J. G., Numerical simulation of LNG dispersion under two-phase release conditions. *Journal of loss prevention in the process industries* **2013**, 26, (1), 245-254.
179. Würtz, J.; Bartzis, J.; Venetsanos, A.; Andronopoulos, S.; Statharas, J.; Nijsing, R., A dense vapour dispersion code package for applications in the chemical and process industry. *Journal of hazardous materials* **1996**, 46, (2-3), 273-284.
180. Bartzis, J. G. *ADREA-HF :A three-dimensional finite volume code for vapour cloud dispersion in complex terrain: final report*; Commission of the european communities, Joint research center, Institute for safety technology: Brussels, Luxembourg, 1991.
181. Venetsanos A.G; E., P.; G., B. J., The ADREA-HF CFD code for consequence assessment of hydrogen applications. *International journal of hydrogen energy international* **2010**, 35, (8), 3908-3918.
182. Vesovic, V., The influence of ice formation on vaporization of LNG on water surfaces. *Journal of hazardous materials* **2007**, 140, (3), 518-26.
183. Siuta, D.; Markowski, A. S.; Mannan, M. S., Uncertainty techniques in liquefied natural gas (LNG) dispersion calculations. *Journal of loss prevention in the process industries* **2013**, 26, (3), 418-426.
184. Britter, R. E.; McQuaid, J., *Workbook on the dispersion of dense gases*. Health & Safety Executive: Bootle, Merseyside [England], 1988.
185. Ivings, M. J.; Lea, C. J.; Webber, D. M.; Jagger, S. F.; Coldrick, S., A protocol for the evaluation of LNG vapour dispersion models. *Journal of loss prevention in the process industries* **2013**, 26, (1), 153-163.
186. Carissimo, B.; Jagger, S. F.; Daish, N. C.; Halford, A.; Selmer-Olsen, S.; Riikonen, K.; Perroux, J. M.; Wurtz, J.; Bartzis, J. G.; Duijm, N. J., The SMEDIS database and validation exercise. *International journal of environment and pollution* **2001**, 16, 614-629.

187. Daish, N. C.; Britter, R. E.; Linden, P. F.; Jagger, S. F.; Carissimo, B., SMEDIS: scientific model evaluation of dense gas dispersion models. *International journal of environment and pollution* **2000**, 14, 39-51.
188. Duijm, N. J.; Carrissimo, B. *Evaluation methodologies for dense gas dispersion models*; McGraw-Hill: 2002.
189. Ivings, M. J.; Jagger, S. F.; Lea, C. J.; Webber, D. M. *Evaluating vapour dispersion models for safety analysis of LNG facilities*; Fire Protection Research Foundation: Quincy, Massachusetts 2007.
190. Hansen, O. R.; Gavelli, F.; Ichard, M.; Davis, S. G., Validation of FLACS against experimental data sets from the model evaluation database for LNG vapor dispersion. *Journal of loss prevention in the process industries* **2010**, 23, (6), 857-877.
191. Raj, P. P.; Moussa, A. N.; Aravamudan, K. *Experiments involving pool and vapor fires from spills of liquefied natural gas on water*; DTIC Document: 1979.
192. Schneider, A. L.; Lind, C. D.; Parnarouskis, M. C. *US Coast Guard Liquefied Natural Gas Research at China Lake*; DTIC Document: 1980.
193. Raj, P.; Moussa, N.; Aravamudan, K.; Lind, C., LNG spill fire tests on water: an overview of the results. *Am. Gas Assoc., Oper. Sect., Proc.,(United States)* **1979**.
194. Schneider, A. L., Liquefied natural gas spills on water-fire modelling. *Journal of Fire Flamability* **1980**, (12), 302 - 313.
195. Mizner, G.; Eyre, J., Large-Scale LNG and LPG pool fires. *EFCE Publication Series (European Federation of Chemical Engineering)* **1982**, 25, 147-161.
196. Hirst, W.; Eyre, J., Maplin Sands experiments 1980: Combustion of large LNG and refrigerated liquid propane spills on the sea. In *Heavy Gas and Risk Assessment—II*, Springer: 1983; pp 211-224.
197. Rodean, H.; Hogan, W.; Urtiew, P.; Goldwire Jr, H.; McRae, T.; Morgan Jr, D. *Vapor burn analysis for the Coyote Series LNG spill experiments*; Lawrence Livermore National Lab., CA (USA): 1984.
198. Mizner, G.; Eyre, J., Radiation from liquefied gas fires on water. *Combustion Science and Technology* **1983**, 35, (1-4), 33-57.
199. Nedelka, D.; Moorehouse, J.; Tucker, R. In *The montoir 35 m diameter LNG pool fire experiments, TRCP. 3148R*, Proceedings of the Ninth International Conference & Expo on LNG, LNG IX IX, Nice, France, 1989; 1989.
200. Lowesmith, B. J.; Hankinson, G.; Acton, M. R.; Chamberlain, G., An Overview of the Nature of Hydrocarbon Jet Fire Hazards in the Oil and Gas Industry and a Simplified Approach to Assessing the Hazards. *Process Safety and Environmental Protection* **2007**, 85, (3), 207-220.
201. Studer, E.; Jamois, D.; Jallais, S.; Leroy, G.; Hebrard, J.; Blanchetière, V., Properties of large-scale methane/hydrogen jet fires. *International Journal of Hydrogen Energy* **2009**, 34, (23), 9611-9619.
202. Wu, Y.; Lu, Y.; Al-Rahbi, I. S.; Kalghatgi, G. T., Prediction of the liftoff, blowout and blowoff stability limits of pure hydrogen and hydrogen/hydrocarbon mixture jet flames. *International Journal of Hydrogen Energy* **2009**, 34, (14), 5940-5945.
203. Brown, L. E., Predict LNG fire radiation. *Hydrocarbon Process* **1974**, 141 - 143.
204. Raj, P.; Atallah, S., Thermal radiation from LNG spill fires. *Advanced Cryogen Engineering* **1975**, (20), 143 - 150.

205. Lautkasi, R., Validation of flame drag correlations with data from large pool fires. *Journal of Loss Prevention in the Process Industries* **1992**, 5, 175 - 180.
206. Johnson, A. D. In *A model for predicting thermal radiation hazards from large-scale LNG pool fires*, Major Hazards Onshore and Offshore, Manchester, 1992; Institute of Chemical Engineers: Manchester, 1992; pp 507 - 524.
207. Moorhouse, J.; Pritchard, M. J., Thermal radiation hazards from large pool fires and fireballs - a literature review. In *Institute of Chemical Engineers Symposium*, Institute of Chemical Engineers: Solihull, England, 1982; pp 397 - 428.
208. SFPE, *The SFPEHandbook of Fire Protection Engineering*. 2nd ed.; 1995.
209. Gavelli, F.; Davis, S. G.; Hansen, O. R., Evaluating the potential for overpressures from the ignition of an LNG vapor cloud during offloading. *Journal of loss prevention in the process industries* **2011**, 24, (6), 908-915.
210. Abe, A.; Katayama, M.; Kim, D.; Usuba, S.; Castillo, M.; Wakatsuki, M.; Kakudate, Y.; Tanaka, K.; Watanabe, Y., Numerical prediction of blast effects caused by large-scale explosion of LOX/LNG fuel. In *Internation Symposium on Structures*, Japan, 2008.
211. Fay, J. A., Risks of LNG and LPG. *Annual review of energy* **1980**, 5, (1), 89-105.
212. Raj, P. K., Field tests on human tolerance to (LNG) fire radiant heat exposure, and attenuation effects of clothing and other objects. *Journal of hazardous materials* **2008**, 157, (2-3), 247-259.
213. Pérez, J. F. S.; Ferradás, E. G.; Alonso, F. D.; García, D. P.; Cano, M. V. M.; Cotorruelo, J. Á. B., New Probit equations for the calculation of thermal effects on humans. *Process Safety and Environmental Protection* **2010**, 88, (2), 109-113.
214. Alonso, F. D.; Ferradás, E. G.; Sánchez, T. d. J. J.; Aznar, A. M.; Gimeno, J. R.; Alonso, J. M., Consequence analysis to determine the damage to humans from vapour cloud explosions using characteristic curves. *Journal of Hazardous Materials* **2008**, 150, (1), 146-152.
215. TNO, *Methods for the determination of possible damage*. The Hague: The Netherlands, 1989.
216. Pitblado, R. M.; D.F., B., Thermal hazards in the process industry. *American Institute of Chemical Engineers* **1989**, 85, 69 - 75.
217. Stoll, A. M.; Chianta, M. A., Heat transfer through fabrics as related to thermal injury. *Transactions of the New York Academy of Sciences* **1971**, 33, (7 Series II), 649-670.
218. Lihou, D.; Maund, J. In *Thermal radiation hazard from fireballs*, IChemE Symp. Series, 1982; 1982; pp 191-224.
219. Bernatik, A.; Senovsky, P.; Pitt, M., LNG as a potential alternative fuel – Safety and security of storage facilities. *Journal of loss prevention in the process industries* **2011**, 24, (1), 19-24.
220. NIPP *National infrastructure protection plan*; N/A, 2009.
221. Yun, G.; Rogers, W. J.; Mannan, M. S., Risk assessment of LNG importation terminals using the Bayesian–LOPA methodology. *Journal of Loss Prevention in the Process Industries* **2009**, 22, (1), 91-96.
222. Rathnayaka, S.; Khan, F.; Amyotte, P., Accident modeling approach for safety assessment in an LNG processing facility. *Journal of loss prevention in the process industries* **2012**, 25, (2), 414-423.
223. Parihar, A.; Vergara, C.; Clutter, J. K., Methodology for consequence analysis of LNG releases at deepwater port facilities. *Safety science* **2011**, 49, (5), 686-694.

224. Li, J.; Huang, Z., Fire and explosion risk analysis and evaluation for LNG ships. *Procedia engineering* **2012**, 45, (0), 70-76.
225. Pitblado, R., Potential for BLEVE associated with marine LNG vessel fires. *Journal of hazardous materials* **2007**, 140, (3), 527-534.
226. Zhang, Q.-x.; Liang, D., Thermal Radiation and Impact Assessment of the LNG BLEVE Fireball. *Procedia Engineering* **2013**, 52, (0), 602-606.
227. Abbasi, T.; Abbasi, S. A., The boiling liquid expanding vapour explosion (BLEVE): Mechanism, consequence assessment, management. *Journal of Hazardous Materials* **2007**, 141, (3), 489-519.
228. Grossel, S. S., LNG Fire Protection & Emergency Response. *Journal of Loss Prevention in the Process Industries* **2008**, 21, (4), 492.
229. Cheng, S.-R.; Lin, B.; Hsu, B.-M.; Shu, M.-H., Fault-tree analysis for liquefied natural gas terminal emergency shutdown system. *Expert Systems with Applications* **2009**, 36, (9), 11918-11924.
230. Keshavarz, G.; Thodi, P.; Khan, F., Risk-based shutdown management of LNG units. *Journal of Loss Prevention in the Process Industries* **2012**, 25, (1), 159-165.
231. Suardin, J. A.; Wang, Y.; Willson, M.; Mannan, M. S., Field experiments on high expansion (HEX) foam application for controlling LNG pool fire. *Journal of Hazardous Materials* **2009**, 165, (1-3), 612-622.
232. Suardin, J. A.; Qi, R.; Cormier, B. R.; Rana, M.; Zhang, Y.; Mannan, M. S., Application of fire suppression materials on suppression of LNG pool fires. *Journal of loss prevention in the process industries* **2011**, 24, (1), 63-75.
233. Sun, B.; Guo, K., LNG accident dynamic simulation: Application for hazardous consequence reduction. *Journal of Loss Prevention in the Process Industries* **2013**, 26, (6), 1246-1256.
234. Taylor, D. W., The role of consequence modeling in LNG facility siting. *Journal of hazardous materials* **2007**, 142, (3), 776-785.
235. Raj, P. K.; Lemoff, T., Risk analysis based LNG facility siting standard in NFPA 59A. *Journal of Loss Prevention in the Process Industries* **2009**, 22, (6), 820-829.
236. Tanabe, M.; Miyake, A., Safety design approach for onshore modularized LNG liquefaction plant. *Journal of loss prevention in the process industries* **2010**, 23, (4), 507-514.
237. Tanabe, M.; Miyake, A., Approach enhancing inherent safety application in onshore LNG plant design. *Journal of loss prevention in the process industries* **2012**, 25, (5), 809-819.
238. Vanem, E.; Antão, P.; Østvik, I.; de Comas, F. D. C., Analysing the risk of LNG carrier operations. *Reliability Engineering & System Safety* **2008**, 93, (9), 1328-1344.
239. Vandebroek, L.; Berghmans, J., Safety Aspects of the use of LNG for Marine Propulsion. *Procedia Engineering* **2012**, 45, (0), 21-26.
240. Moon, K.; Song, S.-R.; Ballesio, J.; Fitzgerald, G.; Knight, G., Fire risk assessment of gas turbine propulsion system for LNG carriers. *Journal of Loss Prevention in the Process Industries* **2009**, 22, (6), 908-914.
241. Chang, D.; Rhee, T.; Nam, K.; Chang, K.; Lee, D.; Jeong, S., A study on availability and safety of new propulsion systems for LNG carriers. *Reliability Engineering & System Safety* **2008**, 93, (12), 1877-1885.

242. IMO, *International code for the construction and equipment of ships carrying liquefied gases in bulk : IGC Code*. International Maritime Organisation: London, 1993.
243. CFR *Minimum relief capacities for cargo tanks containing compressed or liquefied gas*; U.S. Coast Guard: N/A.
244. Havens, J.; Venart, J., Fire performance of LNG carriers insulated with polystyrene foam. *Journal of hazardous materials* **2008**, 158, (2–3), 273-279.
245. Bang, C. S.; Kim, J. G.; Lee, D. G., Cryogenic Performance of Adhesively Bonded Metal Joints for LNG Containment System. *Journal of Adhesion Science and Technology* **2012**, 26, (7), 969-986.
246. Lee, J.-S.; Ryu, Y.-S.; Kim, N.-I.; Kim, B.-J.; Kim, Y.-K.; Kim, M.-H., Stud welding for fixation of cryogenic insulation of membrane tanks in LNG ship building. *Transactions of Nonferrous Metals Society of China* **2009**, 19, Supplement 1, (0), s271-s275.
247. Kim, B. G.; Lee, D. G., Leakage characteristics of the glass fabric composite barriers of LNG ships. *Composite Structures* **2008**, 86, (1–3), 27-36.
248. Yu, Y. H.; Kim, B. G.; Lee, D. G., Cryogenic reliability of composite insulation panels for liquefied natural gas (LNG) ships. *Composite structures* **2012**, 94, (2), 462-468.
249. Yu, Y. H.; Kim, B. G.; Lee, D. G., Cryogenic reliability of the sandwich insulation board for LNG ship. *Composite structures* **2013**, 95, (0), 547-556.
250. Chul Kim, B.; Ho Yoon, S.; Gil Lee, D., Pressure resistance of the corrugated stainless steel membranes of LNG carriers. *Ocean engineering* **2011**, 38, (4), 592-608.
251. Graczyk, M.; Moan, T., Structural response to sloshing excitation in membrane LNG tank. *Journal of offshore mechanics and arctic engineering* **2010**, 133, (2), 021103-021103.
252. Pistani, F.; Thiagarajan, K., Experimental measurements and data analysis of the impact pressures in a sloshing experiment. *Ocean Engineering* **2012**, 52, (0), 60-74.
253. Mitra, S.; Wang, C. Z.; Reddy, J. N.; Khoo, B. C., A 3D fully coupled analysis of nonlinear sloshing and ship motion. *Ocean Engineering* **2012**, 39, (0), 1-13.
254. Goldwire, H. C. J.; Rodean, H. C.; Cederwall, R. T.; Kansa, E. J.; Koopman, R. P.; McClure, J. W.; McRae, T. G.; Morris, L. K.; Kamppinen, L.; Kiefer, R. D. *Coyote series data report - LLNL/NWC 1981LNG spill tests dispersion, vapor burn, and rapid-phase-transition*; Lawrence Livermore National Labarotory: Berkeley, CA, 1983a.
255. Goldwire, H. C. J.; Rodean, H. C.; Cederwall, R. T.; Kansa, E. J.; Koopman, R. P.; McClure, J. W.; McRae, T. G.; Morris, L. K.; Kamppinen, L.; Kiefer, R. D. *Coyote series data report - LLNL/NWC 1981LNG spill tests dispersion, vapor burn, and rapid-phase-transition*; Lawrence Livermore National Labarotory: Berkeley, CA, 1983b.
256. Brown, T. C.; Cederwall, R. T.; Chan, S. T.; Ermak, D. L.; Koopman, R. P.; Lamson, K. C.; McClure, J. W.; Morris, L. K. *Falcon series data report: 1987 LNG vapor barrier verification field trials*; Lawrence Livermore National Laboratory: CA, USA, 1990.
257. Colenbrander, G. W.; Evans, A.; Puttock, J. S. *Spill tests of LNG and refrigerated liquid propane on the sea, Maplin Sands 1980: Dispersion Data Digest; Trial 27*; Thornton Research Center: 1984.

258. Feldbauer, G. F.; Heigl, J. J.; McQueen, W.; Whipp, R. H.; W.G, M. *Spills of LNG on Water: Vaporization & Downwind Drift of Combustible Mixtures*; EESO Research and Engineering Company: 1972.
259. Kneebone, A.; Prew, L. R. In *Shipboard jettison test of LNG onto the sea*, Proceedings on the 4th International Conference on LNG, Algiers, 1974; 1974; pp 1-25.
260. Koopman, R. P.; Bowman, B. R.; Ermak, D. L. *Data and calculations of dispersion of 5m³ LNG spill tests*; Lawrence Livermore National Laboratory: 1979.
261. Tauseef, S. M.; Rashtchian, D.; Abbasi, S. A., CFD-based simulation of dense gas dispersion in presence of obstacles. *Journal of Loss Prevention in the Process Industries* **2011**, 24, (4), 371-376.
262. Koopman, R. P.; Cederwall, R. T.; Ermak, D. L.; Goldwire Jr, H. C.; Hogan, W. J.; McClure, J. W.; McRae, T. G.; Morgan, D. L.; Rodean, H. C.; Shinn, J. H., Analysis of Burro series 40-m³ lng spill experiments. *Journal of Hazardous Materials* **1982**, 6, (1-2), 43-83.
263. ANSYS *ANSYS FLUENT 14 Theory guide*; ANSYS Inc: USA, 2015.
264. Marek, R.; Straub, J., Analysis of the evaporation coefficient and the condensation coefficient of water. *International Journal of Heat and Mass Transfer* **2001**, 44, (1), 39-53.
265. Havens, J. A.; Spicer, T. O., Further Analysis Of Catastrophic LNG Spill Vapor Dispersion. In *Heavy Gas and Risk Assessment — II: Proceedings of the Second Symposium on Heavy Gases and Risk Assessment, Frankfurt am Main, May 25–26, 1982*, Hartwig, S., Ed. Springer Netherlands: Dordrecht, 1983; pp 181-210.
266. Ishii, M.; Hibiki, T., Interfacial Transport. In *Thermo-Fluid Dynamics of Two-Phase Flow*, Springer New York: New York, NY, 2011; pp 143-154.
267. Ikealumba, W. C.; Wu, H., Modeling of Liquefied Natural Gas Release and Dispersion: Incorporating a Direct Computational Fluid Dynamics Simulation Method for LNG Spill and Pool Formation. *Industrial & Engineering Chemistry Research* **2016**, 55, (6), 1778-1787.
268. Dyer, A. J., A review of flux-profile relationships. *Boundary-Layer Meteorology* **1974**, 7, (3), 363-372.
269. Foken, T., 50 Years of the Monin–Obukhov Similarity Theory. *Boundary-Layer Meteorology* **2006**, 119, (3), 431-447.
270. Lees, F., *Lees' Loss Prevention in the Process Industries: Hazard Identification, Assessment and Control*. Elsevier Science: 2012.
271. Otterman, B., Analysis of large LNG spills on water part 1: Liquid spread and evaporation. *Cryogenics* **1975**, 15, (8), 455-460.
272. ABS Consulting, I. *Consequence Assessment Methods for Incidents Involving Releases from Liquefied Natural Gas Carriers*; May 13, 2004.
273. BP *BP Statistical review of world energy 2015*; British Petroleum (BP): London, 2015.
274. OSPO Sea Surface Temperature (SST) Contour Charts. <http://www.ospo.noaa.gov/Products/ocean/sst/contour/>
275. Ikealumba, W. C.; Wu, H., Effect of Air and Sea Surface Temperatures on Liquefied Natural Gas Dispersion. *Energy & Fuels* **2016**, 30, (11), 9266-9274.
276. Noble, P. G.; Ronning, L.; Paulling, J.; Zhao, R.; Lee, H., A novel LNG tank containment design for large LNG carriers. Discussion. *Transactions-Society of Naval Architects and Marine Engineers* **2005**, 113, 612-633.
277. Foss, M. M. *Introduction to LNG*; The University of Texas: Austin, TX, 2013.

278. Chang, H.-M., A thermodynamic review of cryogenic refrigeration cycles for liquefaction of natural gas. *Cryogenics* **2015**, 72, 127-147.
279. Lee, C.-J.; Song, K.; Shin, S.; Lim, Y.; Han, C., Process Design for the Offshore Production of Liquefied Natural Gas with Nonflammable Refrigerants. *Industrial & Engineering Chemistry Research* **2015**, 54, (44), 11106-11112.
280. Fahmy, M.; Nabih, H.; El-Aziz, M. A., Investigation and Performance Improvement of the Propane Precooling Cycle in the Propane Precooled Mixed Refrigerant Cycle Liquefaction Process. *Industrial & Engineering Chemistry Research* **2016**, 55, (10), 2769-2783.
281. White, M.; Phua, D. Natural Gas Imports into China - Prospects for Growth. http://www.kslaw.com/library/newsletters/EnergyNewsletter/2014/September/article_1.html (Accessed 2015)
282. Weather, O. Current Marine Data. <http://www.oceanweather.com/data/>
283. Pasquill, F., The estimation of the dispersion of windborne material. *Meteorol. Mag* **1961**, 90, (1063), 33-49.
284. Ermak, D. L.; Chapman, R.; Goldwire Jr, H. C.; Gouveia, F. J.; Rodean, H. C. *Heavy gas dispersion test summary report*; DTIC Document: 1989.
285. Ikealumba, W. C.; Wu, H., Effect of atmospheric and sea stability on liquefied natural gas (LNG) dispersion: Implications to Australian LNG marine transport. *Fuel* **2017**, 197, 8-19.
286. NOAA/NCEP *User manual and system documentation of WAVEWATCH III version 4.18*; U.S. Department of Commerce: U.S., 2014.
287. Lin, P., *Numerical modeling of water waves*. CRC Press: 2008.
288. Godderidge, B.; Tan, M.; Turnock, S.; Earl, C., A verification and validation study of the application of computational fluid dynamics to the modelling of lateral sloshing. **2006**.
289. Ibrahim, R. A.; Pilipchuk, V.; Ikeda, T., Recent advances in liquid sloshing dynamics. *Applied Mechanics Reviews* **2001**, 54, (2), 133-199.
290. Chwang, A. T.; Wang, K., Nonlinear impulsive force on an accelerating container. *Journal of fluids engineering* **1984**, 106, (2), 233-240.
291. Popov, G.; Sankar, S.; Sankar, T.; Vatistas, G., Liquid sloshing in rectangular road containers. *Computers & fluids* **1992**, 21, (4), 551-569.
292. Faltinsen, O. M.; Rognebakke, O. F.; Timokha, A. N., Resonant three-dimensional nonlinear sloshing in a square-base basin. Part 2. Effect of higher modes. *Journal of Fluid Mechanics* **2005**, 523, 199-218.
293. NewsComAu Typhoon Meranti hits China with 300km/h winds. <http://www.news.com.au/technology/environment/super-typhoon-meranti-is-worlds-largest-since-2013/news-story/0b5c5ac30c6da23bbe23e687d371a3d2> (15 September),

Every reasonable effort has been made to acknowledge the owners of copyright material. I would be pleased to hear from any copyright owner who has been omitted or incorrectly acknowledged.

APPENDIX COPYRIGHT PERMISSION STATEMENTS

- A. *Chapter 2, reprinted with permission from (Ikealumba, Walter Chukwunonso, and Hongwei Wu. "Some recent advances in liquefied natural gas (LNG) production, spill, dispersion, and safety." Energy & Fuels 28.6 (2014): 3556-3586). Copyright (2014) America Chemical Society and is available under the terms of the ACS AuthorChoice license*

Some Recent Advances in Liquefied Natural Gas (LNG) Production, Spill, Dispersion, and Safety

Walter Chukwunonso Ikealumba and Hongwei Wu*

School of Chemical and Petroleum Engineering, Curtin University, GPO Box U1987, Perth, Western Australia 6845, Australia

Energy Fuels, 2014, 28 (6), pp 3556–3586

DOI: 10.1021/ef500626u

Publication Date (Web): April 23, 2014

Copyright © 2014 American Chemical Society

*Telephone: +61-8-92667592. Fax: +61-8-92662681. E-mail: h.wu@curtin.edu.au.

 ACS AuthorChoice - This is an open access article published under an ACS AuthorChoice License, which permits copying and redistribution of the article or any adaptations for non-commercial purposes.

Note

There were errors in values given in Table 3 of the version of this paper published May 16, 2014. The correct version published June 9, 2014.

Abstract

The global demand of liquefied natural gas (LNG) has risen rapidly in recent years for the reasons of energy security and sustainable development. This has led to considerable recent research interests and efforts in the LNG production chain and associated risks in handling, storage, and transport of LNG, largely driven by the intrinsic process safety issues of LNG, potential terrorist threats, and public confidence in LNG safety. This review presents an overview on some recent advances in the LNG value chain, covering upstream gas production and gathering, liquefaction, shipping, and regasification processes. Recent developments in the experimentation and modeling of LNG spills associated with the LNG value chain are then summarized, covering the events following a LNG spill, including LNG pool formation, vapor dispersion, and combustion. The consequent hazards and safety issues are also discussed, with a focus on the methods for improving the safety of personnel, facilities, and ships. The key technical gaps in the related research areas have been identified, and future research directions are outlined.

- B.** Chapter 4, reprinted with permission from (Ikealumba, Walter Chukwunonso, and Hongwei Wu. "Modelling of Liquefied Natural Gas Release and Dispersion: Incorporating a Direct Computational Fluid Dynamics Simulation Method for LNG Spill and Pool Formation." *Industrial & Engineering Chemistry Research* 55.6 (2016): 1778-1787). Copyright (2016) America Chemical Society

 Copyright Clearance Center 

 ACS Publications **Title:** Modeling of Liquefied Natural Gas Release and Dispersion: Incorporating a Direct Computational Fluid Dynamics Simulation Method for LNG Spill and Pool Formation

Author: Walter Chukwunonso Ikealumba, Hongwei Wu

Publication: Industrial & Engineering Chemistry Research

Publisher: American Chemical Society

Date: Feb 1, 2016

Copyright © 2016, American Chemical Society

 If you're a copyright.com user, you can login to RightsLink using your copyright.com credentials. Already a RightsLink user or want to learn more?

PERMISSION/LICENSE IS GRANTED FOR YOUR ORDER AT NO CHARGE

This type of permission/license, instead of the standard Terms & Conditions, is sent to you because no fee is being charged for your order. Please note the following:

- Permission is granted for your request in both print and electronic formats, and translations.
- If figures and/or tables were requested, they may be adapted or used in part.
- Please print this page for your records and send a copy of it to your publisher/graduate school.
- Appropriate credit for the requested material should be given as follows: "Reprinted (adapted) with permission from (COMPLETE REFERENCE CITATION). Copyright (YEAR) American Chemical Society." Insert appropriate information in place of the capitalized words.
- One-time permission is granted only for the use specified in your request. No additional uses are granted (such as derivative works or other editions). For any other uses, please submit a new request.

 BACK

 CLOSE WINDOW

Copyright © 2016 [Copyright Clearance Center, Inc.](#). All Rights Reserved. [Privacy statement](#). [Terms and Conditions](#).
Comments? We would like to hear from you. E-mail us at customercare@copyright.com

C. Chapter 5, reprinted with permission from (Ikealumba, Walter Chukwunonso, and Hongwei Wu. "Effect of Air and Sea Surface Temperatures on LNG Dispersion." *Energy & Fuels*. Copyright (2016) America Chemical Society

 **RightsLink®**

 ACS Publications Most Trusted. Most Cited. Most Read.

Title: Effect of Air and Sea Surface Temperatures on LNG Dispersion
Author: Walter Chukwunonso Ikealumba, Hongwei Wu
Publication: Energy & Fuels
Publisher: American Chemical Society
Date: Oct 1, 2016
Copyright © 2016, American Chemical Society

Home **Create Account** **Help** 

LOGIN

If you're a copyright.com user, you can login to RightsLink using your copyright.com credentials. Already a RightsLink user or want to learn more?

PERMISSION/LICENSE IS GRANTED FOR YOUR ORDER AT NO CHARGE

This type of permission/license, instead of the standard Terms & Conditions, is sent to you because no fee is being charged for your order. Please note the following:

- Permission is granted for your request in both print and electronic formats, and translations.
- If figures and/or tables were requested, they may be adapted or used in part.
- Please print this page for your records and send a copy of it to your publisher/graduate school.
- Appropriate credit for the requested material should be given as follows: "Reprinted (adapted) with permission from (COMPLETE REFERENCE CITATION). Copyright (YEAR) American Chemical Society." Insert appropriate information in place of the capitalized words.
- One-time permission is granted only for the use specified in your request. No additional uses are granted (such as derivative works or other editions). For any other uses, please submit a new request.

BACK

CLOSE WINDOW

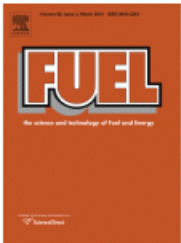
Copyright © 2016 [Copyright Clearance Center, Inc.](#) All Rights Reserved. [Privacy statement](#). [Terms and Conditions](#).
Comments? We would like to hear from you. E-mail us at customercare@copyright.com

- D.** Chapter 6, reprinted with permission from (Ikealumba, Walter Chukwunonso, and Hongwei Wu. "Effect of atmospheric and sea stability on liquefied natural gas (LNG) dispersion: Implications to Australian LNG marine transport" Fuels. Copyright (2017) Elsevier



Copyright Clearance Center RightsLink®

Home **Account Info** **Help**



Title: Effect of atmospheric and sea stability on liquefied natural gas (LNG) dispersion: Implications to Australian LNG marine transport
Author: Walter Chukwunonso Ikealumba, Hongwei Wu
Publication: Fuel
Publisher: Elsevier
Date: 1 June 2017
 © 2017 Elsevier Ltd. All rights reserved.

Logged in as:
 Walter Ikealumba
 Account #: 3000783197

[LOGOUT](#)

Order Completed

Thank you for your order.

This Agreement between Walter Ikealumba ("You") and Elsevier ("Elsevier") consists of your license details and the terms and conditions provided by Elsevier and Copyright Clearance Center.

Your confirmation email will contain your order number for future reference.

[Printable details.](#)

License Number	4082791267191
License date	Apr 05, 2017
Licensed Content Publisher	Elsevier
Licensed Content Publication	Fuel
Licensed Content Title	Effect of atmospheric and sea stability on liquefied natural gas (LNG) dispersion: Implications to Australian LNG marine transport
Licensed Content Author	Walter Chukwunonso Ikealumba, Hongwei Wu
Licensed Content Date	1 June 2017
Licensed Content Volume	197
Licensed Content Issue	n/a
Licensed Content Pages	12
Type of Use	reuse in a thesis/dissertation
Portion	full article
Format	both print and electronic
Are you the author of this Elsevier article?	Yes
Will you be translating?	No
Order reference number	
Title of your thesis/dissertation	Mathematical Modelling of LNG dispersion Under Various Conditions
Expected completion date	May 2017
Estimated size (number of pages)	191